ON FINITE ELEMENT NONLINEAR ANALYSIS OF GENERAL SHELL STRUCTURES

by

SAID BOLOURCHI

B.Sc., Queen Mary College, London University
(1973)

S.M., Massachusetts Institute of Technology
(1975)

SUBMITTED IN PARTIAL FULFILLMENT
OF THE REQUIREMENTS FOR THE
DEGREE OF

DOCTOR OF PHILOSOPHY

at the

MASSACHUSETTS INSTITUTE OF TECHNOLOGY

(May 1979)

Signature of Author . . . . . [redacted] . . . . . .
Department of Mechanical Engineering, May 16, 1979

Certified by . . . . . .
Thesis Supervisor

Accepted by . . . . . .
Chairman, Department Committee on Graduate Students

ON FINITE ELEMENT NONLINEAR ANALYSIS OF GENERAL SHELL STRUCTURES

by

SAID BOLOURCHI

Submitted to the Department of Mechanical Engineering on May 16, 1979 in partial fulfillment of the requirements for the Degree of Doctor of Philosophy.

ABSTRACT

Continuum mechanics-based total Lagrangian and updated Lagrangian formulations of structural elements are presented for large displacement and rotation analysis. It is shown that the two formulations yield identical element matrices, when they are applied to a straight Hermitian-based beam element, but the updated Lagrangian-based beam element is computationally more effective.

A comparison of the straight beam element with an isoparametric bending element with independent nodal element displacement and rotation degrees-of-freedom shows that the isoparametric displacement/rotation method is the more effective technique for fomulating general structural elements.

A displacement-based isoparametric displacement/rotation shell element is formulated and developed as a variable-number-nodes element. The element is described using linear, quadratic or cubic interpolating displacement fields, and can be a quadrilateral or a triangle. The element can also be employed as a fully compatible transition element to model shell to solid regions or shell intersections. Shell structures with eccentric and non-eccentric stiffeners can be modeled using the shell element and a compatible bending element.

The shell element can be employed in analysis of general shell structures with linear and geometric and material nonlinear behavior. Various sample solutions of linear and highly nonlinear problems are presented to illustrate the effectiveness of the element in analyzing practical engineering problems.

Thesis Supervisor: Klaus-Jürgen Bathe
Title: Associate Professor of Mechanical Engineering

ACKNOWLEDGEMENTS

I wish to express my deep appreciation to Professor K. J. Bathe for his supervision and guidance throughout this research. I am also grateful to the other members of my thesis committee: Professor T. H. H. Pian, Professor G. W. Strang and Professor J. H. Williams, Jr.. I am grateful to S. Ramaswamy for some fruitful discussions. I also like to thank M. D. Snyder. I give special thanks to Prudence Young for typing this manuscript.

The work reported in this report has been supported financially by the ADINA users group. I acknowledge this support.

I especially thank my parents Aghdas and Asghar for their patience and support throughout my life.

TABLE OF CONTENTS

TABLE OF CONTENTS (Continued)

TABLE OF CONTENTS (Continued)

LIST OF TABLES

LIST OF FIGURES

LIST OF FIGURES (Continued)

LIST OF FIGURES (Continued)

NOTATION

All notation is defined in the text when used first. The following is only a list of some frequently used symbols.

A bar (-) on a quantity denotes that the quantity is referred or measured in local coordinates.

With regard to tensor and vector subscripts and superscripts, the following convention is employed:

A left superscript denotes the time of the configuration in which the quantity occurs.

A left subscript can have two different meanings. If the quantity considered is a derivative, the left subscript denotes the time of the configuration, in which is measured the coordinate with respect to which is differentiated. Otherwise the left subscript denotes the time of the configuration in which the quantity is measured.

Right lower case subscripts denote the components of a tensor or vector. Components are referred to a fixed global Cartesian coordinate system; i,j, ... = 1,2,3. Differentiation is denoted by a right lower case subscript following a comma, with the subscript indicating the coordinate with respect to which is differentiated , i.e., ${}_{t}u_{i,j} = \partial u_i / \partial {}^{t}x_j$.
A local variable with a right lower case subscript following a comma denotes the derivative of the local variable with respect to the local coordinate axis, i.e., ${}_{0}\bar{u}_{i,j}$ denotes $\partial {}_{0}\bar{u}_i / \partial {}^{0}\bar{x}_j$.

t, $t+\Delta t$ = time t and $t+\Delta t$, before and after time increment Δt

δ	=	denoting "variation in"
${}_0V$, ${}_tV$, ${}_{t+\Delta t}V$	=	volume of body in the configuration at time 0,t,t+Δt
${}_0A$	=	area of body in the configuration at time 0
${}_0x_i$, ${}_tx_i$, ${}_{t+\Delta t}x_i$	=	fixed Cartesian coordinate in the configuration at time 0,t,t+Δt
${}_0\bar{x}_i$, ${}_t\bar{x}_i$, ${}_{t+\Delta t}\bar{x}_i$	=	local convected Cartesian coordinate in the configuration at time 0,t,t+Δt
${}_0x_i^k$, ${}_tx_i^k$, ${}_{t+\Delta t}x_i^k$	=	Cartesian coordinate of nodal point k in the configuration at time 0,t,t+Δt
${}_0^t x_{i,j}$, ${}_0^t x_{i,j}$	=	derivative of coordinate in the configuration at time 0,t with respect to coordinate ${}_tx_j$, ${}_0x_j$
r, s,t	=	natural element coordinates
${}_0V_{ti}^k$, ${}_tV_{ti}^k$, ${}_{t+\Delta t}V_{si}^k$	=	component of unit vector in the direction t of nodal point k at time 0,t,t+Δt
${}_0V_{si}^k$, ${}_tV_{si}^k$, ${}_{t+\Delta t}V_{si}^k$	=	Component of unit vector in the direction s of nodal point k at time 0,t,t+Δt

$^{0}V_{ni}^{k}$, $^{t}V_{ni}^{k}$, $^{t+\Delta t}V_{ni}^{k}$ = Component of unit normal vector to shell mid-surface at the nodal point k at time 0,t,t+Δt

$^{t}u_{i}$, $^{t+\Delta t}u_{i}$ = component of displacement vector from the initial configuration at time 0 to the configuration at time t, t+Δt

u_{i} = increment in displacement component, $u_{i} = {}^{t+\Delta t}u_{i} - {}^{t}u_{i}$

$^{t}u_{i}^{k}$ = displacement component of nodal point k in the configuration at time t

u_{i}^{k} = increment in $^{t}u_{i}^{k}$

V_{ni}^{k} = increment in unit normal vector $^{t}V_{ni}^{k}$ at nodal point k, i.e., $V_{ni}^{k} = {}^{t+\Delta t}V_{ni}^{k} - {}^{t}V_{ni}^{k}$

V_{si}^{k} , V_{ti}^{k} = increment in $^{t}V_{si}^{k}$, $^{t}V_{ti}^{k}$

$^{t}_{0}u_{i,j}$, $^{t+\Delta t}_{0}u_{i,j}$ = derivative of displacement component in the configuration at time t, t+Δt with respect to coordinate $^{0}x_{j}$

$^{0}u_{i,j}$, $^{t}u_{i,j}$, $^{t+\Delta t}u_{i,j}$ = derivative of displacement increment with respect to coordinate $^{0}x_{j}$, $^{t}x_{j}$, $^{t+\Delta t}x_{j}$

${}^{t}\varepsilon_{ij}$, ${}^{t+\Delta t}\varepsilon_{ij}$	=	component of Almansi strain tensor in the configuration at time t,t+Δt referred to the configuration at time 0
${}^{t}_{0}\varepsilon_{ij}$, ${}^{t+\Delta t}_{0}\varepsilon_{ij}$	=	component of Green-Lagrange strain tensor in the configuration at time t,t+Δt referred to the confjguration at time 0
${}^{t+\Delta t}_{t}\varepsilon_{ij}$	=	component of Green-Lagrange strain tensor in the configuration at time t+Δt referred to the configuration at time t (i.e., using displacement increments from the configuration at time t to time t+Δt)
${}_{0}\varepsilon_{ij}$, ${}_{t}\varepsilon_{ij}$	=	component of Green-Lagrange strain increment tensor referred to the configuration at time 0,t
${}^{t}e_{ij}$, ${}^{t+\Delta t}e_{ij}$	=	component of total infinitesimal strain tensor at time t, t+Δt
e_{ij}	=	increment in ${}^{t}e_{ij}$
${}_{0}e_{ij}$, ${}_{t}e_{ij}$	=	linear part of strain increment ${}_{0}\varepsilon_{ij}$, ${}_{t}\varepsilon_{ij}$
${}_{0}\eta_{ij}$, ${}_{t}\eta_{ij}$	=	nonlinear part of strain increment ${}_{0}\varepsilon_{ij}$, ${}_{t}\varepsilon_{ij}$

C_{ijrs}	=	component of constant constitutive tensor
${}^{t}_{0}C_{ijrs}$, ${}^{t}_{t}C_{ijrs}$	=	component of constitutive tensor at time t referred to the configuration at time 0,t
${}^{0}_{0}C_{ijrs}$, ${}^{t}_{t}C_{ijrs}$	=	component of tangent constitutive tensor at time t referred to the configuration at time 0,t
${}^{0}\rho$, ${}^{t}\rho$	=	specific mass of body in the configuration at time 0,t
${}^{t+\Delta t}_{0}f_{i}$	=	component of body force vector per unit mass, at time t+Δt, referred to the configuration at time 0
${}^{t+\Delta t}_{0}t_{i}$	=	component of surface traction vector per unit area, at time t+Δt, referred to the configuration at time 0
${}^{t+\Delta t}R$	=	external virtual work expression corresponding to the configuration at time t+Δt defined in Eq. (2.2)
${}^{t}\sigma_{ij}$	=	component of stress tensor at time t, calculated assuming infinitesimal displacement conditions
σ_{ij}	=	increment in ${}^{t}\sigma_{ij}$

${}^{t}\tau_{ij}$, ${}^{t+\Delta t}\tau_{ij}$	=	component of Cauchy stress tensor in the configuration at time t,t+Δt
${}^{t}_{0}S_{ij}$, ${}^{t+\Delta t}_{0}S_{ij}$	=	component of 2nd Piola-Kirchhoff stress tensor in the configuration at time t,t+Δt referred to the configuration at time 0
${}^{t+\Delta t}_{t}S_{ij}$	=	component of 2nd Piola-Kirchhoff stress tensor in the configuration at time t+Δt referred to the configuration at time t
${}_{0}S_{ij}$, ${}_{t}S_{ij}$	=	component of 2nd Piola-Kirchhoff stress increment at time t
D_{ij}	=	component of deviatoric stresses
h_k	=	finite element interpolation function associated with nodal point k
${}_{0}h^{i}_{k}$, ${}_{t}h^{i}_{k}$	=	finite element Hermitian interpolation function in the local direction i associated with the kth degree of freedom of the beam element, and measured in the local configuration at time 0,t, respectively.

$^{0}R_{ij}$, $^{t}R_{ij}$ = component of the transformation matrix of the beam local axes at time 0,t with respect to the global axis

$^{t}\bar{R}_{ij}$, $^{t+\Delta t}\bar{R}_{ij}$ = component of the transformation matrix of the beam local axes at time t,t+Δt with respect to original beam local axes

Matrices

$^{t}_{0}\underline{B}_{L}$, $^{t}_{t}\underline{B}_{L}$ = linear strain-displacement matrix in the configuration at time t referred to the configuration at time 0,t

$\underline{B}_{L}$ = linear strain-displacement matrix assuming small displacements

$^{t}_{0}\underline{B}_{NL}$, $^{t}_{t}\underline{B}_{NL}$ = nonlinear strain-displacement matrix in the configuration at time t referred to the configuration at time 0,t

$\underline{C}$ = stress-strain material property matrix

$^{0}\underline{C}$, $^{t}\underline{C}$ = tangent material property matrix at time t and referred to the configuration at time 0,t

${}^{t}\underline{F}$, ${}^{t}_{0}\underline{F}$, ${}^{t}_{t}\underline{F}$	=	vector of nodal point forces at time t
$\underline{K}$	=	time independent linear elastic, small displacement stiffness matrix
${}^{t}_{0}\underline{K}_{L}$, ${}^{t}_{t}\underline{K}_{L}$	=	linear strain stiffness matrix in the configuration at time t referred to the configuration at time 0,t
${}^{t}_{0}\underline{K}_{NL}$, ${}^{t}_{t}\underline{K}_{NL}$	=	nonlinear strain stiffness matrix in the configuration at time t, referred to the configuration at time 0,t
${}^{t}\underline{K}$	=	tangent stiffness matrix at time t
$\underline{M}$	=	mass matrix
${}^{t+\Delta t}\underline{R}$	=	vector of external loads at time t+Δt
${}^{t}_{0}\underline{S}$, ${}^{t}_{0}\hat{\underline{S}}$	=	2nd Piola-Kirchhoff stress matrix and vector in the configuration at time t and referred to the configuration at time 0
${}^{t}\underline{u}$, ${}^{t+\Delta t}\underline{u}$	=	vector of element nodal point displacements at time t,t+Δt
${}_{0}\bar{\underline{u}}$, ${}_{t}\bar{\underline{u}}$, ${}_{t+\Delta t}\bar{\underline{u}}$	=	vector of element nodal point incremental displacements at time t and referred to the local axes at time 0, t, t+Δt

$\underline{u}$ = vector of element nodal point incremental displacements at time t

$^{t}\underline{U}$, $^{t+\Delta t}\underline{U}$ = vector of element assemblage nodal point displacements at time t,t+Δt

$\underline{U}$ = vector of element assemblage incremental nodal point displacements at time t

$^{t}\hat{\Sigma}$ = vector of stresses at time t in materially nonlinear analysis only

$^{t}\underline{\tau}$ $^{t}\hat{\underline{\tau}}$ = Cauchy stress matrix and vector in the configuration at time t

$^{t}\underline{D}$ = deviatoric stress matrix in the configuration at time t

$^{0}\underline{R}$, $^{t}\underline{R}$, $^{t+\Delta t}\underline{R}$ = matrix transforming the beam nodal points displacements measured in the beam local axis at time 0,t,t+Δt to the global axis

$^{t}\bar{\underline{R}}$, $^{t+\Delta t}\bar{\underline{R}}$ = matrix transforming the straight beam nodal points displacements measured in the local axes at time t,t+Δt to the beam local axes in the configuration at time 0

1. INTRODUCTION

A very important element of a structure is in many cases a shell, since it is an efficient load carrying member. Shells are used in various structures such as spacecrafts, missiles, pressure vessels and so on. Thus reliable linear and nonlinear analysis of shell structures are of much importance. For decades, a large amount of research effort has been spent to develop capabilities of general shell analysis. Fung and Sechler [1] have given a comprehensive survey of thin shell structural capabilities. In addition many governing equations of the behavior of thin shells have been derived, depending on the specific assumptions made on the behavior or geometry of the structure. One of these thin shell theories derived for geometrically linear and nonlinear general shell structural behavior is presented by Reissner [1]. More detailed discussions of shell theory assumptions are given in [2].

The nonlinear partial differential equations governing the behavior of shell structures are extremely complex. Analytical closed form solutions to these equations hardly exist except for a few small deflection analyses of simple cases of geometry and loading. Some series solution techniques have been used to predict the approximate solution for simple nonlinear shell problems. However, it is impossible to extend these methods to the analysis of realistic engineering shell structures with complex geometries (e.g. variable thickness, cut outs, branches, intersections and connection with other types of structural

members). These difficulties are specially observed due to the complex loading of the engineering shell structures and the high degree of precision which is needed in determining the safety of these structures. The short coming of the classical analytical techniques has forced the designers to search for numerical methods.

Advances in numerical methods and the availability of high speed digital computers has created the new field of computational mechanics. In the past two decades a large number of papers have been devoted to the numerical analysis of shell structures. A detailed review of all the papers on this topic is beyond the scope of this study. The two basic numerical techniques employed in the analyses of plate and shell structures are, the finite element method [3-5], and the finite difference method [6-7]. In this study we concentrate on the finite element method because of its generalities and flexibilities.

The finite element method has proved to be a powerful, effective and reliable approximate technique for solving many solid mechanics problems. Finite element analyses of thin shell structures may be divided into two approaches as follows; firstly, what may be called a classical procedure, and secondly, an assumed displacement isoparametric element formulation.

In the first approach a classical concept is employed in which a plate or shell theory is used as the starting point of the finite element formulation. This plate or shell theory has been developed from the three-dimensional field equations by incorporating various assumptions

appropriate to the structural behavior. Using variational formulations based on these theories various finite element models have been developed; namely, displacement, hybrid and mixed formulations [8]. Atluri and Pian [9] have given a comprehensive review and systematic classification of finite element formulations for the linear analysis of general shells.

In recent years, many elements have been developed based on the classical procedure by employing different plate or shell assumptions to analyze shell structures. Many researchers have approximated the shell geometry using flat elements. Among the recent papers on this subject, [10-13] deal with linear analysis and [3, 14-16] deal with geometrically nonlinear analysis of shells of large deflections and rotations, using flat elements. Displacement type formulation were used in [11,13,14], and hybrid stress formulations are employed in [12,15,16]. A number of authors have concentrated on the analysis of shells of revolution, formulations for linear analysis are presented in [17,18] while [19] deals with nonlinear analysis of shells of revolution. A general shell theory has been employed in [20,21] to formulate shell elements for analyzing the linear behavior of general shell structures. A mixed isoparametric formulation was employed by Noor et al. [22] to study the large deflection behavior of general shells. Boland and Pian [23] used shallow shell theory in formulating shell elements to analyze the elastic behavior of general shells.

In the second approach, isoparametric elements with indepen-

dent rotational and displacement degrees of freedom are employed. This procedure was originally introduced by Ahmad et. al. [24] for the linear analysis of moderately thick and thin shells, and has been further developed for the linear analysis of elastic thin shells [25-27]. A similar approach has recently been applied to the geometrically nonlinear analysis of shells by Ramm [28]. Kråkeland [29] has extended this work to analyze also the materially nonlinear behavior of shells.

In considering current capabilities for the computer analysis of shell structures, reference may also be made to the comparative study of the linear and nonlinear finite element shell solutions reported by Hartung and Ball [31], in which several specific problems solved by different members of the structures community have been compared. The comparison of the results shows good agreement for linear analysis. However, the nonlinear results (geometric nonlinearity only) shows virtually no agreement and the reason for the differences could not be explained.

The conceptual advantage of the displacement/rotation isoparametric elements is their inherent generality, which is analogous to the generality of the isoparametric elements in the analysis of two- and three dimensional continuum problems [34,35]. In contrast to the classical approach, no specific classical plate or shell theory is employed; instead, the geometry and the displacement field of the structure is directly discretized and interpolated as in the analysis of continuum problems. This approach is equivalent to using a general shell theory and can be employed efficiently for the analysis of general structural

configurations by using variable-number-nodes elements [32,33].

The basic ideas for the development of the displacement/rotation isoparametric elements evolved from the difficulties that are encountered when using the usual displacement isoparametric elements in the analysis of plates and shells. Firstly, computational difficulties can result when these isoparametric elements are very thin, because the stiffness coefficients corresponding to the transverse displacement degrees of freedom are considerably larger than those corresponding to the longitudinal displacements. Secondly, errors are introduced in the analysis because erroneous strain energy corresponding to the normal stresses in the thickness direction is included. These two difficulties are overcome in the approach introduced by Ahmad et.al., because it is assumed that the normal to the shell surface remains straight and does not extend, and the normal stresses in the direction of the shell thickness are ignored in the element formulation.

Scope of Present Study

The objective in this investigation is to present a general variable-number-nodes displacement/rotation isoparametric shell element for geometric and material nonlinear analysis of general plate and shell structures. The element formulations are based on the consistance continuum mechanics principles.

We first present the basic continuum mechanics virtual work theory and then define an updated Lagrangian (U.L.) and a total Lagrangian (T.L.) formulation, Chapter 2. These formulations allow for very large displacements and rotations as well as the material nonlinear

behavior of the continuum. The linearization of these formulations, and the finite element discretization are also presented in this chapter.

In Chapter 3, the T.L. and the U.L. formulations are employed to formulate a straight beam element, in which Hermitian polynomials are employed to interpolate displacements within the element. It is shown in this chapter that both formulations are identical for this example.

In Chapter 4, a variable-number-nodes Lagrangian bending element with independent displacement and rotation is presented. It is shown that it is more effective to employ the Lagrangian bending element than the Hermitian beam element to analyze curved structures.

The general variable-number-nodes displacement/rotation isoparametric shell element is presented in Chapter 5. This element can be employed to analyze general shell structures with geometric and material nonlinear behavior. In this chapter, we present the derivation of the element matrices based on the T.L. and the U.L. formulation. We also present the lumped and consistent mass matrices, elastic and elastic-plastic constitutive relations to be employed in the element formulation.

In Chapter 6, the Lagrangian interpolation functions of the variable-number-nodes general shell element are presented. The tables of interpolation functions are presented for both the quadrilateral and the triangular elements. The shell element can possess 3 to 16 mid-surface nodes. Each mid-surface node has three displacement degrees of freedom and two rotational degrees-of-freedom. The interpolation function can be linear, quadratic, or cubic polynomial. The quadri-

lateral element can have 1 or 4 internal nodes. The 9-nodes element (including one internal node), and 16-nodes element (including four internal nodes) represent quadratic and cubic Lagrangian element, respectively. In this chapter, the interpolation functions of transition element are also presented. This element can have mid-surface nodes and top- and bottom- surface nodes. This element can be used for connecting the shell element to solid continuum elements. Each top- or bottom- surface node has three displacement degrees-of-freedom.

In Chapter 7, we describe some important aspects pertaining to the implementation and the usage of the element such as; geomerty discription, spatial integration over quadrilateral and triangular space, connectivity of the element with other continuum elements, modeling of sharp edges and branches by using constraint equations, and the effect of the element aspect ratio on the response prediction.

Some linear and highly nonlinear numerical examples are presented in Chapter 8. These examples demonstrate some of the capabilities and the effectiveness of the element. The numerical results are compared to analytical or experimental results when available.

Finally the conclusions of this study and recommendations for further studies are given.

2. INCREMENTAL CONTINUUM MECHANICS FORMULATION

Consider the large displacement motion of a general body as a function of time and assume that the solutions for the static and kinematic variables are known for the discrete time points, 0, Δt, $2\Delta t$, ...,t. The motion of the body is considered in a fixed Cartesian coordinate system, Fig. 2.1. The basic aim of the analysis is to establish an equation of virtual work from which the unknown static and kinematic variables in the configuration at time $t+\Delta t$ can be solved. Since the displacement-based finite element procedure shall be employed for numerical solution, we use the principle of virtual displacements to express the equilibrium of the body.

Assuming that the direction and magnitude of the body and surface loading are independent of the body configuration, the principle of virtual displacements is:

$$\int_{t+\Delta t_V} {}^{t+\Delta t}\tau_{ij}\ \delta\, {}_{t+\Delta t}e_{ij}\ {}^{t+\Delta t}dv = {}^{t+\Delta t}R \qquad (2.1)$$

where ${}^{t+\Delta t}\tau_{ij}$ = Cartesian components of Cauchy stress tensor at time $t+\Delta t$ and measured in the configuration at time $t+\Delta t$ [Physically equal to force per unit area of the deformed body];

${}_{t+\Delta t}e_{ij}$ = Cartesian components of infinitesimal strain tensor increment measured in the configuration at time $t+\Delta t$,which are defined to be ${}_{t+\Delta t}e_{ij} = \frac{1}{2}\left(\frac{\partial u_i}{\partial\, {}^{t+\Delta t}x_j} + \frac{\partial u_j}{\partial\, {}^{t+\Delta t}x_i}\right)$

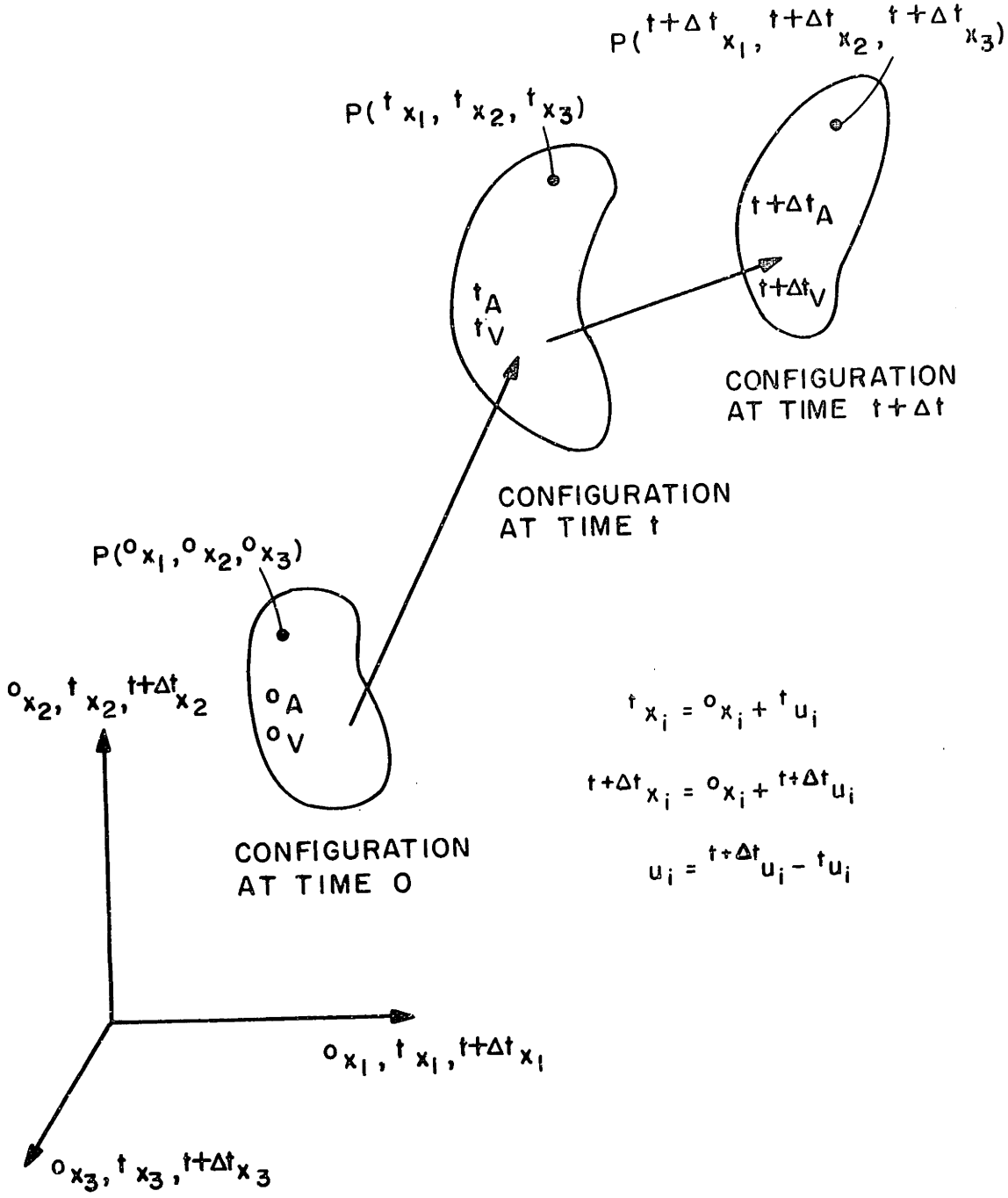

FIGURE 2.1 MOTION OF BODY IN CARTESIAN COORDINATE SYSTEM

and, ${}^{t+\Delta t}R$ is the total external virtual work expression due to the surface tractions with components ${}^{t+\Delta t}_{0}t_k$, and body forces with components ${}^{t+\Delta t}_{0}f_k$,

$$ {}^{t+\Delta t}R = \int_{0_A} {}^{t+\Delta t}_{0}t_k \, \delta u_k \, {}^{0}da + \int_{0_V} {}^{0}\rho \, {}^{t+\Delta t}_{0}f_k \, \delta u_k \, {}^{0}dv \tag{2.2} $$

It should be noted that Eq. (2.1) is identical to the virtual work principle for linear analysis, except that in the linear formulation the integral is performed over the original volume.

Equation (2.1) is an integral equation over the unknown deformed volume of the body at time $t+\Delta t$. The quantities in this equation can be referred back to any of the known configurations at time $0, \Delta t, 2\Delta t, \ldots t$, i.e. the integral can be evaluated over the known volume ${}^{0}V$, ${}^{\Delta t}V$, ${}^{2\Delta t}V$, $\ldots {}^{t}V$. Here we show how to refer the Eq. (2.1) to the configuration at time $\hat{t}$ (where $\hat{t}$ could be $0, \Delta t, 2\Delta t, \ldots t$). Define a mathematical stress measure, 2nd Piola-Kirchhoff stress†, [36, pp. 220-224]

$$ {}^{t+\Delta t}_{\hat{t}}S_{ij} = \frac{\hat{t}_\rho}{{}^{t+\Delta t}\rho} \, {}^{\hat{t}}_{t+\Delta t}x_{i,s} \, {}^{t+\Delta t}\tau_{sr} \, {}^{\hat{t}}_{t+\Delta t}x_{j,r} \tag{2.3} $$

†Although some pictorial representation of the 2nd Piola-Kirchhoff stress are given (e.g. see Fung [37] page 437, Malvern [36] page 221), there is no physical representation of this stress measure. This stress tensor is merely used for mathematical convenience.

where $\hat{t}\rho$, $^{t+\Delta t}\rho$ = density at time $\hat{t}$, $t+\Delta t$

$$^{t+\Delta t}x_i = {}^{0}x_i + {}^{t+\Delta t}u_i$$

$$\hat{t}x_{t+\Delta t}{}_{i,s} = \frac{\partial \hat{t}x_i}{\partial {}^{t+\Delta t}x_s}$$

Inverting Eqn. (2.3),

$$^{t+\Delta t}\tau_{ij} = \frac{^{t+\Delta t}\rho}{\hat{t}\rho} \; \hat{t}x_{i,r} \; \hat{t}S_{rs} \; \hat{t}x_{j,s} \qquad (2.4)$$

Substituting Eqn. (2.4) into Eqn. (2.1) we obtain;

$$^{t+\Delta t}R = \int_{\hat{t}V} \frac{^{t+\Delta t}\rho}{\hat{t}\rho} \; \hat{t}S_{rs} \; \hat{t}x_{i,r} \; \hat{t}x_{j,s} \; \delta \, {}^{t+\Delta t}e_{ij} \; {}^{t+\Delta t}dv \qquad (2.5)$$

Introducing the increment in the Green-Lagrange strain measure

$$\hat{t}\varepsilon_{rs} = \hat{t}x_{i,r} \; \hat{t}x_{j,s} \; {}^{t+\Delta t}e_{ij} \qquad (2.6)$$

and the total Green-Lagrange strain at time $t+\Delta t$ is

$$^{t+\Delta t}_{\hat{t}}\varepsilon_{rs} = {}^{t}_{\hat{t}}\varepsilon_{rs} + \hat{t}\varepsilon_{rs} \qquad (2.7)$$

where ${}^{t}_{\hat{t}}\varepsilon_{rs}$ = component of Green-Lagrange strain tensor at time t measured in the configuration at time $\hat{t}$.

Using Eq. (2.7), the variation in the Green-Lagrange strain becomes;

$$\delta {}^{t+\Delta t}_{\hat{t}}\varepsilon_{rs} = \delta {}^{\hat{t}}_{\hat{t}}\varepsilon_{rs} \tag{2.8}$$

Using Eqs. (2.5) to (2.8) and since from the conservation of mass

$${}^{t+\Delta t}\rho \; {}^{t+\Delta t}dv = {}^{\hat{t}}\rho \; {}^{\hat{t}}dv \tag{2.9}$$

the virtual work principle becomes

$${}^{t+\Delta t}R = \int_{\hat{t}V} {}^{t+\Delta t}_{\hat{t}}S_{rs} \; \delta \; {}^{t+\Delta t}_{\hat{t}}\varepsilon_{rs} \; {}^{\hat{t}}dv \tag{2.10}$$

It should be noted that Eqs. (2.1) and (2.10) are equivalent. It should also be noted that a large number of stress and strain measures could have been used to transform Eq. (2.1) into a form other than the one in Eq. (2.10). However, the well known 2nd Piola-Kirchhoff stress tensor is used in this study, because it is a simple and symmetric tensor (see Eq. (2.3)), which results in a symmetric stiffness matrix.

In order to solve for the static and kinematic variables of the body at time t+Δt, in essence, two different formulations can be employed [34]. In the total Lagrangian (T.L.) formulation all static and kinematic variables are referred to the initial configuration at time 0. The up-

dated Lagrangian (U.L.) formulation is based on the same procedures that are used in the T.L. formulation, but in the solution all static and kinematic variables are referred to the last calculated configuration at time t. Various applications of both formulations in the analysis of continuum problems are presented in [35,38] where it was shown, in particular that both the T.L. and U.L. formulations include all nonlinear effects due to large displacements, large strains and material nonlinearities. The only advantage of using one formulation rather than the other is its better numerically efficiency.

2.1 Updated Lagrangian Formulation

In the U.L. formulation the virtual work principle expressing the equilibrium and compatibility requirements of the body at time $t+\Delta t$ referred to the configuration at time t, is

$$\int_{{}^tV} {}^{t+\Delta t}_{t}S_{ij} \; \delta {}^{t+\Delta t}_{t}\varepsilon_{ij} \; {}^{t}dv = {}^{t+\Delta t}R \tag{2.11}$$

where the ${}^{t+\Delta t}_{t}S_{ij}$ and the ${}^{t+\Delta t}_{t}\varepsilon_{ij}$ are the components of the 2nd Piola-Kirchhoff stress tensor and Green-Lagrange strain tensor both referred to the configuration at time t respectively; ${}^{t+\Delta t}R$ is the external virtual work defined by Eq. (2.2). The above relation represents a nonlinear equation in the unknown static and kinematic variables of the body at time $t+\Delta t$. The first step is to obtain an approximate solution to Eq. (2.11) by linearizing the equation about the last calculated configuration

at time t. This approximate solution can then be improved by equilibrium iteration until Eq. (2.11) is satisfied to a required tolerance. Using our usual notation, Table 1 summarizes the linearization and solution of Eq. (2.11) by the modified Newton-Raphson iteration.

The objective is to perform static and dynamic analysis, where in dynamic analysis the applied body forces include inertia forces. Assuming that the mass of the body is preserved, the inertia forces are conservative and can, in both the T.L. and U.L. formulations, be evaluated using $\int_{{}^0V} {}^0\rho \; {}^{t+\Delta t}\ddot{u}_k \; \delta u_k \; {}^0dv$. Corresponding to the linearized equation given in the table the equations of motion to be solved in the U.L. formulation by finite element discretization are:

$$\int_{{}^0V} {}^0\rho \;\; {}^{t+\Delta t}\ddot{u}_k \; \delta u_k \; {}^0dv \;+\; \int_{{}^tV} {}^tC_{ijrs} \; {}^te_{rs} \;\; \delta \, {}^te_{ij} \; {}^tdv \qquad (2.12)$$

$$+ \quad \int_{{}^tV} {}^t\tau_{ij} \;\; \delta \, {}^t\eta_{ij} \;\; {}^tdv \;=\; {}^{t+\Delta t}R \;-\; \int_{{}^tV} {}^t\tau_{ij} \;\; \delta \, {}^te_{ij} \;\; {}^tdv$$

where the definition for ${}^{t+\Delta t}R$ is still given in Eq. (2.2), but it should be noted that the body forces no longer include inertia forces, and ${}^tC_{ijrs}$ is the incremental material property tensor, referred to the configuration at time t. The derivation of ${}^tC_{ijrs}$ is presented in Section 5.3. The ${}^t\tau_{ij}$

are given Cauchy stresses acting in the configuration at time t, and ${}^{t}e_{ij}$, ${}^{t}\eta_{ij}$ are the linear and nonlinear incremental strains referred to the configuration at time t.

2.2 Total Lagrangian Formulation

In the T.L. formulation, the same basic concepts as in the U.L. formulation are employed, but the initial configuration at time 0 is used as reference. Thus, the governing virtual work principle is

$$\int_{{}^{0}V} {}^{t+\Delta t}_{0}S_{ij} \; \delta {}^{t+\Delta t}_{0}\varepsilon_{ij} \; {}^{0}dv = {}^{t+\Delta t}R \tag{2.13}$$

where the ${}^{t+\Delta t}_{0}S_{ij}$ and ${}^{t+\Delta t}_{0}\varepsilon_{ij}$ are the components of the 2nd Piola-Kirchhoff stress tensor and Green-Lagrange strain tensor, both referred to the initial configuration at time 0. Equation (2.13) represents a nonlinear equation in the unknown static and kinematic variables of the body at time t+Δt. Using our usual notation, Table 2 summarizes the linearization and solution of Eq. (2.13) by the modified Newton-Raphson iteration. Separating the inertia forces from the body forces in the linearized equations of motion given in the table leads to the equations to be solved in the T.L. formulation by finite element discretization:

$$\int_{{}^{0}V} {}^{0}\rho \; {}^{t+\Delta t}\ddot{u}_k \; \delta u_k \; {}^{0}dv + \int_{{}^{0}V} {}^{0}C_{ijrs} \; {}^{0}e_{rs} \; \delta {}^{0}e_{ij} \; {}^{0}dv \tag{2.14}$$

$$+ \int_{{}^{0}V} {}^{t}_{0}S_{ij} \; \delta {}^{0}\eta_{ij} \; {}^{0}dv = {}^{t+\Delta t}R - \int_{{}^{0}V} {}^{t}_{0}S_{ij} \; \delta {}^{0}e_{ij} \; {}^{0}dv$$

where ${}_0C_{ijrs}$ is the incremental material property tensor referred to the configuration at time 0, ${}^t_0S_{ij}$ are given 2nd Piola-Kirchhoff stresses acting at time t, and ${}_0e_{ij}$, ${}_0\eta_{ij}$ are the linear and nonlinear incremental strains referred to the configuration at time 0.

2.3 Finite Element Discretization

The basic aim is to establish and solve the equations of motion of a complete structure. Referring to the standard procedures for assembling the structure matrices, in the derivation of the required finite element matrices, attention need only be given to the calculation of the matrices corresponding to a single element [33].

In the U.L. formulation, using Eq. (2.12), the following matrix equations are obtained,

$$\underline{M}\,{}^{t+\Delta t}\underline{\ddot{u}} + \left({}^t_t\underline{K}_L + {}^t_t\underline{K}_{NL}\right)\underline{u} = {}^{t+\Delta t}\underline{R} - {}^t_t\underline{F} \tag{2.15}$$

In the T.L. formulation, using Eq. (2.14), the following matrix equations are obtained in the finite element derivations,

$$\underline{M}\,{}^{t+\Delta t}\underline{\ddot{u}} + \left({}^t_0\underline{K}_L + {}^t_0\underline{K}_{NL}\right)\underline{u} = {}^{t+\Delta t}\underline{R} - {}^t_0\underline{F} \tag{2.16}$$

where $\underline{M}$ = mass matrix

${}^t_0\underline{K}_L$, ${}^t_t\underline{K}_L$ = linear strain incremental stiffness matrices;

${}^t_0\underline{K}_{NL}$, ${}^t_t\underline{K}_{NL}$ = nonlinear strain (geometric or initial stress) incremental stiffness matrices;

$^{t+\Delta t}\underline{R}$ = vector of externally applied element nodal loads at time $t+\Delta t$;

$^{t}_{0}\underline{F}$, $^{t}_{t}\underline{F}$ = vectors of nodal point forces equivalent to the element stresses at time t;

$\underline{u}$ = vector of incremental nodal displacements, assembled from u_j^k ;

$^{t+\Delta t}\underline{u}$ = vector of nodal displacements at time $t+\Delta t$, assembled from $^{t+\Delta t}u_j^k$;

$^{t+\Delta t}\ddot{\underline{u}}$ = vector of nodal point accelerations at time $t+\Delta t$.

Using our usual notation, Table 3 summarizes the various integrals considered and the corresponding matrix evaluations.

3. COMPARISON OF THE T.L. AND U.L. FORMULATION FOR A STRUCTURAL ELEMENT

The total and the updated Lagrangian formulations were employed successfully in formulating continuum elements [32,39]. In this study we apply these formulations in formulating bending elements. It is important to show that both formulations yield identical element matrices, and the only difference in these formulations is their relative computational efficiency . In this chapter it is shown that the two formulations are identical when they are applied to a straight 2-node beam element.

The general three-dimensional straight beam element is formulated based on the T.L. and the U.L. formulations [40,41]. The element has two nodes with 6 degrees of freedom per node, and can transmit an axial force, two shear forces, two bending moments and a torque. Figure 3.1 shows a typical beam element.

The element is assumed to be straight and of constant cross-section. It is assumed that plane sections of the beam element normal to the neutral axis remain plane and normal during deformation. The element can undergo large deflections and rotations, but small strains conditions are assumed. Thus, the cross-sectional area and the length of the beam element do not change during deformation.

The principal moment of inertia axes of the beam element define the local coordinate system r,s,t as shown in Fig. 3.1. The two end nodes of the element, 1 and 2, plus a third auxiliary node, 3, are used to define these axes, where it should be noted that in the computations the r-s plane is defined by nodes 1, 2, and 3.

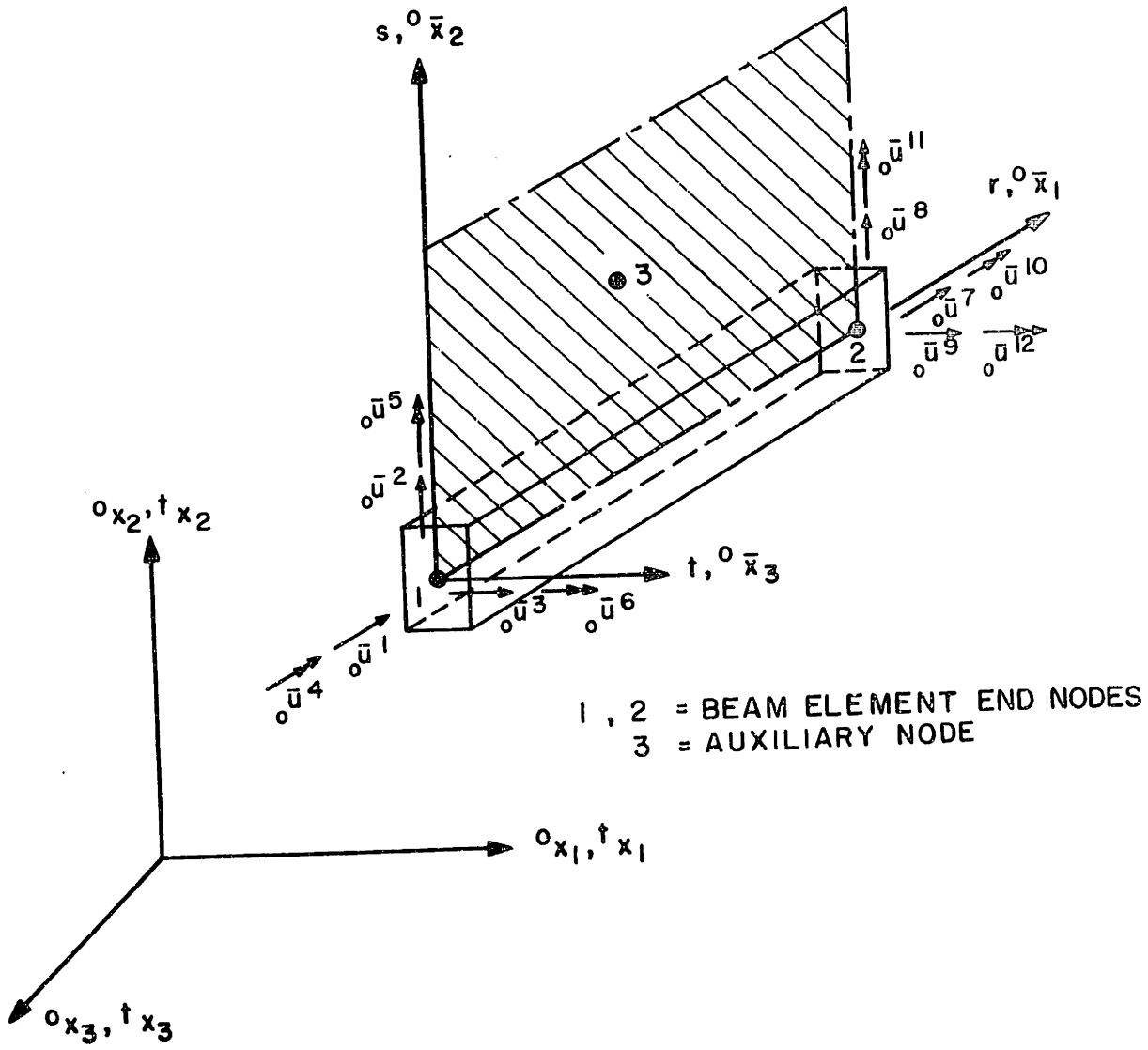

FIGURE 3.1 SCHEMATIC VIEW OF THE 3/D BEAM ELEMENT LOCAL COORDINATE AXES

Considering a typical straight beam element it is more effective to first evaluate the finite element matrices corresponding to the local principal axes ${}^{\tau}\bar{x}_i$ of the element (see Fig. 3.2), and then transform the resulting matrices to correspond to the global Cartesian coordinates prior to the element assemblage process [33]. The finite element matrices corresponding to the axes ${}^{\tau}\bar{x}_i$ are simply obtained by measuring all static and kinematic quantities in this coordinate system. These new quantities are denoted by a bar (-) placed over them.

3.1 U.L. Formulation of Beam Element

To describe the motion of a beam element the incremental displacement field within the element as a function of the incremental nodal point displacement components is required,

$$ {}^{t}\bar{u}_i = \sum_{k=1}^{12} {}_{t}h_k^i \; {}^{t}\bar{u}^k \tag{3.1} $$

where the ${}_{t}h_k^i$ are the interpolation functions corresponding to the local axis ${}^{t}\bar{x}_i$, and the ${}_{t}\bar{u}^k$ are the nodal point displacement increments measured in the local axis at time t, see Fig. 3.2.

The interpolation functions in Eq. (3.1) are Hermitian functions where bending displacements varying cubically and axial and torsional displacements varying linearly, Table 4.A. The kinematic assumptions used in defining these interpolation functions hold for small strains, small rigid body incremental rotations in each solution step, but any size translational displacements. These assumptions are appropriate for the up-

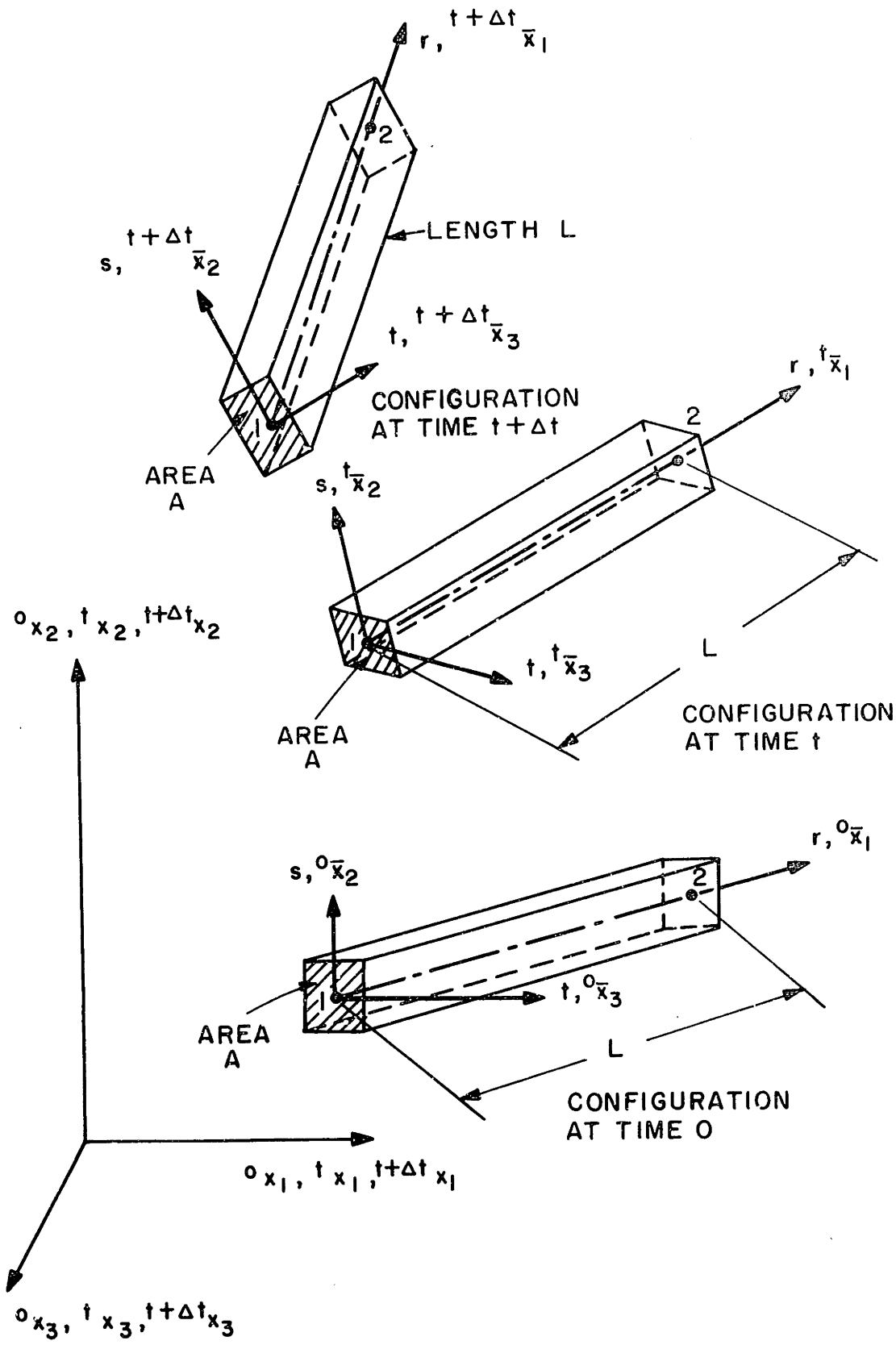

FIGURE 3.2 MOTION OF 3/D BEAM ELEMENT AND ITS LOCAL COORDINATE AXIS SHOWN IN GLOBAL COORDINATE SYSTEM

dated Lagrangian formulation of beams, because the kinematic variables are linearized about the last-known position.

A typical derivative required in the calculation of strain-displacement transformation matrices is $(\partial_t \bar{u}_i / \partial {}^t\bar{x}_j)$. This derivative is calculated using Eq. (3.1) and noting that the axes ${}^t\bar{x}_j (j = 1,2,3)$ correspond to convected coordinates axes r,s,t at time t (i.e. ${}^t\bar{x}_j \equiv r,s,t$ $(j = 1,2,3)$). Table 4.B summarizes the calculation of the matrices ${}^t_{t}\bar{B}_L$ and ${}^t_{t}\bar{B}_{NL}$ that are required to evaluate the tangent stiffness matrix and nodal point force vector of an element corresponding to coordinate axes ${}^t\bar{x}_i$ (i=1,2,3). The element matrices have to be transformed to the global coordinate system prior to their assemblage into a system of beam elements.

3.2 T.L. Formulation of Beam Element

The displacement increments within the element at time t measured in the local axes at time 0 are related to the nodal point displacement increments of the element in its local axes using, see Figs. 3.1 and 3.2,

$$ {}_0\bar{u}_i = \sum_{k=1}^{12} {}_0h_k^i \; {}_0\bar{u}^k \qquad (3.2) $$

where the ${}_0\bar{u}^k$ are the element nodal point displacement increments at time t, but measured in the ${}^0\bar{x}_i$ (i=1,2,3) coordinate system. The functions ${}_0h_k^i$ (i=1,2,3) are the interpolation functions corresponding to the convected axes r,s,t and measured in the coordinate system ${}^0\bar{x}_j$ (j=1,2,3). The interpolation functions ${}_0h_k^i$ are obtained using

$$ {}_0h_k^i = \sum_{m=1}^{3} \sum_{n=1}^{12} {}^t\bar{R}_{im} \; {}_th_n^m \; {}^t\bar{R}_{nk} \tag{3.3} $$

where ${}^t\bar{R}_{im}$ is the element (i,m) of the matrix ${}^t\underline{\bar{R}}$, which transforms displacements measured in the coordinate system ${}^t\bar{x}_i$ (i=1,2,3) to displacements measured in the system ${}^0\bar{x}_i$ (i=1,2,3). This matrix is incrementally calculated at each time step [41].

A typical derivative required in the calculation of the strain-displacement transformation matrix is $(\partial_0\bar{u}_i/\partial {}^0\bar{x}_j) = \sum_{k=1}^{12} (\partial_0 h_k^i/\partial {}^0\bar{x}_j)_0\bar{u}^k$.

To evaluate these derivatives it should be noted that the axes ${}^0\bar{x}_j$ (j=1,2,3) correspond to the convected axes r,s,t at time 0 (i.e., ${}^0\bar{x}_1 \equiv r$, ${}^0\bar{x}_2 \equiv s$, ${}^0\bar{x}_3 \equiv t$). Using Eq. (3.3) we have

$$ \frac{\partial_0\bar{u}_i}{\partial {}^0\bar{x}_j} = \sum_{k=1}^{12} \sum_{m=1}^{3} \sum_{n=1}^{12} {}^t\bar{R}_{im} \; \frac{\partial_t h_n^m}{\partial {}^0\bar{x}_j} \; {}^t\bar{R}_{nk} \; {}_0\bar{u}^k \tag{3.4} $$

Therefore double transformations are needed at each integration point for the strain calculation in the T.L. formulation. In comparison, the U.L. Formulation does not require the above transformation.

In order to evaluate the strain increments it is also necessary to calculate the derivatives of the total displacements. The kinematics of the rigid body rotations of the beam give;

$$ {}_0^t\bar{u}_{i,j} = {}^t\underset{\sim}{\bar{R}}_{ij} - \delta_{ij} \qquad \begin{pmatrix} i=1,2,3 \\ j=1,2,3 \end{pmatrix} \tag{3.5} $$

where the ${}^t\underset{\sim}{\bar{R}}_{ij}$ are the direction cosine of the ${}^t\bar{x}_i$ axis with respect to the ${}^0\bar{x}_j$ axis, and δ_{ij} is the Kronecker delta.

3.3 Comparison of T.L. and U.L. Formulations

The total and updated Lagrangian formulations are compared for the straight beam element presented in the previous sections.

The reference coordinate system used in the U.L. formulation is defined by the principal axes of the beam element in the position at time t, i.e., ${}^{t}\bar{x}_i$ (i=1,2,3). Therefore, the local stiffness matrix and the nodal point force vector are referred to this coordinate system. These matrices are transformed to the global coordinate system using

$$
\begin{aligned}
{}^{t}_{t}\underline{K} &= {}^{t}\underline{R}^{T}\ {}^{t}_{t}\bar{\underline{K}}\ {}^{t}\underline{R} \\
{}^{t}_{t}\underline{F} &= {}^{t}\underline{R}^{T}\ {}^{t}_{t}\bar{\underline{F}} \qquad (3.6) \\
\underline{u} &= {}^{t}\underline{R}^{T}\ {}_{t}\bar{\underline{u}} \\
{}^{t}\underline{R} &= {}^{t}\bar{\underline{R}}\ {}^{0}\underline{R}
\end{aligned}
$$

where ${}^{t}\bar{\underline{R}}$ is the transformation matrix relating the incremental nodal point displacements measured in ${}^{t}\bar{x}_i$ to ${}^{0}\bar{x}_i$ (i=1,2,3), and ${}^{0}\underline{R}$ is the transformation matrix that expresses the nodal point displacements measured in the beam local coordinate system ${}^{0}\bar{x}_i$ (i=1,2,3) in terms of the global nodal point displacement

In the T.L. formulation the reference coordinate system used is given by the element principal axes of inertia in the configuration at time 0, ${}^{0}\bar{x}_i$ (i=1,2,3). Therefore, the complete stiffness matrix (including the linear and nonlinear strain stiffness matrices), the nodal point force vector, and the local displacement increments are

referred to this coordinate system and must be transformed to the global coordinate system ${}^{0}x_i$ (i=1,2,3);

$$
\begin{aligned}
{}^{t}_{0}\underline{K} &= {}^{0}_{\underline{R}}\underline{R}^{T}\ {}^{t}_{0}\bar{\underline{K}}\ {}^{0}_{\underline{R}}\underline{R} \\
{}^{t}_{0}\underline{F} &= {}^{0}_{\underline{R}}\underline{R}^{T}\ {}^{t}_{0}\bar{\underline{F}} \\
\underline{u} &= {}^{0}_{\underline{R}}\underline{R}^{T}\ {}_{0}\bar{\underline{u}}
\end{aligned}
\tag{3.7}
$$

The principal difference between the U.L. and the T.L. formulations is that in the T.L. formulation the transformation on the interpolation functions in Eq. (3.3) is carried out to refer the displacement interpolations to the original configuration, and the ${}^{t}_{0}\bar{\underline{B}}_{L1}$ matrix is included in the calculations. The transformations on the interpolation functions and the use of the ${}^{t}_{0}\bar{\underline{B}}_{L1}$ matrix in the T.L. formulation together are equivalent to the additional transformation matrix ${}^{t}\bar{\underline{R}}$ that is employed on Eq. (3.6) in the U.L. formulation.

Indeed, as we have shown in detail [40], using Eqs. (3.1) to (3.5), Table 4, and some algebra we obtain,

$$
{}^{t}_{t}\bar{\underline{B}}_{L}\ {}^{t}\bar{\underline{R}} = \left[{}^{t}_{0}\bar{\underline{B}}_{L0} + {}^{t}_{0}\bar{\underline{B}}_{L1}\right] \equiv {}^{t}_{0}\bar{\underline{B}}_{L} \tag{3.8}
$$

Substituting the above relation into Table 3, when the ${}^{0}\bar{x}_j$ (j=1,2,3) are used as the reference coordinate system to evaluate the linear strain stiffness matrices, we obtain

$$
{}^{t}\bar{\underline{R}}^{T}\ {}^{t}_{t}\bar{\underline{K}}_{L}\ {}^{t}\bar{\underline{R}} = {}^{t}_{0}\bar{\underline{K}}_{L} \tag{3.9}
$$

Therefore the two formulations lead to identical linear-strain stiffness matrices corresponding to the global coordinate system. The components of the Cauchy stress tensor referred to the ${}^{t}\underline{x}_i$ axes are numerically equal to the components of the 2nd Piola-Kirchhoff stress tensor referred to the ${}^{0}\underline{x}_i$ axes [52], it follows from Eq. (3.8), Table 3, and the above fact, that the nodal point force vectors corresponding to the global axes are equal in both formulations.

Bathe and Bolourchi [40] have shown that the two formulations lead to identical nonlinear strain stiffness matrices corresponding to the global coordinate system;

$$ {}^{t}\underline{R}^{T} \; {}^{t}_{t}\underline{K}_{NL} \; {}^{t}\underline{R} = {}^{t}_{0}\underline{K}_{NL} \tag{3.10} $$

Although the same final element stiffness matrices and nodal point force vectors are generated in the two formulations, it is noted that using numerical integration the transformation on the interpolation functions in Eq. (3.3) and the evaluation of the ${}^{t}_{0}\underline{B}_{L1}$ matrix is carried out at each integration point. Therefore, the U.L. formulation is computationally more effective.

4. COMPARISON OF HERMITIAN AND LAGRANGIAN BENDING ELEMENTS

Hermitian polynomials to interpolate nodal displacements were employed in the previous chapter to develop a straight beam element. The element was used to evaluate an updated and a total Lagrangian formulation. In the formulations of the straight beam element displacements and slopes considered as dependent variables, and the Hermitian functions used to interpolate displacements were referred to the beam convected coordinate axes. A specific difficulty using this approach lies in that the different displacement components are not interpolated alike; namely, the use of polynomials of different order for the bending, torsional and axial displacements establishes an interpolation directionality that requires special attention. This difficulty is clearly shown in the need for double transformations required in the evaluation of the convected interpolation functions which are employed in the T.L. formulation, Eq. (3.3).

An alternative method is to formulate a general nonlinear beam bending element in which the transverse displacements, axial displacements and the rotations are interpolated independently using the same polynomials, Fig. 4.1. Since the same functions are employed for all these kinematic variables, the problem of interpolation directionality under large rotations does not arise.

In this chapter we first present the updated and total Lagrangian formulations of a 2 to 4 variable-number-nodes Lagrangian beam bending element, Fig. 4.1. The straight beam formulation presented in the previous chapter is then compared to this formulation.

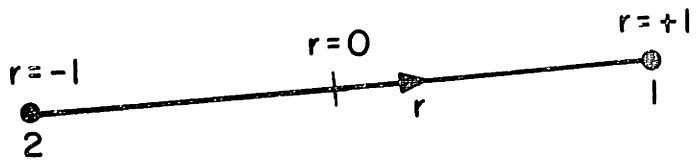

2-NODE BENDING ELEMENT (N=2)

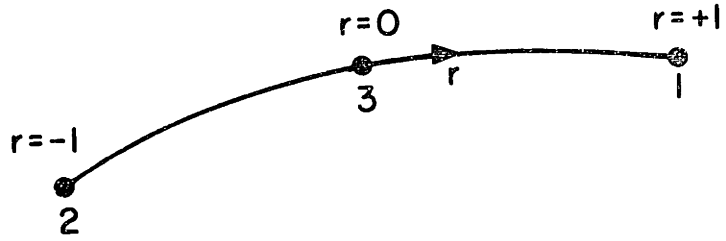

3-NODE BENDING ELEMENT (N=3)

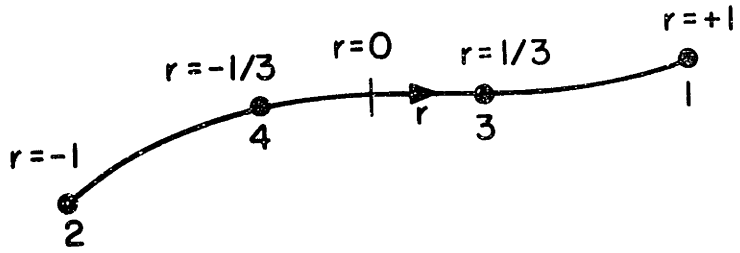

4-NODE BENDING ELEMENT (N=4)

FIGURE 4.1 VARIABLE-NUMBER-NODES BENDING ELEMENT

4.1 U.L. Formulation of Lagrangian Bending Element

The virtual work principle at time t+Δt, and its linearization is given in Table 1. Although in the table the general three-dimensional continuum formulation is presented, the stress matrices and stain-displacement transformation matrices in the evaluation of element stiffness matrix and force vector only corresponding to the three nonzero convected beam element stress components.

Geometry and Displacement Interpolation

In the derivation of the bending element below, we follow the work presented for continuum element [38], but use displacement and rotational degrees-of-freedom [42]. Considering a rectangular cross-section and the notation defined in Fig. 4.2 the geometry of the bending element at time t is interpolated using

$$ {}^{t}x_i = \sum_{k=1}^{N} h_k \, {}^{t}x_i^k + \frac{t}{2} \sum_{k=1}^{N} a_k h_k \, {}^{t}V_{ti}^k + \frac{s}{2} \sum_{k=1}^{N} b_k h_k \, {}^{t}V_{si}^k \qquad (4.1) $$

where

${}^{t}x_i$ = Cartesian coordinate of any point on the element at time t

$h_k(r)$ = Lagrangian isoparametric interpolation functions, defined in section 6.1.

${}^{t}x_i^k$ = Cartesian coordinate of nodal point k at time t

a_k = thickness of element in t-direction at nodal point k

b_k = thickness of element in s-direction at nodal point k

$^tV^k_{ti}$ = component i of unit vector in t-direction, $^t\underline{V}^k_t$ at nodal point k at time t

$^tV^k_{si}$ = component i of unit vector in s-direction, $^t\underline{V}^k_s$ at nodal point k at time t.

Also, in Eq. (4.1) the variable N is equal to the number of nodes used, which can be 2, 3 or 4 as shown in Fig. 4.1.

The displacement increments $u_i = {}^{t+\Delta t}x_i - {}^t x_i$ are evaluated using Eq. (4.1),

$$u_i = \sum_{k=1}^{N} h_k u_i^k + \frac{t}{2} \sum_{k=1}^{N} a_k h_k V_{ti}^k + \frac{s}{2} \sum_{k=1}^{N} b_k h_k V_{si}^k \qquad (4.2)$$

where

$$V_{ti}^k = {}^{t+\Delta t}V_{ti}^k - {}^tV_{ti}^k$$
$$V_{si}^k = {}^{t+\Delta t}V_{si}^k - {}^tV_{si}^k \qquad (4.3)$$

For the finite element solution we express the components V_{ti}^k and V_{si}^k in terms of rotation increments. To do so we use the unit vectors $^t\underline{V}^k_s$ and $^t\underline{V}^k_t$ corresponding to the configuration at time t which is known (the initial vectors $^0\underline{V}^k_t$ and $^0\underline{V}^k_s$ corresponding to the configuration at time 0 are defined and input to the analysis). Then we have approximately, for small incremental changes in $^t\underline{V}^k_t$ and $^t\underline{V}^k_s$,

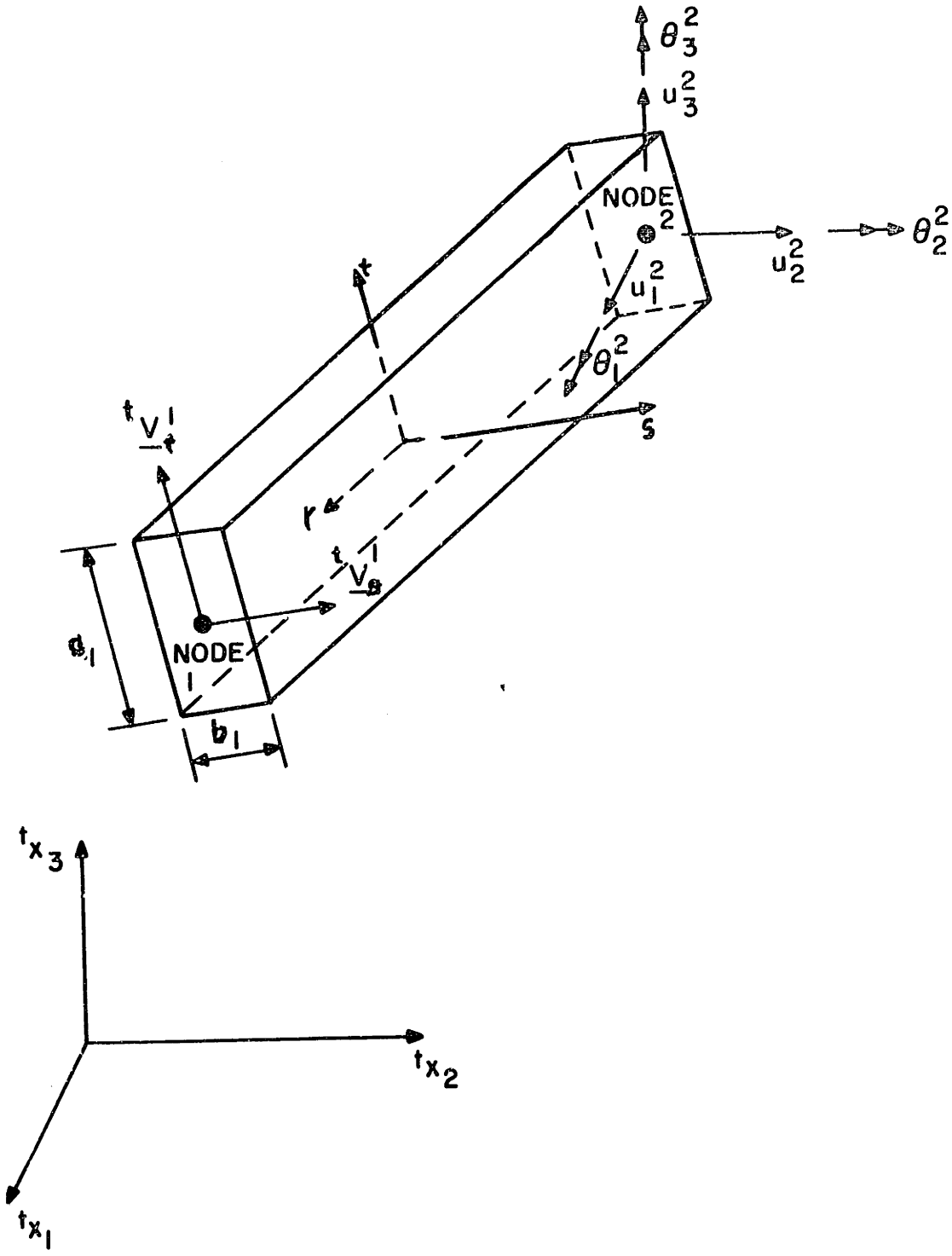

FIGURE 4.2 DEFINITION OF TWO-NODE BENDING ELEMENT

$$\underline{V}_{t}^{k} = \underline{\theta}^{k} \times {}^{t}\underline{V}_{t}^{k}$$

$$\underline{V}_{s}^{k} = \underline{\theta}^{k} \times {}^{t}\underline{V}_{s}^{k} \tag{4.4}$$

where $\underline{\theta}^{k}$ is a vector listing three small increments in rotations at node k about the ${}^{t}\underline{x}_{1}$, ${}^{t}\underline{x}_{2}$ and ${}^{t}\underline{x}_{3}$ axes, respectively.

Substituting from Eq. (4.4) into Eq. (4.2) the incremental displacements in the beam are obtained in terms of incremental nodal point displacements and rotations. The finite element solution gives these nodal point quantities, which can then be employed to evaluate the vectors ${}^{t+\Delta t}\underline{V}_{t}^{k}$ and ${}^{t+\Delta t}\underline{V}_{s}^{k}$ accurately,

$$ {}^{t+\Delta t}\underline{V}_{t}^{k} = {}^{t}\underline{V}_{t}^{k} + \int_{0}^{\underline{\theta}^{k}} d\underline{\theta}^{k} \times {}^{\tau}\underline{V}_{t}^{k}$$

$$ {}^{t+\Delta t}\underline{V}_{s}^{k} = {}^{t}\underline{V}_{t}^{k} + \int_{0}^{\underline{\theta}^{k}} d\underline{\theta}^{k} \times {}^{\tau}\underline{V}_{s}^{k} \tag{4.5}$$

If $\underline{\theta}^{k}$ is small the integrations can be carried out to sufficient accuracy using the Euler method, which corresponds to the assumption in Eq. (4.4).

Calculation of Element Matrices

Considering a single bending element, the linear strain-displacement transformation matrix, ${}^{t}_{t}\bar{B}_{NL}$, the nonlinear strain-displacement matric ${}^{t}_{t}\bar{B}_{NL}$, the stress matrix, ${}^{t}\bar{\tau}$ are required.

To evaluate the strain-displacement matrices we obtain from Eqs. (4.2) and (4.4)

$$\begin{bmatrix} u_{i,r} \\ u_{i,s} \\ \\ u_{i,t} \end{bmatrix} = \sum_{k=1}^{N} \begin{bmatrix} h_{k,r} & [1 & {}^{t}(g)^{k}_{1i} & {}^{t}(g)^{k}_{2i} & {}^{t}(g)^{k}_{3i}\ ] \\ h_{k} & [0 & {}^{t}(gs)^{k}_{1i} & {}^{t}(gs)^{k}_{2i} & {}^{t}(gs)^{k}_{3i}] \\ \\ h_{k} & [0 & {}^{t}(gt)^{k}_{1i} & {}^{t}(gt)^{k}_{2i} & {}^{t}(gt)^{k}_{3i}] \end{bmatrix} \begin{bmatrix} u^{k}_{i} \\ \theta^{k}_{1} \\ \theta^{k}_{2} \\ \theta^{k}_{3} \end{bmatrix} \tag{4.6}$$

where we use the notation

$${}^{t}(\underline{gs})^{k} = \frac{1}{2} b_{k} \begin{bmatrix} 0 & -{}^{t}V^{k}_{s3} & {}^{t}V^{k}_{s2} \\ {}^{t}V^{k}_{s3} & 0 & -{}^{t}V^{k}_{s1} \\ -{}^{t}V^{k}_{s2} & {}^{t}V^{k}_{s1} & 0 \end{bmatrix} \tag{4.7}$$

$${}^{t}(\underline{gt})^{k} = \frac{1}{2} a_{k} \begin{bmatrix} 0 & -{}^{t}V^{k}_{t3} & {}^{t}V^{k}_{t2} \\ {}^{t}V^{k}_{t3} & 0 & -{}^{t}V^{k}_{t1} \\ -{}^{t}V^{k}_{t2} & {}^{t}V^{k}_{t1} & 0 \end{bmatrix} \tag{4.8}$$

and

$${}^{t}(g)^{k}_{ij} = {}^{s}t(gs)^{k}_{ij} + {}^{t}t(gt)^{k}_{ij} \tag{4.9}$$

To obtain the displacement derivatives corresponding to the axes ${}^{t}x_i$, i=1,2,3 we employ the Jacobian transformation [33]

$$\frac{\partial}{\partial {}^{t}\underline{x}} = {}^{t}\underline{J}^{-1} \frac{\partial}{\partial \underline{r}} \tag{4.10}$$

where the Jacobian matrix, ${}^{t}\underline{J}$, contains the derivatives of the current coordinates ${}^{t}x_i$, i=1,2,3 with respect to the isoparametric coordinates r,s and t. Substituting from Eq. (4.6) into Eq. (4.10) we obtain

$$\begin{bmatrix} \frac{\partial u_i}{\partial {}^{t}x_1} \\ \frac{\partial u_i}{\partial {}^{t}x_2} \\ \frac{\partial u_i}{\partial {}^{t}x_3} \end{bmatrix} = \sum_{k=1}^{N} \begin{bmatrix} {}^{t}h_{k,1} & {}^{t}(G1)^{k}_{i1} & {}^{t}(G2)^{k}_{i1} & {}^{t}(G3)^{k}_{i1} \\ {}^{t}h_{k,2} & {}^{t}(G1)^{k}_{i2} & {}^{t}(G2)^{k}_{i2} & {}^{t}(G3)^{k}_{i2} \\ {}^{t}h_{k,3} & {}^{t}(G1)^{k}_{i3} & {}^{t}(G2)^{k}_{i3} & {}^{t}(G3)^{k}_{i3} \end{bmatrix} \begin{bmatrix} u^{k}_{i} \\ \theta^{k}_{1} \\ \theta^{k}_{2} \\ \theta^{k}_{3} \end{bmatrix} \tag{4.11}$$

where

$${}^{t}(Gm)^{k}_{in} = \left({}^{t}J^{-1}_{n1}\ {}^{t}(g)^{k}_{mi}\right) h_{k,r} + \left({}^{t}J^{-1}_{n2}\ {}^{t}(gs)^{k}_{mi} + {}^{t}J^{-1}_{n3}\ {}^{t}(gt)^{k}_{mi}\right) h_k \tag{4.12}$$

With the displacement derivatives defined in Eq. (4.11) we can now directly assemble the strain-displacement matrices ${}^{t}_{t}\underline{B}_{L}$ and ${}^{t}_{t}\underline{B}_{NL}$. Namely, Eq. (4.11) is employed to establish the global strain components (corresponding to the ${}^{t}x_i$, i = 1,2,3, axes) which are then employed to calculate using a second order tensor transformation the local strain

components ${}^t\bar{e}_{rr}$, ${}^t\bar{\gamma}_{rs}$ and ${}^t\bar{\gamma}_{st}$ corresponding to the r,s and t axes. Thus, we obtain

$$\begin{bmatrix} {}^t\bar{e}_{rr} \\ {}^t\bar{\gamma}_{rs} \\ {}^t\bar{\gamma}_{st} \end{bmatrix} = {}^t_{t}\bar{\underline{B}}_L \, \underline{u} \qquad (4.13)$$

The elements in ${}^t_{t}\bar{\underline{B}}_L$ are defined by the elements in Eq. (4.11) and the direction cosines of the r, s and t axes with respect to the global Cartesian axes ${}^t x_i$, i = 1,2,3. The elements in the nonlinear strain-displacement matrix ${}^t_{t}\bar{\underline{B}}_{NL}$ are defined analogously.

4.2 T.L. Formulation of Lagrangian Bending Element

The virtual work principle at time t+Δt and its linearization in the case of the total Lagrangian formulation is presented in Table 2. In this table the general three-dimensional continuum formulation is given, however, in the element implementation specialized such that the stress matrix and strain-displacement transformation matrices and force vector only correspond to the three non-zero stress components. The main difference to the U.L. formulation (see Table 1) is that in the T.L. formulation an initial displacement effect is present in the calculation of the linear strain-displacement transformation matrix. This initial displacement effect is taken into account using Eq. (4.1) at time t and time 0. Then, because ${}^t u_i = {}^t x_i - {}^0 x_i$, we have

$$ {}^{t}u_i = \sum_{k=1}^{N} h_k \, {}^{t}u_i^k + \frac{s}{2} \sum_{k=1}^{N} b_k h_k ({}^{t}V_{si}^k - {}^{0}V_{si}^k) + \frac{t}{2} \sum_{k=1}^{N} a_k h_k ({}^{t}V_{ti}^k - {}^{0}V_{ti}^k) \tag{4.14} $$

and using Eqs. (4.10) and (4.14) corresponding to the coordinates ${}^{0}x_i$, i=1,2,3 we obtain

$$ \begin{aligned} \frac{\partial {}^{t}u_i}{\partial {}^{0}x_j} = & \sum_{k=1}^{N} {}^{0}J_{j1}^{-1} h_{k,r} \left({}^{t}u_i^k + \frac{s}{2} b_k ({}^{t}V_{si}^k - {}^{0}V_{si}^k) + \frac{t}{2} a_k ({}^{t}V_{ti}^k - {}^{0}V_{ti}^k) \right) \\ & + \frac{1}{2} \sum_{k=1}^{N} {}^{0}J_{j2}^{-1} b_k h_k ({}^{t}V_{si}^k - {}^{0}V_{si}^k) \\ & + \frac{1}{2} \sum_{k=1}^{N} {}^{0}J_{j3}^{-1} a_k h_k ({}^{t}V_{ti}^k - {}^{0}V_{ti}^k) \end{aligned} \tag{4.15} $$

The strain-displacement transformation matrices ${}^{t}_{0}B_L$ and ${}^{t}_{t}B_{NL}$ can now be obtained using Eq. (4.11) corresponding to the coordinates ${}^{0}x_i$, i=1,2,3 and Eq. (4.15). The details of the evaluation are as in the U.L. formulation.

4.3 Comparison of Hermitian Beam and Lagrangian Bending Element

Comparing the straight beam element formulation given in the previous chapter, and the displacement /rotation , isoparametric bending element formulation presented in this chapter the following differences are identified;

(a) The geometry of the straight beam element is assumed to always

remain straight. In the Lagrangian bending element, however, the curved geometry of the original or deformed structure can be modeled with a higher order of accuracy because more nodes are used along the element. Also, it should be noted that the geometry of the element is interpolated to the same order as displacements, Eqs. (4.1), (4.2).

This difference in geometry interpolation and representation is very important for modelling of curved structures (especially when it is expanded for shell analyses).

(b) In the formulations of the straight beam element Hermitian interpolation polynomials, referred to the beam convected coordinate axes, were employed. A specific difficulty of this approach lies in determining the relative contributions of nodal displacements, and/or angles to the bending and/or axial displacements. This establishes the interpolation directionality which requires extra transformations as shown in Eq. (3.3). The above difficulty is not present in the displacement/rotation isoparametric formulation with Lagrangian interpolation functions, as was demonstrated in the bending element formulation.

(c) The other advantage of the Lagrangian bending element is that the displacements and rotations are interpolated independently using the same functions. As the rotations are assumed to be independent variables, the shear deformation energy is approximately included in the formulation. In comparison, the inclusion of shear de-

formation effects requires special attention for straight beams with Hermitian polynomial interpolation.

The above differences indicate that the use of isoparametric displacement/rotation elements with Lagrangian interpolation functions is the more effective approach to expand for the analysis of two-dimensional bending structures, especially for shell structures where the accurate definition of the geometry is of importance.

5. FORMULATIONS OF THE NONLINEAR GENERAL SHELL ELEMENT

In Section 4.3, we showed the advantages of employing independent nodal point rotation and displacement degrees of freedom. We also pointed out the importance of interpolating the geometry and the displacements and rotations using the same function. This, in effect, is the displacement/rotation isoparametric element formulation.

In the formulations of the displacement/rotation isoparametric shell elements no specific shell theory is assumed. This is in contrast to the classical approach of formulating shell elements. The geometry and displacement field of the structure are discretized and interpolated as in the analysis of continuum problems [32]. The other advantage of the displacement/rotation isoparametric shell element is its generality which is analogous to the well known isoparametric two- and three-dimensional continuum elements [4].

The objective in this chapter is to present the formulations of a general 3 to 32 variable-number-nodes displacement/rotation isoparametric element for geometric and material nonlinear analysis of general shells, Figs. 5.1 to 5.3. The interpolation functions are presented in the next chapter. The element can have nodes on the middle surface only, or have nodes on the top and bottom surfaces and mid-surface, or on the top and bottom surfaces, see Figs. 5.1 to 5.3. The first elements are used for modelling thin shell structures, and elements with nodes on top, bottom and middle surfaces are employed for the transition regions between

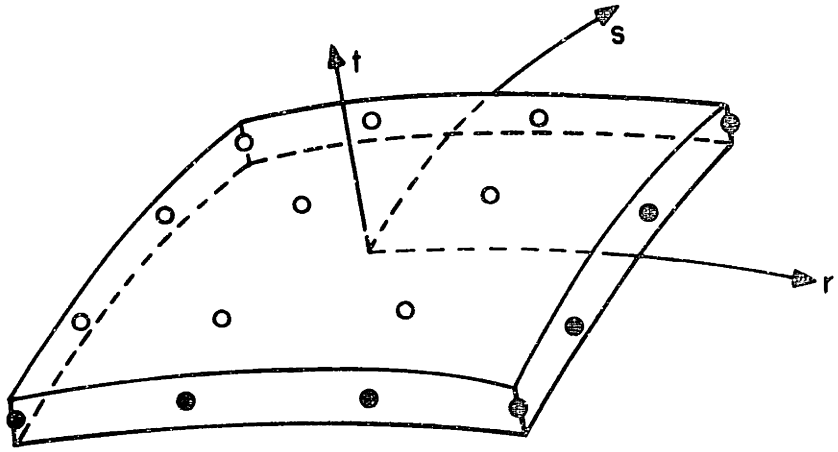

16-NODE CUBIC LAGRANGIAN ELEMENT
(ALL NODES ARE ON THE SHELL MID-SURFACE)

SOME DERIVED ELEMENTS:

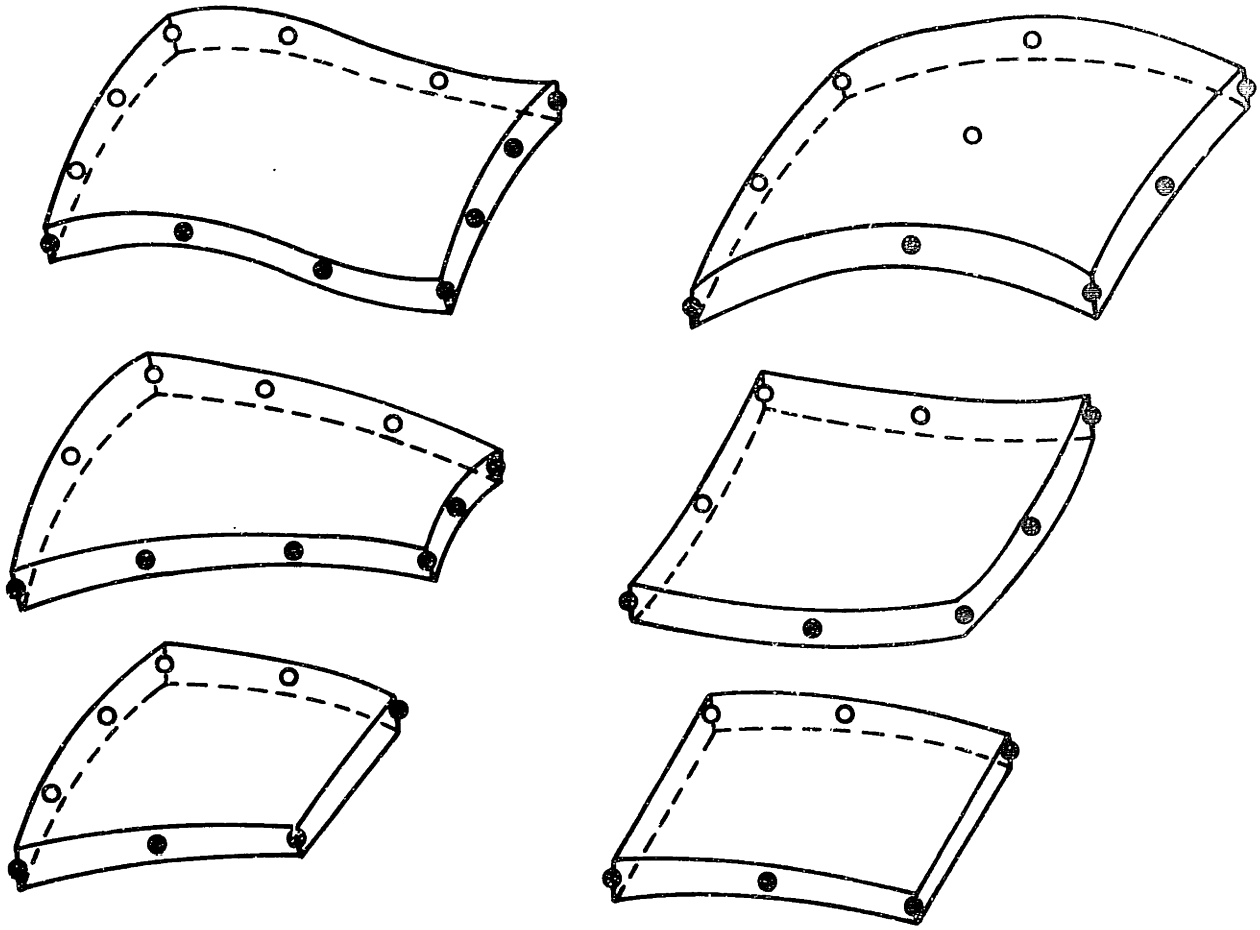

FIGURE 5.1 VARIABLE-NUMBER-NODES QUADRILATERAL SHELL ELEMENTS

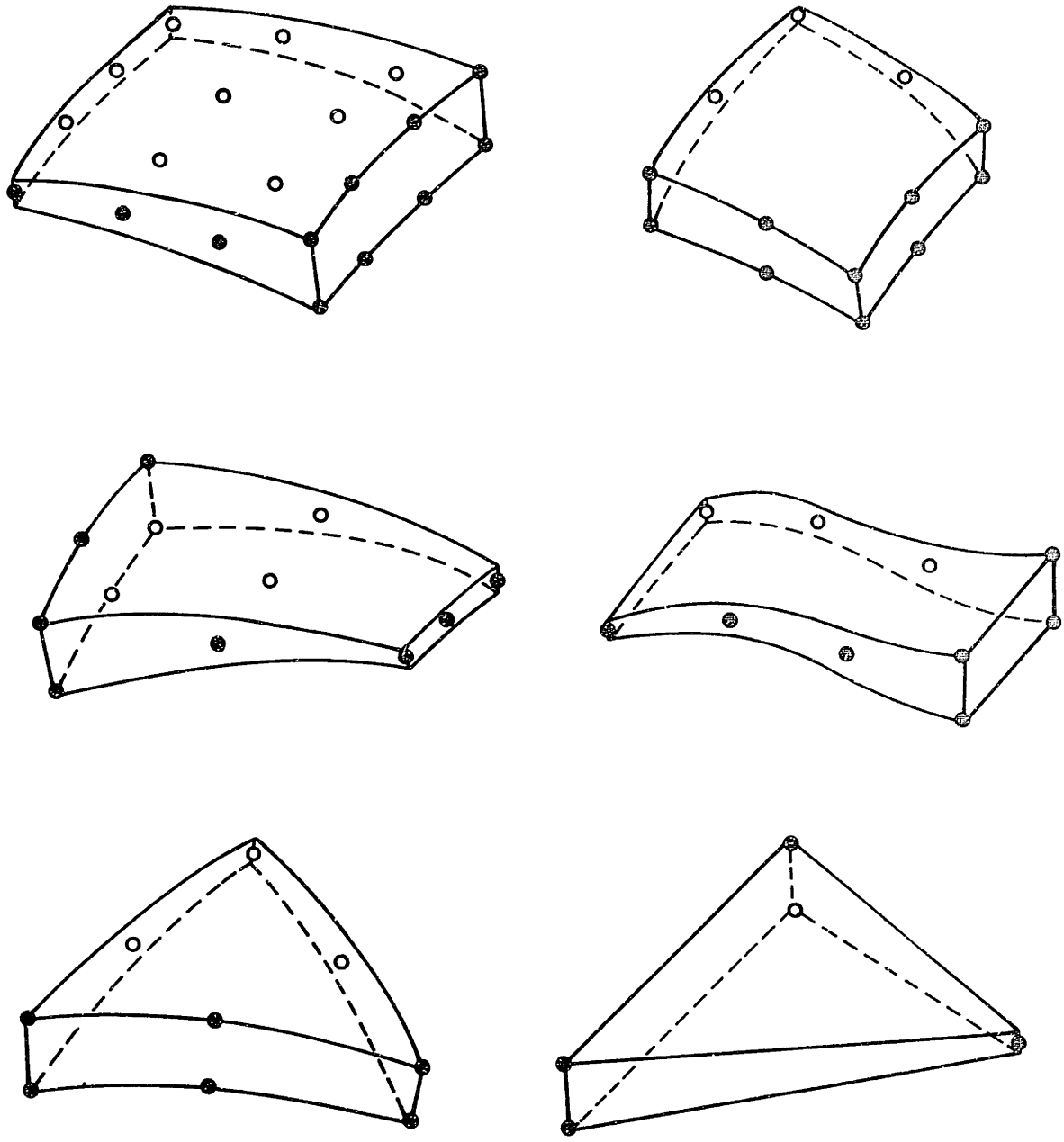

FIGURE 5.3 SOME DERIVED ELEMENTS OF VARIABLE-NUMBER-NODES TRANSITION ELEMENTS

the thin shell section and sections of the structure modelled by continuum elements. The importance of each of the above elements are discussed in the next two chapters. Any top-or bottom-surface node has, in general, three displacement degrees-of-freedom. A mid-surface node, in general, has five degrees of freedom, three displacements and two rotations, see Fig. 5.4.

The following constraints, corresponding to some of the usual shell theory assumptions, are introduced in formulating the element: (a) the strain energy corresponding to the stresses along the normal to the mid-surface is ignored by modifying the three-dimensional material law, and (b) the normal to the shell mid-surface remains straight (not necessarily normal) and does not extend during deformation.

5.1 U.L. Formulation of the Shell Element

The virtual work principle expressing the equilibrium and compatibility requirement of the body at time $t+\Delta t$, in the U.L. formulation, is given in Eq. (2.11). This equation represents a nonlinear expression in the unknown static and kinematic variables of the body at time $t+\Delta t$. Using our usual notation, Table 1 summarizes the linearization and solution of Eq. (2.11) by the modified Newton-Raphson iteration.

Geometry and Displacement Interpolations

In the derivation of an effective shell element, based on the U.L. formulation in Table 1, the displacements and rotational degrees-of-freedom are used. Referring to Fig. 5.4, the geometry of the variable-number-nodes shell element at time t is interpolated using

$$ {}^{t}x_i = \sum_{k=1}^{N} h_k \, {}^{t}x_i^k + \frac{t}{2} \sum_{k=1}^{N} n_k a_k h_k \, {}^{t}V_{ni}^k \qquad (5.1) $$

where

${}^{t}x_i$ = Cartesian coordinate of any point on the shell at time t.

h_k = isoparametric interpolation functions, see Chapter 6.
h_k is a function of r and s only if k is a mid-surface node Figs. 5.1, 5.2 and,
h_k is a function of r, s and a linear function of t if k is a top-or bottom-surface node, Fig. 5.3

${}^{t}x_i^k$ = Cartesian coordinate of nodal point k at time t

$$ n_k = \begin{cases} 0 \text{ if node k is a top-or bottom-surface node} \\ 1 \text{ if node k is a mid-surface node} \end{cases} $$

a_k = thickness of shell (in t direction) at nodal point k

${}^{t}V_{ni}^k$ = component i of unit normal vector, ${}^{t}\underline{V}_n^k$, to the surface of the shell at nodal point k and time t.

Also in Eq. (5.1), the isoparametric element coordinates are r,s and t, and N is the number of nodes of the element.

To obtain an expression for u_i, we use

$$ u_i = {}^{t+\Delta t}x_i - {}^{t}x_i \qquad (5.2) $$

and substitute from Eq. (5.1),

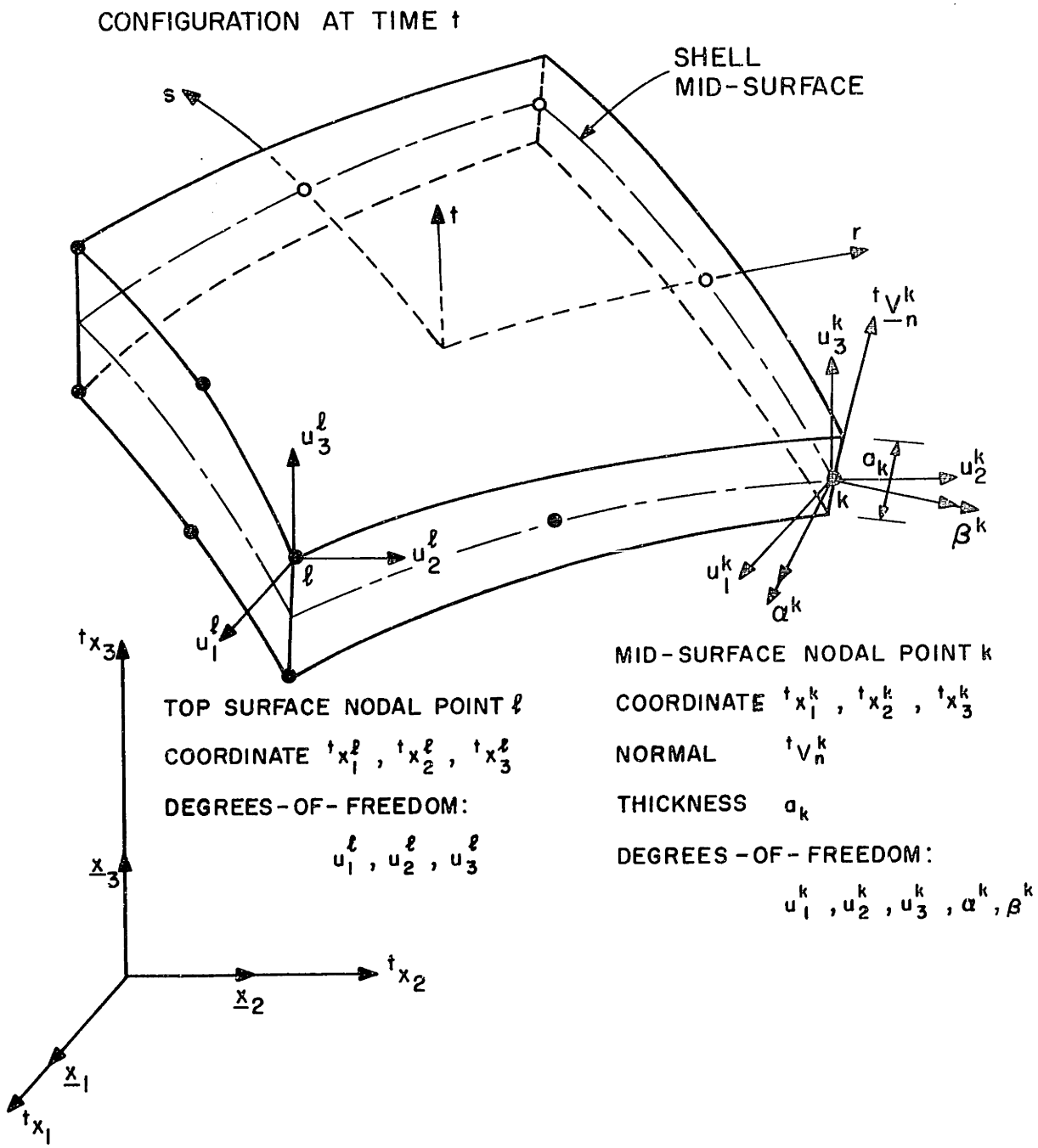

FIGURE 5.4 DEFINITION OF A GENERAL SHELL ELEMENT

$$u_i = \sum_{k=1}^{N} h_k u_i^k + \frac{t}{2} \sum_{k=1}^{N} n_k a_k h_k V_{ni}^k \qquad (5.3)$$

where

$$V_{ni}^k = {}^{t+\Delta t}V_{ni}^k - {}^{t}V_{ni}^k \qquad (5.4)$$

It should be noted that the calculation of increments in the normal vector, $\underline{V}_n^k$, or new normal directions are only performed at mid-surface nodes. For the finite element solution we express the components V_{ni}^k in terms of rotations. To do so we use the vector ${}^{t}\underline{V}_n^k$ corresponding to the configuration at time t which is known. The vector ${}^{t}\underline{V}_n^k$ does not pertain to an element but to mid-surface nodal point k. Thus, all shell elements meeting at mid-surface nodal point k have this same vector as mid-surface normal as illustrated in Fig. 5.5 (for modeling of intersecting shells see Chapter 7). Also, to start the solution, ${}^{0}\underline{V}_n^k$ corresponding to the initial configuration is defined prior to the incremental analysis.

To express the components V_{ni}^k in terms of rotation angles, we first define two unit vectors ${}^{t}\underline{V}_1^k$ and ${}^{t}\underline{V}_2^k$ that are orthogonal to ${}^{t}\underline{V}_n^k$ (see Fig. 5.6).

$${}^{t}\underline{V}_1^k = (\underline{x}_2 \times {}^{t}\underline{V}_n^k)/(\underline{x}_2^T \, {}^{t}\underline{V}_n^k) \qquad (5.5)$$

where we set ${}^{t}\underline{V}_1^k$ equal to $\underline{x}_3$ if ${}^{t}\underline{V}_n^k$ is parallel to $\underline{x}_2$, and

$${}^{t}\underline{V}_2^k = {}^{t}\underline{V}_n^k \times {}^{t}\underline{V}_1^k \qquad (5.6)$$

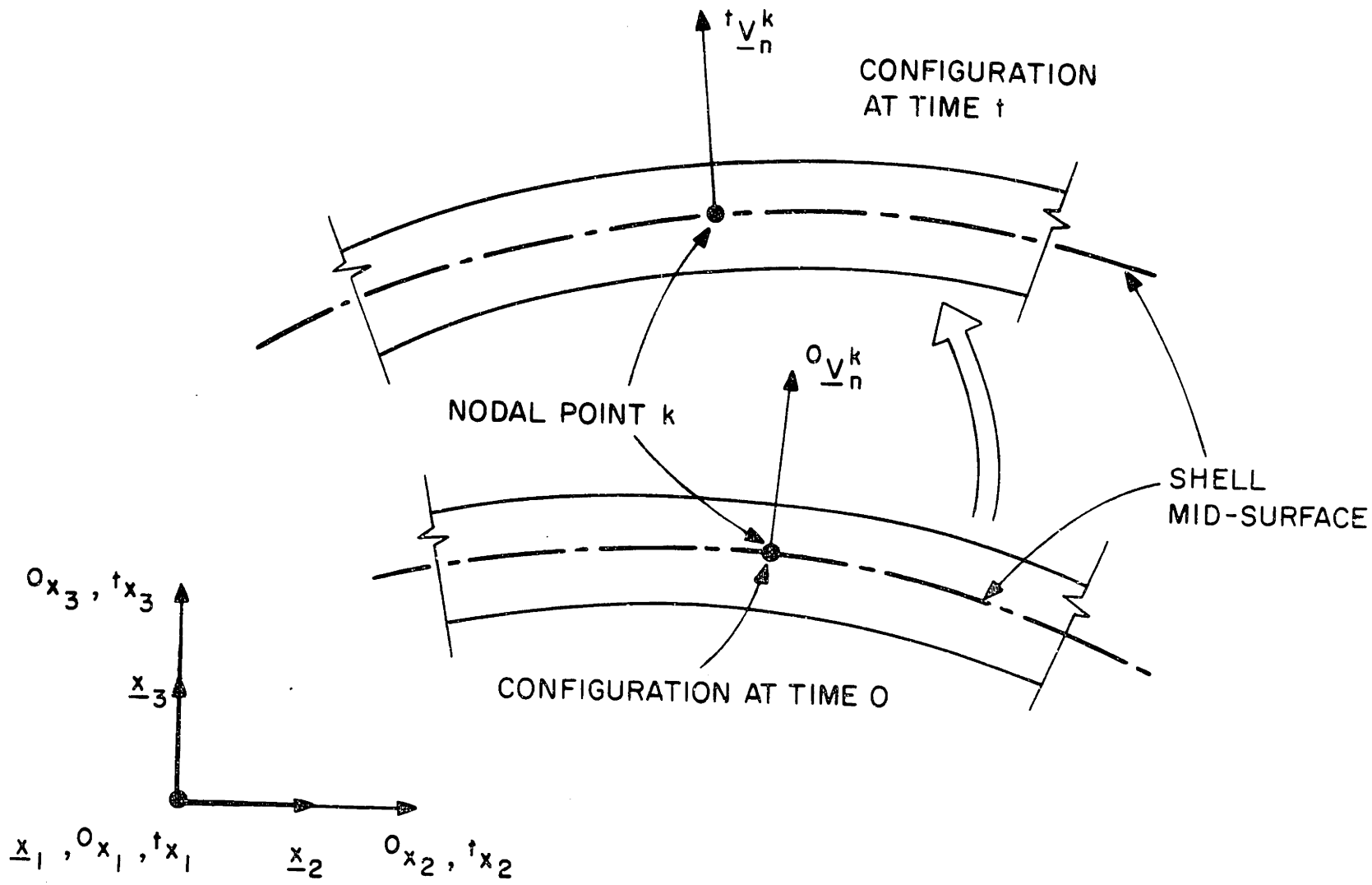

FIGURE 5.5 NORMAL TO SHELL MID-SURFACE

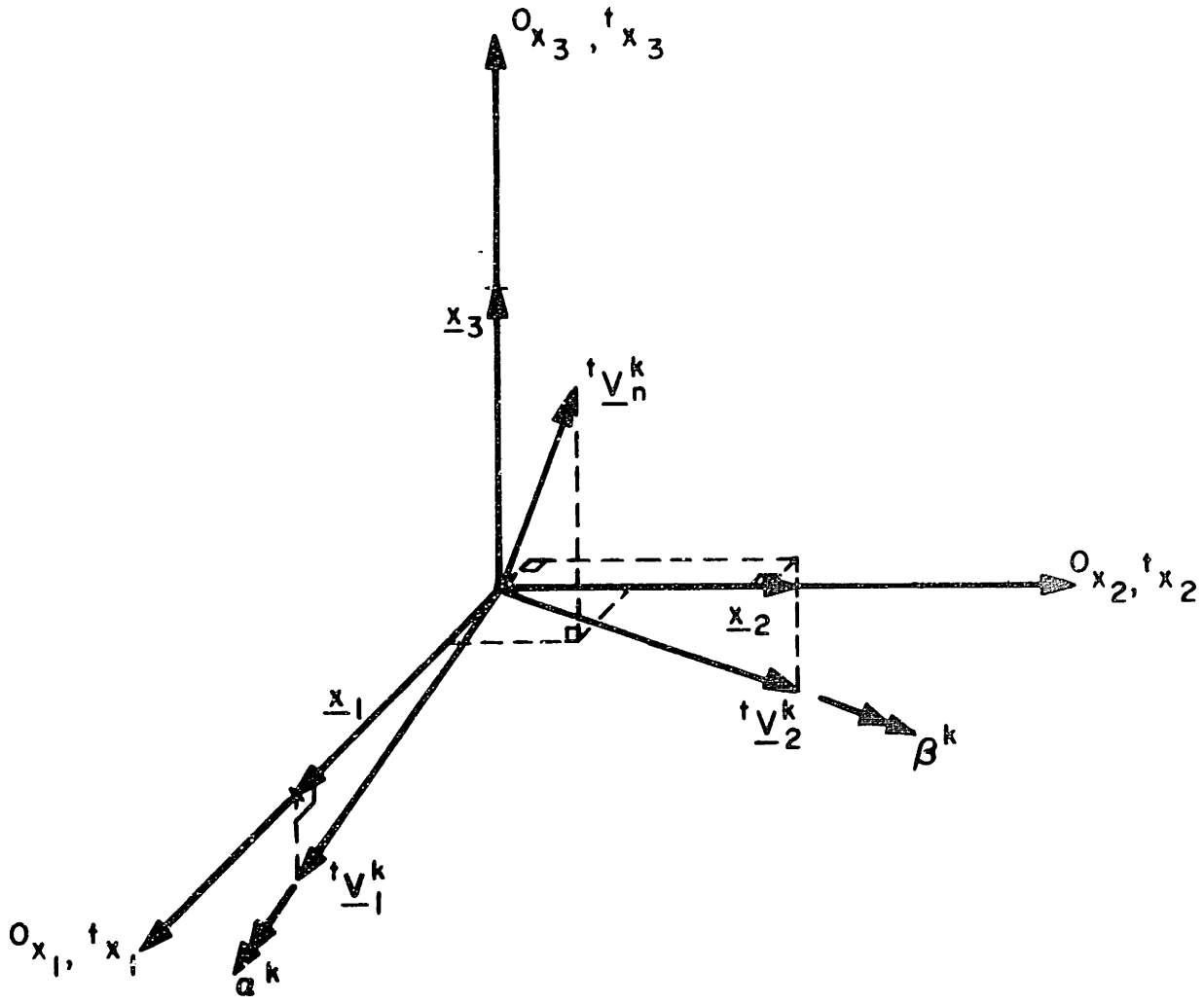

FIGURE 5.6 DEFINITION OF VECTORS AT NODAL POINT k

Let α^k and β^k be the rotations of the normal vector about the vectors ${}^t\underline{V}_1^k$ and ${}^t\underline{V}_2^k$ from the configuration at time t to the configuration at time t+Δt, then approximately (for small incremental angles α^k and β^k)

$$\underline{V}_n^k = - {}^t\underline{V}_2^k \alpha^k + {}^t\underline{V}_1^k \beta^k \tag{5.7}$$

Substituting from Eq. (5.7) into Eq. (5.3) we thus obtain the incremental internal element displacements in terms of the nodal point incremental displacements and rotations

$$u_i = \sum_{k=1}^{N} h_k u_i^k + \frac{t}{2} \sum_{k=1}^{N} n_k a_k h_k [{}^t\underline{V}_{2i}^k \alpha^k + {}^tV_{1i}^k \beta^k] \tag{5.8}$$

The finite element solution will yield the nodal point variables u_i^k if node k is a top-or bottom-surface node, or u_i^k, α^k and β^k if node k is a mid-surface node. The displacements and rotation of mid-surface nodes can then be employed to evaluate accurately ${}^{t+\Delta t}\underline{V}_n^k$,

$${}^{t+\Delta t}\underline{V}_n^k = {}^t\underline{V}_n^k + \int_{\alpha^k,\beta^k} -{}^\tau\underline{V}_2^k \, d\alpha^k + {}^\tau\underline{V}_1^k \, d\beta^k \tag{5.9}$$

If α^k and β^k are small, the integration in Eq. (5.9) can be carried out to sufficient accuracy using the Euler method [33],

$${}^{t+\Delta t}\underline{V}_n^k = {}^t\underline{V}_n^k - {}^t\underline{V}_2^k \alpha^k + {}^t\underline{V}_1^k \beta^k \tag{5.10}$$

which corresponds to the assumption employed in Eq. (5.7).

Calculation of Element Matrices

Considering a single shell element, as summarized in Table 1 and 3, the linear strain-displacement transformation matrix, ${}^{t}_{t}B_{L}$, the stress matrix, ${}^{t}\underline{\tau}$, and the stress vector, ${}^{t}\hat{\tau}$, are required.

To evaluate the strain-displacement matrices we obtain from Eq. (5.8)

$$\begin{bmatrix} u_{i,r} \\ u_{i,s} \\ u_{i,t} \end{bmatrix} = \sum_{k=1}^{N} \begin{bmatrix} h_{k,r}\,[1 & {}^{t}g^{k}_{1i} & {}^{t}g^{k}_{2i}] \\ h_{k,s}\,[1 & {}^{t}g^{k}_{1i} & {}^{t}g^{k}_{2i}] \\ h_{k,t} & h_{k}\,{}^{t}g^{k}_{1i} & h_{k}\,{}^{t}g^{k}_{2i} \end{bmatrix} \begin{bmatrix} u^{k}_{i} \\ \alpha^{k} \\ \beta^{k} \end{bmatrix} \tag{5.11}$$

where we use the notation

$$\begin{aligned} {}^{t}g^{k}_{1i} &= -\frac{1}{2}\, n_k a_k\, {}^{t}V^{k}_{2i} \\ {}^{t}g^{k}_{2i} &= \frac{1}{2}\, n_k a_k\, {}^{t}V^{k}_{1i} \end{aligned} \tag{5.12}$$

To obtain the displacement derivatives corresponding to the axes ${}^{t}x_{i}$, i=1,2,3, we now employ the inverse Jacobian transformation ${}^{t}\underline{J}^{-1}$,

$$\frac{\partial}{\partial\, {}^{t}\underline{x}} = {}^{t}\underline{J}^{-1}\, \frac{\partial}{\partial \underline{r}} \tag{5.13}$$

where the Jacobian matrix, ${}^{t}\underline{J}$, contains the derivatives of the current coordinates ${}^{t}x_i$, i=1,2,3 of Eq. (5.1) with respect to the isoparametric coordinates r,s and t,

$$ {}^{t}\underline{J} = \begin{bmatrix} {}^{t}x_{1,r} & {}^{t}x_{2,r} & {}^{t}x_{3,r} \\ {}^{t}x_{1,s} & {}^{t}x_{2,s} & {}^{t}x_{3,s} \\ {}^{t}x_{1,t} & {}^{t}x_{2,t} & {}^{t}x_{3,t} \end{bmatrix} \tag{5.14} $$

Substituting from Eq. (5.11) into Eq. (5.13) we obtain

$$ \begin{bmatrix} \frac{\partial u_i}{\partial {}^{t}x_1} \\ \frac{\partial u_i}{\partial {}^{t}x_2} \\ \frac{\partial u_i}{\partial {}^{t}x_3} \end{bmatrix} = \sum_{k=1}^{N} \begin{bmatrix} {}^{t}h_{k,1} & {}^{t}g_{1i}^{k}\ {}^{t}G_1^k & {}^{t}g_{2i}^{k}\ {}^{t}G_1^k \\ {}^{t}h_{k,2} & {}^{t}g_{1i}^{k}\ {}^{t}G_2^k & {}^{t}g_{2i}^{k}\ {}^{t}G_2^k \\ {}^{t}h_{k,3} & {}^{t}g_{1i}^{k}\ {}^{t}G_3^k & {}^{t}g_{2i}^{k}\ {}^{t}G_3^k \end{bmatrix} \begin{bmatrix} u_i^k \\ \alpha^k \\ \beta^k \end{bmatrix} \tag{5.15} $$

where

$$ \begin{aligned} {}^{t}h_{k,i} &= {}^{t}J_{i1}^{-1}\ h_{k,r} + {}^{t}J_{i2}^{-1}\ h_{k,s} + {}^{t}J_{i3}^{-1}\ h_{k,t} \\ {}^{t}G_i^k &= t({}^{t}J_{i1}^{-1}\ h_{k,r} + {}^{t}J_{i2}^{-1}\ h_{k,s}) + {}^{t}J_{i3}^{-1}\ h_k \end{aligned} \tag{5.16} $$

and ${}^{t}J^{-1}_{ij}$ is the element (i,j) of the matrix ${}^{t}\underline{J}^{-1}$ in Eq. (5.13).

With the displacement derivatives defined in Eq. (5.15) we can now directly assemble the strain-displacement matrices ${}^{t}_{t}\underline{B}_{L}$ and ${}^{t}_{t}\underline{B}_{NL}$. Table 5 gives these matrices and defines also the corresponding stress matrix ${}^{t}\underline{\tau}$ and stress vector ${}^{t}\underline{\hat{\tau}}$.

5.2 T.L. Formulation of the Shell Element

In the T.L. formulation, the virtual work principle expressing the equilibrium and compatibility requirement of the body at time $t+\Delta t$ is given by Eq. (2.13). This equation represents a nonlinear equation in the unknown static and kinematic variables of the body. Using our usual notation, Table 2 summarizes the linearization and solution of Eq. (2.13) by the modified Newton-Raphson iteration.

Geometry and Displacement Interpolations

In the T.L. formulation of a shell element, not only the geometry and displacement increments are required to be interpolated, but also we need to interpolate the total displacements, see Tables 2 and 6.

The geometry at time t, and the displacement increments of the variable-number-nodes shell element are interpolated using Eq. (5.1) and Eq. (5.3), respectively. The evaluation of the normal vector increments and calculation of the normal vectors at time $t+\Delta t$ are as given in the updated Lagrangian formulation presented in the previous section.

The initial displacement effect (which is present in the calcu-

lation of the linear strain-displacement transformation matrix) is taken into account using Eq. (5.1) at time t and 0. Then because ${}^{t}u_i = {}^{t}x_i - {}^{0}x_i$, we have

$$ {}^{t}u_i = \sum_{k=1}^{N} h_k \, {}^{t}u_i^k + \frac{t}{2} \sum_{k=1}^{N} n_k a_k h_k \left({}^{t}V_{ni}^k - {}^{0}V_{ni}^k \right) \tag{5.17} $$

Calculation of Element Matrices

Consider a single shell element, as summarized in Tables 2 and 3, the linear and nonlinear strain-displacement transformation matrices, ${}^{t}_{0}\underline{B}_L$ and ${}^{t}_{0}\underline{B}_{NL}$, and the stress matrix, ${}^{t}_{0}\underline{S}$, and stress vector, ${}^{t}_{0}\hat{\underline{S}}$, are required.

To obtain the derivates with respect to the axes ${}^{0}x_i$, i=1,2,3, we employ the inverse Jacobian transformation ${}^{0}\underline{J}^{-1}$,

$$ \frac{\partial}{\partial {}^{0}\underline{x}} = {}^{0}\underline{J}^{-1} \frac{\partial}{\partial \underline{r}} \tag{5.18} $$

where the Jacobian matrix, ${}^{0}\underline{J}$, is defined:

$$ {}^{0}\underline{J} = \begin{bmatrix} {}^{0}x_{1,r} & {}^{0}x_{2,r} & {}^{0}x_{3,r} \\ {}^{0}x_{1,s} & {}^{0}x_{2,s} & {}^{0}x_{3,s} \\ {}^{0}x_{1,t} & {}^{0}x_{2,t} & {}^{0}x_{3,t} \end{bmatrix} \tag{5.19} $$

Substituting from Eq. (5.11) into Eq. (5.18) we obtain

$$\begin{bmatrix} \frac{\partial u_i}{\partial {}^0x_1} \\ \frac{\partial u_i}{\partial {}^0x_2} \\ \frac{\partial u_i}{\partial {}^0x_3} \end{bmatrix} = \sum_{k=1}^{N} \begin{bmatrix} {}^0h_{k,1} & {}^t g_{1i}^k \, {}^0G_1^k & {}^t g_{2i}^k \, {}^0G_1^k \\ {}^0h_{k,2} & {}^t g_{1i}^k \, {}^0G_2^k & {}^t g_{2i}^k \, {}^0G_2^k \\ {}^0h_{k,3} & {}^t g_{1i}^k \, {}^0G_3^k & {}^t g_{2i}^k \, {}^0G_3^k \end{bmatrix} \begin{bmatrix} u_i^k \\ \alpha^k \\ \beta^k \end{bmatrix} \tag{5.20}$$

where

$$\begin{aligned} {}^0h_{k,i} &= {}^0J_{i1}^{-1} \, h_{k,r} + {}^0J_{i2}^{-1} \, h_{k,s} + {}^0J_{i3}^{-1} \, h_{k,t} \\ {}^0G_i^k &= t({}^0J_{i1}^{-1} \, h_{k,r} + {}^0J_{i2}^{-1} \, h_{k,s}) + {}^0J_{i3}^{-1} \, h_k \end{aligned} \tag{5.21}$$

and ${}^0J_{ij}^{-1}$ is the element (i,j) of ${}^0\underline{J}^{-1}$ in Eq. (5.16).

Using Eqs. (5.17), (5.18) and (5.21), the derivatives of the initial displacements corresponding to the coordinates ${}^0x_i$, i=1,2,3 are obtained:

$$\frac{\partial {}^t u_i}{\partial {}^0x_j} = \sum_{k=1}^{N} {}^0h_{k,j} \, {}^t u_i^k + \frac{1}{2} \sum_{k=1}^{N} n_k a_k \left({}^t {}^0h_{k,j} + {}^0J_{j3}^{-1} \, h_k \right) ({}^t V_{ni}^k - {}^0V_{ni}^k) \tag{5.22}$$

With the displacement derivatives in Eqn. (5.20) and initial displacement derivatives in Eq. (5.22) we can directly assemble the strain

displacement matrices, ${}^{t}_{0}\underline{B}_{L}$ and ${}^{t}_{0}\underline{B}_{NL}$. Table 6 gives these matrices and defines also the corresponding stress matrix ${}^{t}_{0}\underline{S}$ and stress vector ${}^{t}_{0}\underline{\hat{S}}$.

5.3 Constitutive Relations

In the previous sections we assumed that appropriate constitutive relations are used, Tables 1 and 2. The constitutive tensor, in the U.L. formulation relates Cauchy stresses and Almansi strains, and in the T.L. formulation relates 2nd Piola-Kirchhoff stresses to Green-Lagrange strains.

We should note that in the formulations given so far all the six stress and strain components in the Cartesian coordinate directions are calculated, and the constitutive tensor corresponding to these components is used in Tables 1, 2 and 3. To obtain this tensor constrained by the shell assumption that the stress normal to the shell is zero, we use the usual three-dimensional constitutive relations corresponding to the local orthogonal directions Fig. 5.7, impose the condition that the normal stress in t-direction) is negligible and then transform the modified constitutive relations to correspond to the global Cartesian coordinate axes.

Linear Elastic Material Model

Young's moduli, E, and Poisson's ratio, ν, are employed to define the usual three-dimensional isotropic constitutive tensor [33]. The constraint of zero stress along the normal to the mid-surface is satisfied by

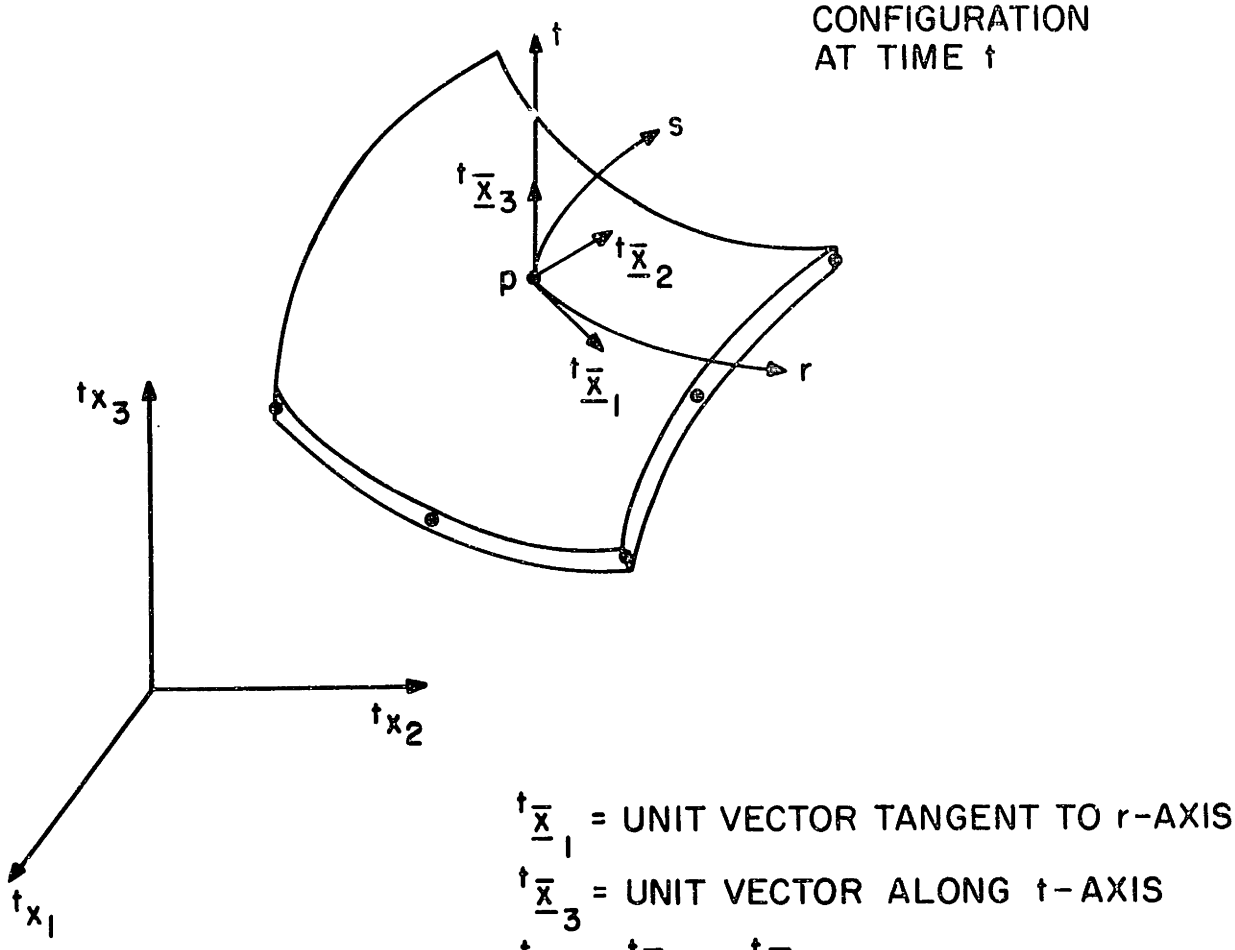

FIGURE 5.7 DEFINITION OF THE SHELL ELEMENT ORTHOGONAL LOCAL COORDINATE AXES

statically condensing out the appropriate row and column of the constitutive tensor. This leads to an anisotropic constitutive relation, in the linear analysis, and in the T.L. formulation,

$$
{}^{t}_{0}\underline{\bar{C}} = \frac{E}{1-\nu^2}
\begin{bmatrix}
1 & \nu & 0 & 0 & 0 & 0 \\
 & 1 & 0 & 0 & 0 & 0 \\
 & & 0 & 0 & 0 & 0 \\
 & & & \frac{1-\nu}{2} & 0 & 0 \\
 & \text{Symmetric} & & & \frac{1-\nu}{2} & 0 \\
 & & & & & \frac{1-\nu}{2}
\end{bmatrix}
\tag{5.23}
$$

The anisotropic constitutive tensor, measured in the ${}^{t}\bar{x}_i$ coordinate system at time t, employed in the U.L. formulation ${}^{t}_{t}\underline{\bar{C}}$, is numerically identical to ${}^{t}_{0}\underline{\bar{C}}$ of Eq. (5.23).

The above constitutive tensors are transformed to global coordinate systems using;

$$
{}^{t}_{\tau}\underline{\bar{C}} = {}^{\tau}\underline{\tilde{Q}}^{T}\ {}^{t}_{\tau}\underline{\bar{C}}\ {}^{\tau}\underline{\tilde{Q}} \qquad (\tau = 0,t) \tag{5.24}
$$

$$
{}^{\tau}\underline{\tilde{Q}} = {}^{\tau}\underline{Q}\ {}^{\tau}\underline{Q} \qquad (\tau = 0,t) \tag{5.25}
$$

where the elements of the matric ${}^{\tau}\underline{Q}$, $\tau = 0,(t)$ are the direction cosines of the orthogonal local axes ${}^{\tau}\bar{x}_i$ with respect to the fixed global axes,

in linear or T.L. (U.L.) formulation. The direction cosines of the unit vectors ${}^{0}\bar{x}_1$ and ${}^{0}\bar{x}_3$ are obtained from the normalized values of the Jacobian matrix ${}^{0}\underline{J}$, Eq. (5.19), i.e.; ${}^{0}\bar{x}_1$ and ${}^{0}\bar{x}_3$ are along the natural coordinate r and t axes at time 0 respectively. The third unit vector is calculated as ${}^{0}\underline{\bar{x}}_2 = {}^{0}\underline{\bar{x}}_3 \times {}^{0}\underline{\bar{x}}_1$, Fig. 5.7. The directions of the unit ${}^{t}\underline{\bar{x}}_1$ (used in U.L. formulation) are obtained similarly by employing Eq. (5.14). It should be noted that the advantage of employing the local orthogonal axes ${}^{\tau}\bar{x}_i$ as a reference system rather than natural coordinates r,s,t is especially seen when triangular or distorted quadrilateral shell elements are formulated where the axes r and s are non-orthogonal. It should also be mentioned that change of density is ignored in Eq. (5.24) because of the small strain assumption.

The constitutive relations in Eq. (5.24) are used in the evaluation of the element stress matrices and stress vectors, i.e., we calculate from total Green-Lagrange or Almansi strains directly the total 2nd Piola-Kirchhoff or Cauchy stresses, respectively. However, in the calculation of the linear strain stiffness matrices at time t, we need the following tangent material property tensors

$$ {}^{0}C_{ijrs} = {}^{t}_{0}C_{ijrs} \; ; \; {}^{t}C_{ijrs} = {}^{t}_{t}C_{ijrs} \tag{5.26} $$

Considering the elastic stress-strain relations, we note that in the analysis the material constants are independent of the history of solution, thus no error due to constitutive evaluation is introduced in the analysis.

Elastic-Plastic Material Model

In this section we present, for completeness, the derivation of the isothermal elastic-plastic incremental constitutive relations used in infinitesimal displacement analysis [35] (materially nonlinear only conditions). The model is also employed in large rotation small strain analysis using the T.L. formulation by employing the incremental 2nd Piola-Kirchhoff stress and Green-Lagrange strain measures. It should be noted that the three-dimensional continuum constitutive relation is first derived to relate the stress and strain increments, which are measured in the shell element local orthogonal coordinate ${}^{0}\bar{x}_i$, Fig. 5.7.

For elastic-plastic analysis, in addition to the elastic constitutive relations the following basic ingredients are used: (1) a yield function; (2) a flow rule, which relates the plastic strain increments to the current stresses and the increments of stresses subsequent to yielding; and (3) a hardening rule.

The initial and subsequent isothermal yield condition can be written as:

$$ {}^{t}F \left({}^{t}\underline{\bar{e}}^{P} , {}^{t}\underline{\bar{\sigma}} \right) = 0 \quad , \tag{5.27} $$

where ${}^{t}\underline{\bar{e}}^{P}$ = total plastic strain vector at time t, and ${}^{t}\underline{\bar{\sigma}}$ = effective stress vector at time t. It should be noted again that a bar (-) on a variable means that it is measured in the local coordinate system. The local orthogonal coordinate systems are ${}^{0}\bar{x}_{i}$, Fig. 5.7.

Since during plastic deformation $d^{t}F = 0$, we have

$$ d^{t}F = \frac{\partial {}^{t}F}{\partial {}^{t}\bar{\sigma}_{ij}} \bar{\sigma}_{ij} + \frac{\partial {}^{t}F}{\partial {}^{t}\bar{e}^{P}_{ij}} \bar{e}^{P}_{ij} = 0 \tag{5.28} $$

where $\bar{e}^{P}_{ij}$ = components of incremental plastic strain, or in matrix notation,

$$ {}^{t}\underline{\bar{q}}^{T} \underline{\bar{\sigma}} = {}^{t}\underline{\bar{P}}^{T} \underline{\bar{e}}^{P} \tag{5.29} $$

where ${}^{t}\bar{q}_{ij} = \partial {}^{t}F / \partial {}^{t}\bar{\sigma}_{ij}$ and ${}^{t}\bar{P}_{ij} = - \partial {}^{t}F / \partial {}^{t}\bar{e}^{P}_{ij}$ and the vector components of strain increments and stresses for a shell element are:

$$ \underline{\bar{e}}^{T} = [\bar{e}_{11} \quad \bar{e}_{22} \quad \bar{e}_{33} \quad 2\bar{e}_{12} \quad 2\bar{e}_{13} \quad 2\bar{e}_{23}] \tag{5.30} $$

$$ \underline{\bar{\sigma}}^{T} = [\bar{\sigma}_{11} \quad \bar{\sigma}_{22} \quad \bar{\sigma}_{33} = 0 \quad \bar{\sigma}_{12} \quad \bar{\sigma}_{13} \quad \bar{\sigma}_{23}] \tag{5.31} $$

Using an associated flow rule, the yield function Eq. (5.27), is the potential function to which the normality rule is applicable; i.e.,

$$\underline{\bar{e}}^P = {}^t\lambda \; {}^t\underline{\bar{q}} \tag{5.32}$$

where ${}^t\lambda$ is a scalar to be determined. The stress increments are calculated using

$$\underline{\bar{\sigma}} = \underline{\bar{C}}^E \; (\underline{\bar{e}} - \underline{\bar{e}}^P) \tag{5.33}$$

where $\underline{\bar{C}}^E$ is the three-dimensional continuum elastic constitutive relation. Using Eqs. (5.29)-(5.33) to eliminate $\underline{\bar{e}}^P$ and ${}^t\lambda$, we obtain the elastic-plastic stress-strain matrix at time t:

$$\underline{\bar{\sigma}} = \underline{\bar{C}}^{EP} \underline{\bar{e}} \tag{5.34}$$

where

$$\underline{\bar{C}}^{EP} = \underline{\bar{C}}^E - \frac{\underline{\bar{C}}^E \, {}^t\underline{\bar{q}} \, (\underline{\bar{C}}^E \, {}^t\underline{\bar{q}})^T}{{}^t\underline{\bar{p}}^T \, {}^t\underline{\bar{q}} + {}^t\underline{\bar{q}}^T \, \underline{\bar{C}}^E \, {}^t\underline{\bar{q}}} \tag{5.35}$$

In this study the von Mises yield condition for isothermal and isotropic hardening is used,

$${}^tF \; ({}^t\underline{\bar{\sigma}} \; , \; {}^t\underline{\bar{e}}^P) = \frac{1}{2} \; {}^t\bar{D}_{ij} \; {}^t\bar{D}_{ij} - \frac{{}^t\sigma_y^2}{3} \tag{5.36}$$

where ${}^t\bar{D}_{ij} = {}^t\bar{\sigma}_{ij} - \frac{1}{3} \, {}^t\bar{\sigma}_{kk} \delta_{ij}$ = deviatoric stress components, and ${}^t\sigma_y$ is the yield stress at time t, which is a function of the plastic work per unit volume ${}^tW^P$:

$${}^tW^P = \int_0^{{}^t\bar{e}^P_{ij}} {}^t\bar{\sigma}_{ij} \; \bar{e}^P_{ij} \tag{5.37}$$

To evaluate $\underline{\bar{C}}^{EP}$ from Eq. (5.35), we need to calculate ${}^{t}\underline{\bar{p}}$ and ${}^{t}\underline{\bar{q}}$. By the definition of ${}^{t}\bar{q}_{ij} = \partial {}^{t}F/\partial {}^{t}\bar{\sigma}_{ij}$, Eq. (5.36), and some algebra, we can obtain,

$$ {}^{t}\underline{\bar{q}} = [{}^{t}\bar{D}_{11} \quad {}^{t}\bar{D}_{22} \quad {}^{t}\bar{D}_{33} \quad 2{}^{t}\bar{D}_{12} \quad 2{}^{t}\bar{D}_{13} \quad 2{}^{t}\bar{D}_{23}] \tag{5.38} $$

To evaluate ${}^{t}\underline{\bar{P}}$, we use the definition ${}^{t}\bar{P}_{ij} = - \partial {}^{t}F/\partial {}^{t}\bar{e}^{P}_{ij}$ and Eq. (5.36) to get

$$ {}^{t}\bar{P}_{ij} = \frac{2}{3} \, {}^{t}\sigma_{y} \frac{d{}^{t}\sigma_{y}}{d{}^{t}W^{P}} \frac{d{}^{t}W^{P}}{d{}^{t}\bar{e}^{P}_{ij}} $$

The above equation and Eq. (5.37) give

$$ {}^{t}\underline{\bar{P}}^{T} = {}^{t}H \, [{}^{t}\bar{\sigma}_{11} \quad {}^{t}\bar{\sigma}_{22} \quad {}^{t}\bar{\sigma}_{33} = 0 \quad {}^{t}\bar{\sigma}_{12} \quad {}^{t}\bar{\sigma}_{13} \quad {}^{t}\bar{\sigma}_{23}] \tag{5.39} $$

where

$$ {}^{t}H = \frac{2}{3} \, {}^{t}\sigma_{y} \quad \frac{d{}^{t}\sigma_{y}}{d{}^{t}W^{P}} \tag{5.40} $$

Assuming linear hardening ${}^{t}H$ is calculated to be

$$ {}^{t}H = \frac{2}{3} \left(\frac{1}{E_T} - \frac{1}{E} \right)^{-1} \tag{5.41} $$

where E_T = linear strain hardening (tangent) modulus. Now, by knowing ${}^{t}\underline{\bar{P}}$ and ${}^{t}\underline{\bar{q}}$ and $\underline{\bar{C}}^{E}$ a general three-dimensional incremental elastic-plastic constitutive relation measured in local coordinate system ${}^{0}\bar{x}_{i}$, i=1,2,3, can be formed, $\underline{\bar{C}}^{EP}$, see Table 7. The shell elastic-plastic incremental

constitutive relation $\underline{\tilde{C}}^{SEP}$, is then formed by imposing the condition zero normal stress in the t-direction. This is done by statictically condensing out the appropriate row and column of the matrix $\underline{\tilde{C}}^{EP}$. The matrix $\underline{C}^{-SEP}$ is then transformed to the global coordinate system by employing Eq. (5.24).

5.4 Mass Matrices

Two different mass discretization methods can be employed in the formulation of the shell element, i.e., a lumped mass matrix, $\underline{M}_{\ell}$, or a consistent mass matrix, $\underline{M}_{c}$.

Lumped Mass Matrix, $\underline{M}_{\ell}$

The lumped mass is the simplest mass representation. A principal advantage of the lumped mass assumption is that it is cheaper to use compared to a consistent mass discretization. The lumped mass matrix is obtained by lumping equal masses, m, at each of the translational degrees of freedom of the top and bottom nodes, and assigning equal masses of 2m to the translational degrees of freedom of the mid-surface nodes. Also including the rotational inertia of $\frac{1}{2}\, m\, (a_k)^2$ to the rotational degrees of freedom of the mid-surface nodes, where the mass m, is defined

$$m = \frac{{}^{0}\rho\ {}^{0}V}{\sum_{k=1}^{N} (1+n_k)} \tag{5.42}$$

where $n_k = 1,(0)$ if node k is, (is not) a mid-surface node, and ${}^{0}V$ = volume of the element at time 0, and a_k is the thickness of the shell at node k. It should be noted that the lumped mass matrix is a diagonal matrix. Masses

allocated to the translational degrees of freedom are independent of the geometry of the element at any time, and remain constant provided the total mass of the element, ${}^0\rho\,{}^0V$, is constant. The inertia lumped to the rotational degrees of freedom is also independent of the element orientation. Because the thickness, a_k, does not change, and the reference axes ${}^tV_1$ and ${}^tV_2$ are shell body coordinate axes. However it should be pointed out that, in the calculation of the nodal acceleration using available time integration schemes (such as Wilson-θ method, Newmark method [32]) stationary reference coordinate systems are assumed. Thus, in performing large rotation dynamic analysis of structures, a modified time integration scheme is needed to evaluate rotational acceleration about non-stationary ${}^tV_1$ and ${}^tV_2$ axes.

The diagonal term of the lumped mass matrix (only non-zero terms) of a transition element, see Section 6.3, is

$$\text{diagonal } [\underline{M}_\ell] = \Big\{ \ldots \underbrace{m\ m\ m}_{\substack{\text{top-or}\\ \text{bottom-}\\ \text{surface node}}} \ldots \underbrace{2m\ 2m\ 2m\ \tfrac{1}{2}m\,(a_k)^2\ \tfrac{1}{2}m\,(a_k)^2}_{\text{mid-surface node k}} \ldots \Big\} \tag{5.43}$$

Consistent Mass Matrix, $\underline{M}_c$

The consistent mass matrix, in the geometric linear analysis, is evaluated for a single element using $\int_{{}^0V} {}^0\rho\ {}^{t+\Delta t}\ddot{\underline{u}}\ \delta\underline{u}\ {}^0dv$. Rewriting the Eq. (5.8) in the linear analysis and using the notation in Eq. (5.12)

$$ {}^{t+\Delta t}u_i = \sum_{k=1}^{N} h_k \left[1 \quad {}^0g_{1i}^k \quad {}^0g_{2i}^k\right] \begin{bmatrix} {}^{t+\Delta t}u_i^k \\ {}^{t+\Delta t}\alpha^k \\ {}^{t+\Delta t}\beta^k \end{bmatrix} \tag{5.44} $$

where ${}^{t\Delta t}\alpha^k$ and ${}^{t+t}\beta^k$ are the total rotation angles of the normal vector from time 0 to time $t+\Delta t$. It should be noted that Eq. (5.44) is justified, because the rotations are small in the linear analysis. Noting that in the isoparametric formulation ${}^{t+\Delta t}\ddot{u}_i$ is interpolated the same as in the above equation.

The variation of the incremental displacement is evaluated similarly,

$$ \delta u_i = \sum_{k=1}^{N} h_k \left[1 \quad {}^0g_{1i}^k \quad {}^0g_{2i}^k\right] \begin{bmatrix} \delta u_i^k \\ \delta\alpha^k \\ \delta\beta^k \end{bmatrix} \tag{5.45} $$

Using the Eqs. (5.44), (5.45) and the definition of the consistent mass matrix, Table 3

$$ [\underline{M}_C]^{t+\Delta t}\underline{\ddot{U}} = \left[\int_{{}^0V} {}^0\rho \; {}^0\underline{H}^T \; {}^0\underline{H} \; {}^0dv\right] {}^{t+\Delta t}\underline{\ddot{U}} \tag{5.46} $$

where ${}^0\underline{H}$ is the matrix of interpolation functions, which is evaluated using Eqs. (5.44), (5.45). This matrix is a function of the natural coordinates r, s, and t, see Table 8. To evaluate the consistent mass matrix using integration over the limits of the natural coordinate system

we get

$$\underline{M}_C = \int_{-1}^{1} \int_{-1}^{1} \int_{-1}^{1} {}^0\rho \; {}^0\underline{H}^T \; {}^0\underline{H} \; {}^0\underline{J} \; dr \; ds \; dt \qquad (5.47)$$

where ${}^0\underline{J}$ is the Jacobian matrix defined in Eq. (5.19).

It is worth noting that the consistent matrix evaluated using Eq. (5.47) is invariant of the element deformation. Therefore, the matrix $\underline{M}_C$ is calculated once before the step-by-step solution.

In the large deflection analysis, the consistent mass matrix is a function of the element geometry at the solution time. This means the inertia forces are not conservative forces, when the body undergoes large rotations. However, in this study only conservative forces are assumed (i.e, path independent forces). Thus it is also assumed that the consistent mass matrix is invarient, i.e. using the matrix $\underline{M}_C$ defined in Eq. (5.47).

6. INTERPOLATION FUNCTIONS FOR SHELL ELEMENTS

In the previous chapter the shell element matrices required in the T.L. or U.L. formulation were derived. The interpolation polynomials, h_K, used in these matrices have not yet been defined. The same interpolation functions are also employed in the definition of the geometry of the element, Eq. (5.1), and the displacement variation within the element, Eqs. (5.3), (5.17).

The basic procedure in the isoparametric finite element formulation is to express the element coordinates and element displacements in the form of interpolation using the natural coordinate system of the element. The natural coordinate system of the shell element is r, s and t. Coordinate r and s define the mid-surface of the shell element, which is in general a curvilinear coordinate system. The coordinate t is along the normal to the mid-surface of the element. Each of the coordinates r, s and t varies from -1 to +1 to define the element domain.

The global coordinate at any point of the shell element, ${}^{t}x_i$, is interpolated using the nodal positions and nodal normal vectors of the element at time t, according to Eq. (5.1). The unknown quantities in this equation are so far the interpolation functions h_k ($k = 1,2,...N$). The fundamental property of the interpolation function h_k is that its value in the natural coordinate system is unity at node k and is zero at all other nodes. Other requirements of the interpolation functions is to satisfy the Patch test [4]. This is insured when these functions satisfy the rigid body modes and constant strain condition. Using these conditions

the functions h_k corresponding to a specific nodal point layout could be solved for in a systematic manner. However, it is possible to construct them by inspection. The computationally effective procedure to construct the interpolation functions for variable-number-nodes shell element is presented in this chapter. To demonstrate this technique it is employed to construct the interpolation functions of a variable-number-nodes one dimensional element.

6.1 Demonstrative One-Dimensional Element Example

The procedure to construct the interpolation functions of a variable-number-nodes element is demonstrated by formulating the interpolation functions of a 2- to 4- nodes element. In this case the interpolation functions are only a function of the natural coordinate r, which vary from -1 to +1.

Construct the interpolations corresponding to a basic two-node element. The nodes 1 and 2 are located at r = +1, and r = -1 respectively. In this case, the interpolation functions are polynomial of linear order in r, Fig. 6.1.

The addition of the third node at r = 0 results into additional quadratic interpolation function and a correction to be applied to the already existing interpolation functions for nodes 1 and 2. The two linear interpolation functions are adjusted by subtracting one half of the quadratic function assigned to the node 3. Hence, the final three interpolation functions are all quadratic functions in r.

If the fourth node is added at position $r = -\frac{1}{3}$ and moving the

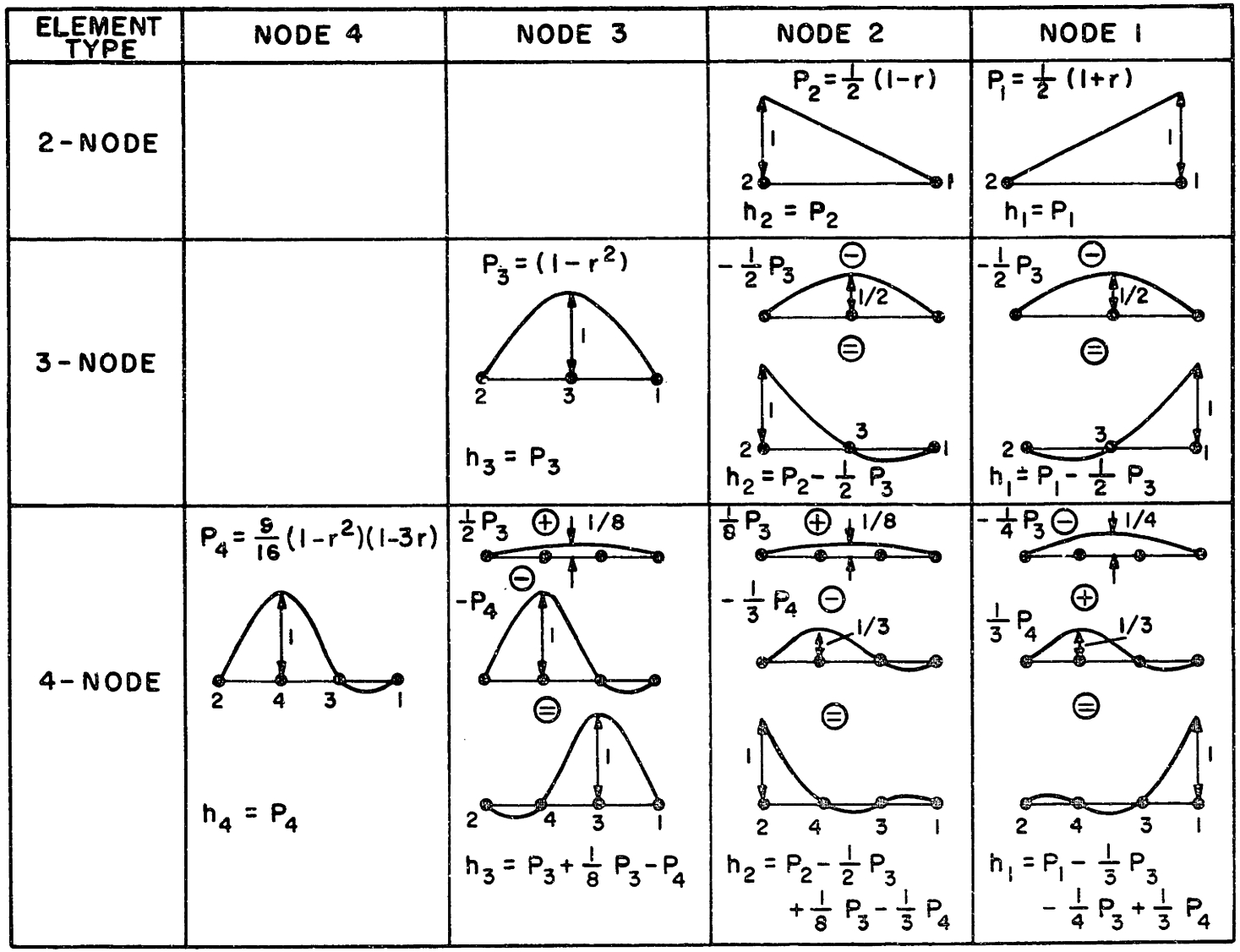

FIGURE 6.1 SCHEMATIC CONSTRUCTION OF A VARIABLE-NUMBER-NODES, ONE DIMENSIONAL ELEMENT INTERPOLATION FUNCTIONS

already existing node 3 to the position $r = \frac{1}{3}$ results in additional cubic interpolation polynomial and correction to be applied to the three previous quadratic interpolation functions. All the final four interpolation functions will be of the cubic power in r.

6.2 Variable - Number - Nodes Quadrilateral Shell Element

The quadrilateral shell element is a 4- to 16- variable-number-nodes element. All the nodes are located on the shell mid-surface. Each node has five degrees-of-freedom, three displacements and two rotations. The node numbering scheme and the parent element nodal position measured in the natural coordinate system are shown in Fig. 6.2.

The procedure to construct the interpolation functions for the variable-number-nodes shell element are analogous to the example given in the previous section. The interpolation functions for the 4- to 16-nodes shell element are presented in the Table 9.A. It should be noted that the interpolation polynomials are only a function of r and s. The construction of the quadratic h_1 and cubic h_6 are shown graphically in Fig. 6.3.

Some of the important elements that can be constructed from different node layouts are; (a) cubic Lagrangian element, this element has 12 boundary nodes and 4 internal nodes. The displacement within the element is interpolated using polynomial of complete cubic terms in r and s plus terms of r^3s, r^2s^2, rs^3 and r^3s^3. (b) 12-nodes serendipity element, all nodes are located on the boundary in this case. The displacement is interpolated with cubic functions in r and s plus terms of

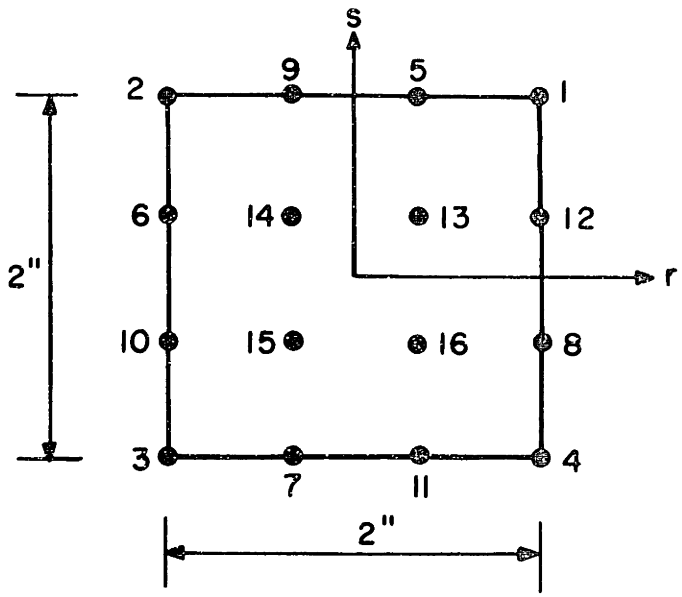

PARENT ELEMENT

NODE	r	s	COMMENTS
1	1	1	LINEAR
2	-1	1	
3	-1	-1	
4	1	-1	
5	γ	1	QUADRATIC
6	-1	γ	
7	$-\gamma$	-1	
8	1	$-\gamma$	
9	-1/3	1	CUBIC
10	-1	-1/3	
11	1/3	-1	
12	1	1/3	
13	η	η	INTERNAL NODES
14	-1/3	1/3	
15	-1/3	-1/3	
16	1/3	-1/3	

$$\gamma = \begin{cases} 0, \text{ IF NODE (i+4) IS NOT PRESENT} \\ \frac{1}{3}, \text{ IF NODE (i+4) IS PRESENT} \end{cases}$$

$$\eta = \begin{cases} 0, \text{ IF ONLY ALL NODES 1 TO 8 ARE PRESENT} \\ \frac{1}{3}, \text{ IF ALL NODES ARE PRESENT} \end{cases}$$

FIGURE 6.2 NODE NUMBERING SCHEME OF A VARIABLE-NUMBER-NODES, QUADRILATERAL SHELL ELEMENT

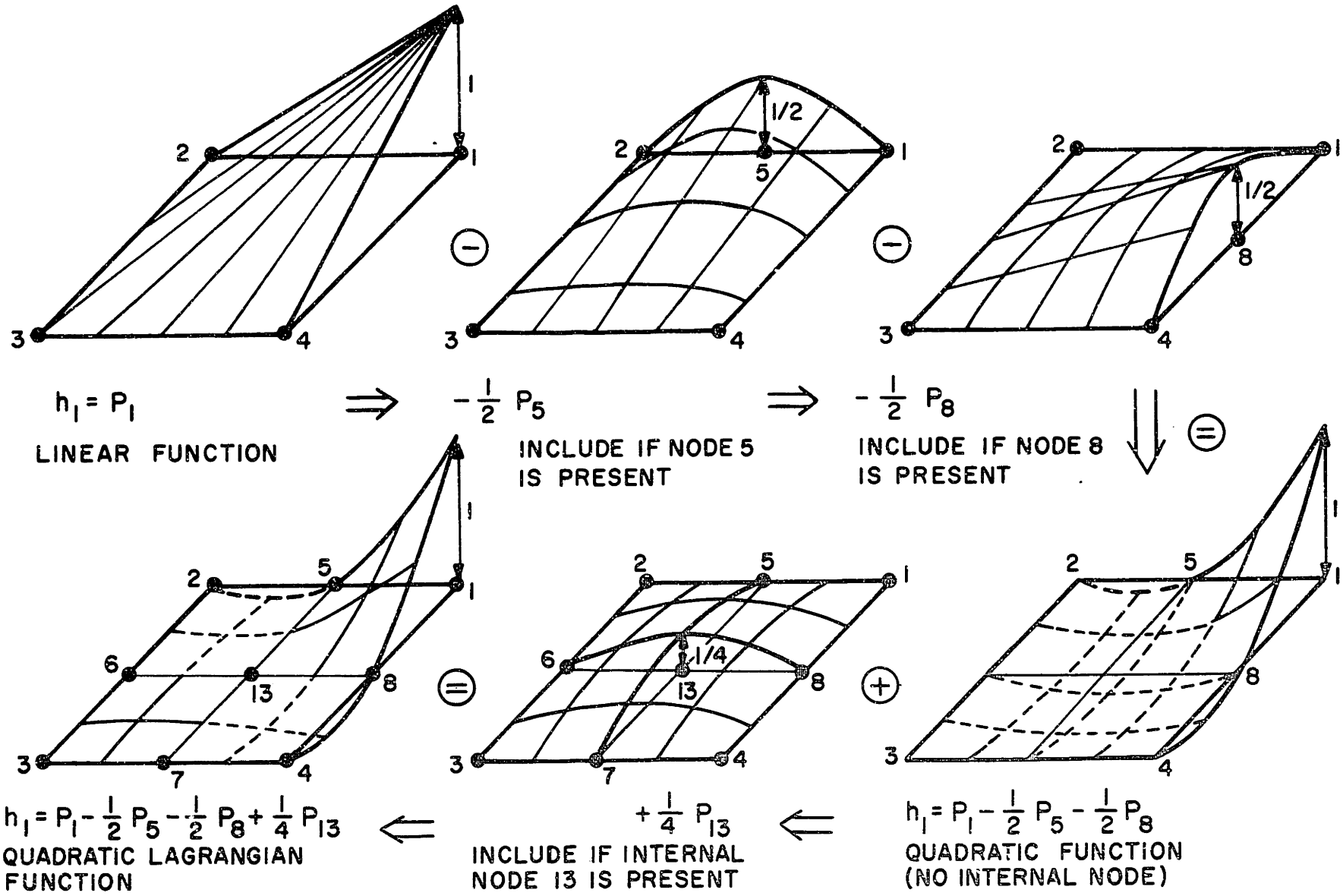

FIGURE 6.3 CONSTRUCTION OF SHELL ELEMENT INTERPOLATION FUNCTIONS

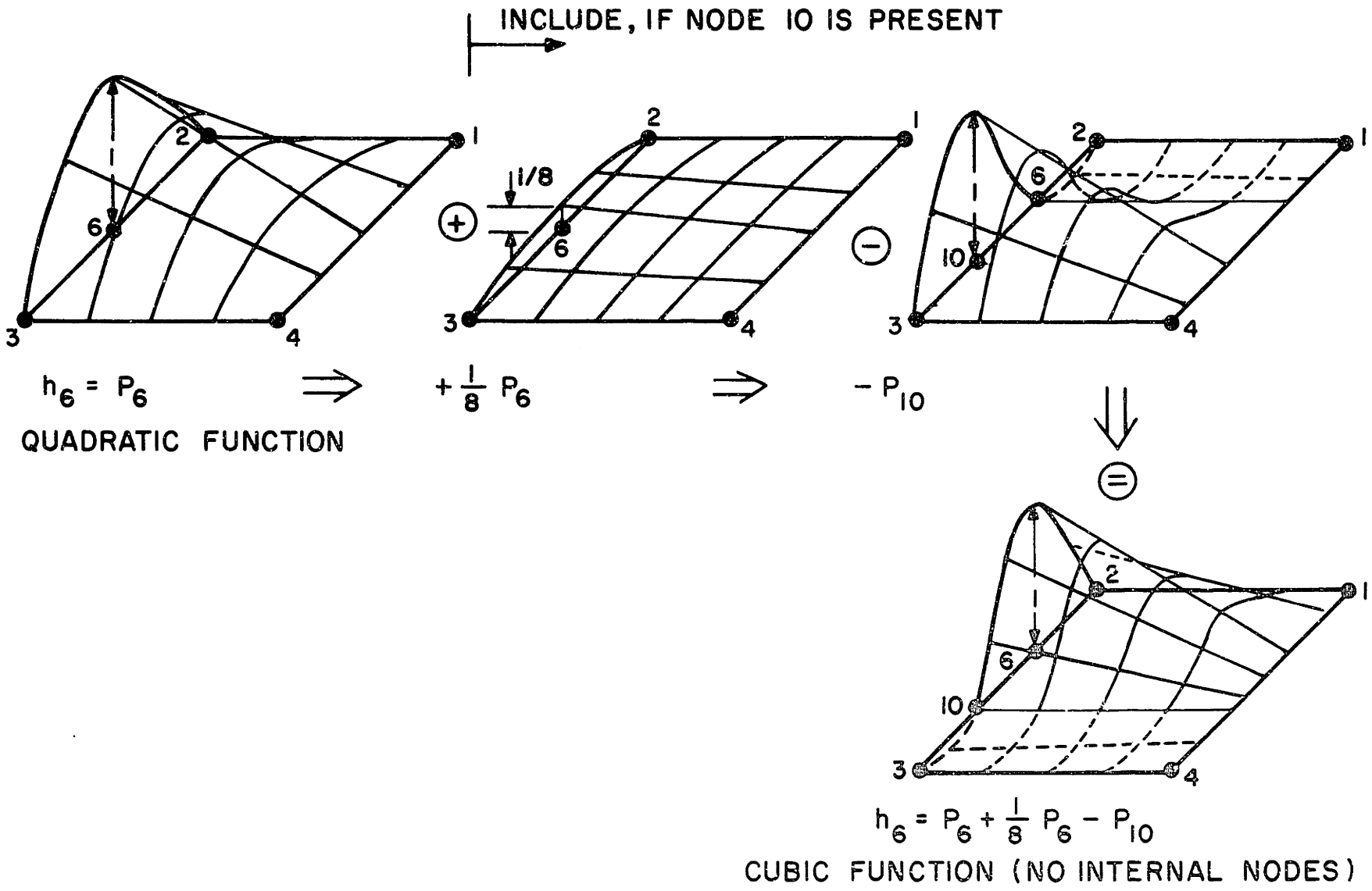

FIGURE 6.3 (Continued)

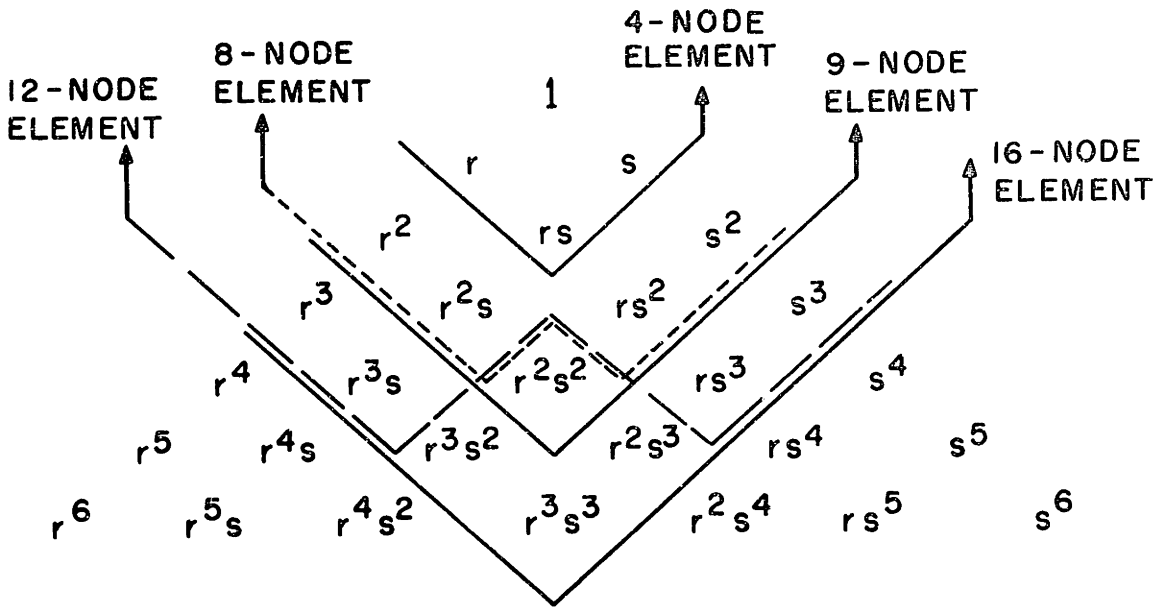

FIGURE 6.4 INTERPOLATION POLYNOMIALS OF SOME OF THE SHELL ELEMENTS

r^3s and rs^3, (c) quadratic Lagrangian element, this element has 8 boundary nodes and one internal node. The displacement in this case is interpolated with complete quadratic functions plus terms of order r^2s, rs^2 and r^2s^2. (d) 8-node serendipity element. The displacement is interpolated with complete quadratic functions in r and s plus terms of r^2s and rs^2 (see Fig. 6.4).

6.3 Variable-Number-Nodes Triangular Shell Element

The triangular shell element is a 3- to 9- variable-number-nodes element. All the nodes are located on the shell mid-surface and each possess five degrees-of-freedom. The element may be formulated either as an independent element, or as an extension to the quadrilateral element. The latter is achieved by collapsing nodes of one side of the element. However, the final interpolation functions of an element formulated by either method should be identical. The node collapsing method is computationally more effective, becuase the traingular element and the quadrilateral element can be combined in one element.

Node collapsing means to assign one global structural node to all collapsed local nodes of an element, i.e., all the collapsed nodes possess the same coordinates and displacements. Without any loss of generality we collapse nodes 1 and 4 (also nodes 8 and 12 if they are included) into one node, Fig. 6.2. Using Eq. (5.1) and noting that all the collapsed nodes have the same positions and normal vector, the effective interpolation function at this node (i.e. triangular element node 1) is:

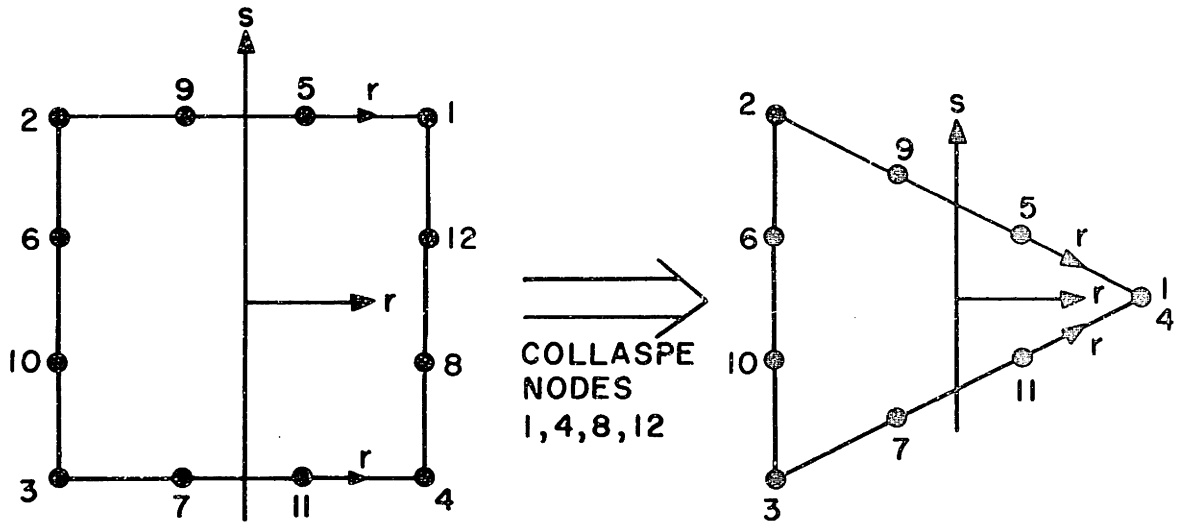

QUADRILATERAL ELEMENT

COLLAPSED TRIANGULAR ELEMENT

(a) NODE COLLAPSING SCHEME, AND TRIANGULAR ELEMENT NODE NUMBERING

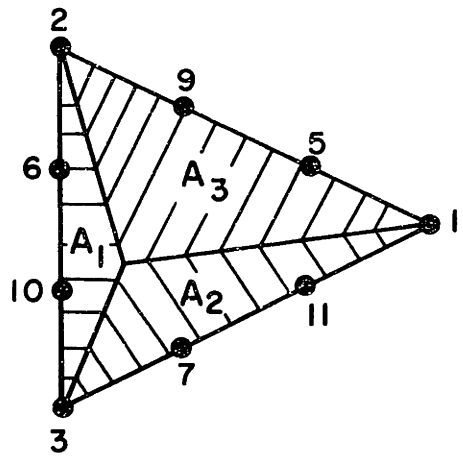

$$L_i = \frac{A_i}{A}$$

A_i = AREA OF SUB-TRIANGLE

A = AREA OF THE TRIANGLE

L_i = AREA COORDINATE

(b) TRIANGULAR ELEMENT, AREA COORDINATE DEFINITION

FIGURE 6.5 NODE NUMBERING OF A VARIABLE-NUMBER-NODES, TRIANGULAR SHELL ELEMENTS

$$h_1^T = h_1 + h_4 + \underline{h_8 + h_{12}} \qquad (6.1)$$

where underline functions are included if nodes 8 or 12 are present. Inclusion of nodes 8 and 12 in the formation of the collapsed node does not alter the effective interpolation function assigned to the collapsed node, see Table 9.A. Therefore, from here on we only consider the collapse of nodes 1 and 4. The node numbering scheme of the collapsed triangular element is shown in Fig. 6.5 (note that the nodes 8, 12 and internal nodes are not present).

The traingular element constructed by node collapsing does not, in general, satisfy the spatial isotropy [33] or geometric invaniance requirement. This means that the displacements of the element as yet are not independent of the orientation of the local element coordinate system, r-s. Therefore the interpolation functions need to be modified to satisfy this requirement.

The interpolation functions of the element based on triangular area coordinate system does staisfy the spatial isotropy condition. The area coordinates ($L_i = A_i/A$, $i = 1,2,3$) are defined in Fig. 6.5. The interpolation functions of the variable-number-nodes element employing area coordinates are given in Table 9.B.

The area coordinates are related to the curvilinear coordinates r and s. The relationships can be identified numerically by matching the values of the two coordinate systems at all the nodes and at every other point within the domain of the element. The relationships are:

$$L_1 = \frac{1}{2}(1+r)$$

$$L_2 = \frac{1}{4}(1-r)(1+s) \qquad (6.2)$$

$$L_3 = \frac{1}{4}(1-r)(1-s)$$

Compare the evaluation procedure of the interpolation functions given in Table 9.A and 9.B, and note the node collapsing effect, Eq. (6.1), it can be observed that both formulations yield identical final functions if the primary polynomials P_i are identical for both the collapsed quadrilateral and triangular element. Using Eq. (6.2), and comparing the primary functions shows that corrections have to be made to the primary functions of nodes 6, 10 and 11. Therefore the corrected primary functions assigned to these nodes are;

$$P_6^c = P_6 + \underline{\left[-\frac{1}{4}(1-r^2)(1-s^2)\right]} \qquad (6.3)$$

$$P_{10}^c = P_{10} + \underline{\left[\frac{27}{128}(1-r^2)(1-s^2)(1-r)(1+s)\right]} \qquad (6.4)$$

$$P_{11}^c = P_{11} + \underline{\left[\frac{27}{64}(1-r^2)(1-s^2)(1-r)\right]} \qquad (6.5)$$

where P_6, P_{10} and P_{11} are defined in Table 9.A, and underline functions are corrections to be made to the primary functions of the quadrilateral element. These corrections insure the spatial isotropy of the collapsed triangular element. Employing the corrected primary functions of Eqs. (6.3) - (6.5) instead of P_6, P_{10} and P_{11} in Table 9.A, leads to the table of interpolation function for variable-number-nodes collapsed tri-

angular element.

6.4 Variable-Number-Nodes Transition Element

The transition element is a 4- to 32- variable-number-nodes element. This element can have nodes on the top-, bottom-, and the mid-surface of the shell. The mid-surface nodes possess the same five degrees of freedom as the shell element, and the top- or bottom- surface nodes have three displacements degrees of freedom. This element can be used to connect the shell elements to solid elements and preserve complete compatibility. The element may have quadrilateral or triangular type base shape.

The interpolation functions of the transition element may be constructed in two steps; first from the interpolation functions, h_i, of an element with all nodes projected to the mid-surface, secondly split each mid=surface node, which is required, into a top-surface node and a bottom-surface node. The interpolation functions for the top-, and bottom-surface nodes are;

$$h_i^{top} = \frac{1}{2}(1+t)\, h_i \tag{6.6}$$

$$h_i^{bot} = \frac{1}{2}(1-t)\, h_i \tag{6.7}$$

The mid-surface nodes interpolation functions, h_i, and the top- and bottom=surface nodes interpolation functions, h_i^{top} and h_i^{bot}, will be written in a compact notation h_i as used in Eq. (5.1), Tables 5 and 6 etc.

7. SOME IMPORTANT FEATURES OF THE SHELL ELEMENT

The variable-number-nodes shell element is a very general and versatile element. In this chapter some of its pertinent theoretical and practical features are discussed.

7.1 Element Description

To describe an assemblage of variable-number-nodes shell elements the following input is required:

(i) the shell nodal point coordinates;

(ii) the shell mid-surface normals, $^{0}\underset{\sim}{V}_{n}^{k}$, at all mid-surface nodes. One normal is defined at each mid-surface node;

(iii) the shell thickness, a_k, at all mid-surface nodes, one thickness is defined at each mid-surface node;

(iv) the material properties of the element.

Where (i) and (ii) pertain to the global nodal layout which define the complete structure, whereas the information of (iii) and (iv) define the geometric and material property of element(s).

7.2 Numerical Integration

It is essential to employ numerical integration in evaluating element matrices (especially in the case of distroted element). Many numerical integration schemes are presented in [4,33]. The Gauss integration method [4, pp.146-148] is proven to be an effective scheme, therefore this method is used for integration through the thickness of the shell, i.e. in t-direction. The integration order of 2 in the t-direction is usually sufficient, but higher integration order may need

to be employed, in particular in material nonlinear analysis.

Different spatial integration schemes over the r-s surface are employed for the quadrilateral and triangular element.

(a) quadrilateral element; Gauss integration is used in the r and s directions. The order of integration in each direction can be selected independently. The error in Gauss integration scheme in any one direction is of the order 2n, i.e., when n integration points are employed in a direction (e.g. r-direction) the polynomial of this variable up to the power (2n-1) is integrated exactly. Thus, Gauss integration order (3x3) and (4x4) in the (rxs) directions integrate exactly the matrices of the undistorted quadratic and cubic elements respectively (i.e., when the determinate of the Jacobian matrix is invarient).

(b) Triangular element, an important requirement of the integration scheme, over the triangular r-s surface of the element, is that the integrating points should be evenly (or symmetrically) spaced with respect to the three vertices of the triangle. This is to have a uniform accuracy in the area coordinate directions L_1, L_2 and L_3, in order to preserve the spatial isotropy of the element. If Gauss integration or Gauss-Radau integration [4, pp.149] methods are used the above requirement will be violated. Various special integration schemes for triangular domains have been derived [43-46], and an effective scheme has been reported by Cowper [47], which is employed in this study with success.

In this study all the element matrices are functions of r and s, thus the integrals are performed over the r-s surface ($-1 \leq r < 1$, and $-1 \leq s \leq 1$).

Therefore the integration scheme reported by Cowper in terms of the area coordinates is transformed to the r-s plane by using Eq. 6.2 (i.e., transforming the integration points coordinates and their weighting factors), see Fig. 7.1. The integration orders of 7 and 13 are recommended for quadratic and cubic triangular elements respectively.

In this section a comment on reduced integration is in order; the cubic element can be employed without reduced or selective integration. When the element is straight it does not display the stiffening effect that is observed in lower order elements, see Section 8.1. Also, when modeling curved structure the cubic element with high order integration shows less stiffening effect and a better rate of convergence than the lower order elements with high integration, see Section 8.3. These observations are important; namely, for numerical reasons reduced integration must be employed with care in practice, especially in nonlinear analysis. Using reduced or selective integration the difficulties are that, for all possible geometric shapes, the finite element must not contain small spurious eigenvalues (or develop such eigenvalues in the incremental solution), and the element must satisfy all convergence requirements and display good accuracy characteristics. The precise effect of reduced integration is very difficult to assess when using an element in general large displacement analysis; and considering materially nonlinear analysis a higher-order integration may be desirable anyway, in order to caputre the variation in the constitutive relations, thus further study in this field is recommended. Therefore the reduced integration is in general helpful, but cubic elements may be employed with high degrees of accuracy

(a) 4-POINT INTEGRATION

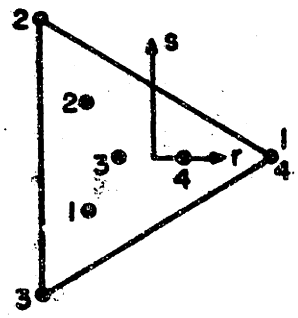

INTEG. POINT	r	s	WEIGHTING FACTOR, W_f
1	-.6000000000000	-.5000000000000	1.3020833333333
2	-.6000000000000	.5000000000000	1.3020833333333
3	-.3333333333333	.0000000000000	-1.6875000000000
4	.2000000000000	.0000000000000	2.6041666666667

(b) 7-POINT INTEGRATION

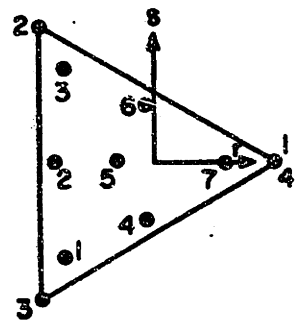

INTEG. POINT	r	s	WEIGHTING FACTOR, W_f
1	-.7974269853530	-.7745966692414	.2802654718574
2	-.8805682564204	.0000000000000	.2816045678459
3	-.7974269853530	.7745966692414	.2802654718574
4	-.0597158717898	-.7745966692414	.4997345281425
5	-.3333333333333	.0000000000000	.6750000000000
6	-.0597158717898	.7745966692414	.4997345281425
7	.5948539707062	.0000000000000	1.2433954321539

FIGURE 7.1 TRIANGULAR INTEGRATION SCHEME

(C) 13-POINT INTEGRATION

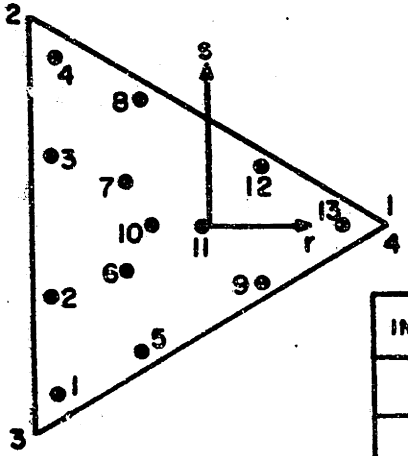

INTEG. POINT	r	s	WEIGHTING FACTOR, W_f
1	-.8697397941956	-.8606648837354	.1141276144935
2	-.9026193691494	-.3422425923378	.1621212569170
3	-.9026193691494	.3422425923378	.1621212569170
4	-.8697397941956	.8606648837354	.1141276144935
5	-.3742690079902	-.8582801034086	.2244502653904
6	-.4793080678420	-.2960331340346	.4748578372573
7	-.4793080678420	.2960331340344	.4748578372573
8	-.3742690079902	.8582801034085	.2244502653904
9	.2768883771396	-.7306622441902	.4265662918555
10	-.3333333333333	.0000000000000	-.4487101334031
11	-.0413838643162	.0000000000000	.6745457211343
12	.2768883771396	.7306622441902	.4265662918555
13	.7394795883912	.0000000000000	.8190872305070

FIGURE 7.1 (Continued)

without selective or reduced integration.

7.3 Modeling of Shell Connections in Engineering Problems

In the analysis of an actual shell structure, it is often necessary to model shell intersections or a shell to solid transitions or shell with discrete stiffeners and eccentric stiffeners. Modelling of these engineering problems are discussed in this section.

7.3.1 Modeling of Shell Intersections

Since rotational degrees of freedom of the shell element are aligned with the mid-surface of the shell (about ${}^{t}V_1^k$ and ${}^{t}V_2^k$ axes, Fig. 5.6), the intersection of shell surfaces can be modeled in three ways as shown in Fig. 7.2;

(a) Use the shell transition element to model the shell intersection. In this case only translational degrees-of-freedom are employed at the shell intersection.

(b) Assign a mean normal at the shell surface intersection.

(c) Assign to each shell surface one node with its shell surface normal, and assign to both nodes the same coordinates, i.e. the location of the intersection of the shell surfaces. Then recognizing that the degrees-of-freedom at the shell surface nodes are those in Fig. 5.4, select one master node and use constraint equations to constrain the degrees-of-freedom at the other nodes to the master degrees-of-freedom.

An example of these techniques is given in Section 8.2.

7.3.2 Modeling of Thin Shell to Solid Transition

Many structural problems have regions that behave as thin shell structures, and regions behaving as solid continuum. For examples; turbine blade with thin top (modeled by shell elements) and thick root (modeled by solid continuum elements) as shown in Fig. 7.3(a); or a dome

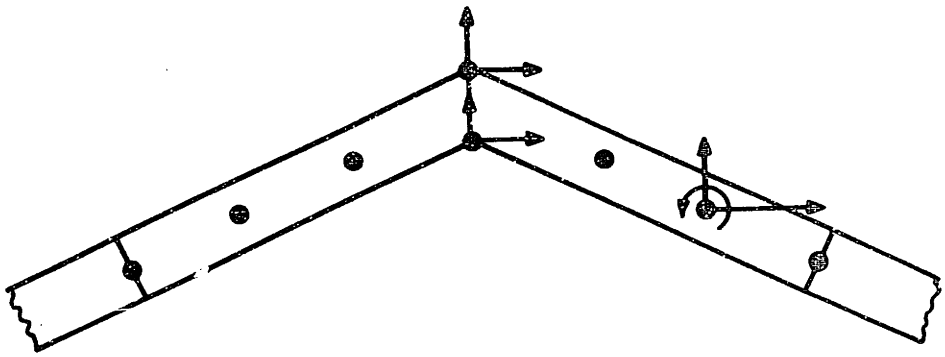

(a) USE OF TRANSITION ELEMENTS

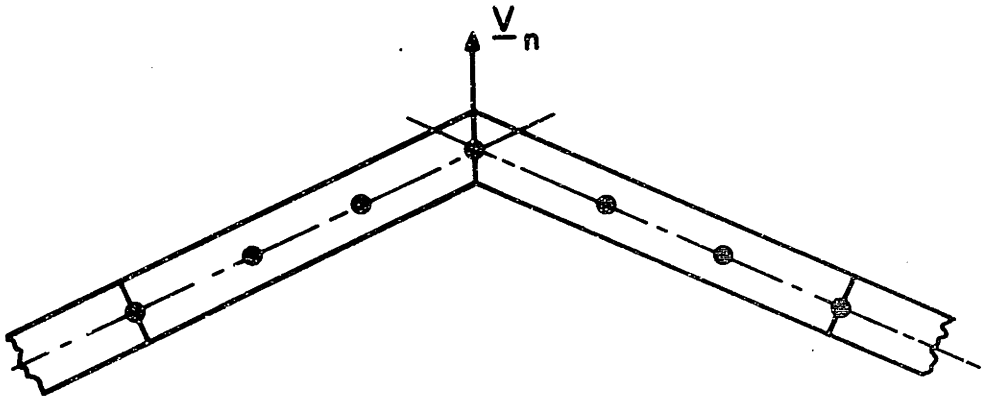

(b) USE OF ONE APPROXIMATE (OR AVERAGE) NORMAL

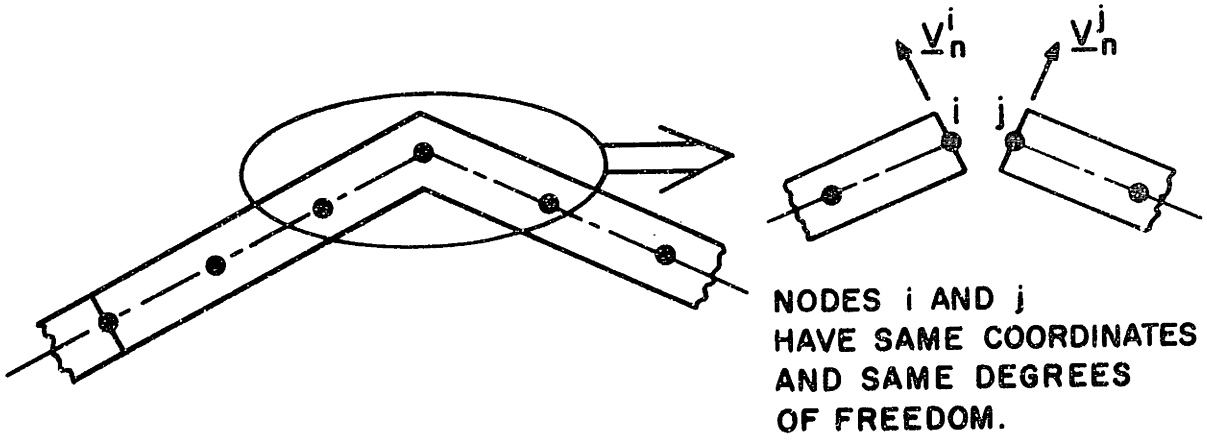

(c) USE OF CONSTRAINT EQUATIONS

FIGURE 7.2 MODELING OF SHELL SURFACES INTERSECTIONS

connected to the ground, Fig. 7.3(b). The Fig. 7.3 is shown in the cases of two-dimensional problems for clarity only. In all such problems a transition element can be employed to idealize the transitional region. This element has mid-surface nodes to couple into shell elements and top- and bottom-surface nodes to connect to the usual continuum isoparametric elements. The top and bottom nodes of the transition elements possess the same global displacements (no rotational) degrees-of-freedom as the continuum elements. The associated interpolation functions corresponding to the top and bottom nodes of transitional elements are compatible to the ones of solid elements. The degrees-of-freedom and interpolation functions associated to the mid-surface nodes of transitional elements and shell elements are fully matched.

A demonstrative example of the usage of the transitional element is given in Section 8.1.

7.3.3 Modeling of Stiffened Shells

The bending elements (formulated in Chapter 4) and the shell elements can be used together effectively to model stiffened shells. Since the same interpolation functions are employed in bending elements as in the formulations of the shell elements, the two elements are compatible. The bending elements can be used to model discrete eccentric and non-eccentric stiffeners. A demonstrative example of a plate with eccentric stiffeners is given in Section 8.1.

The three rotational degrees-of-freedom of the bending element are rotations about the fixed global Cartesian coordinate axes, whereas

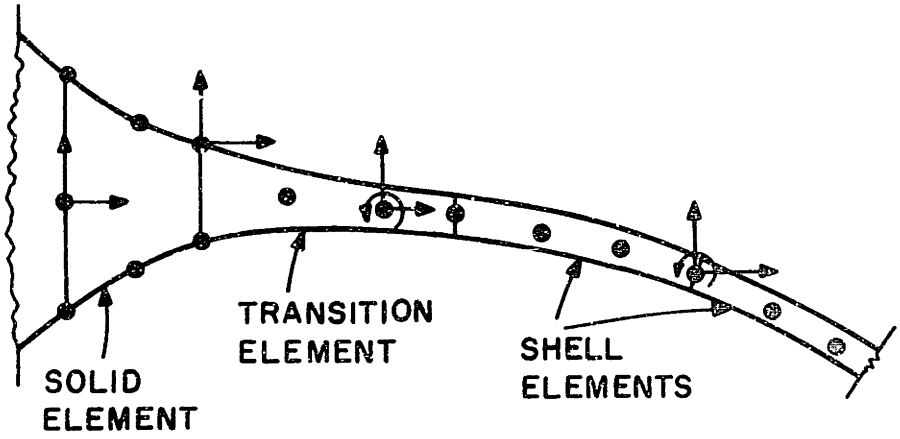

(a) TURBINE BLADE

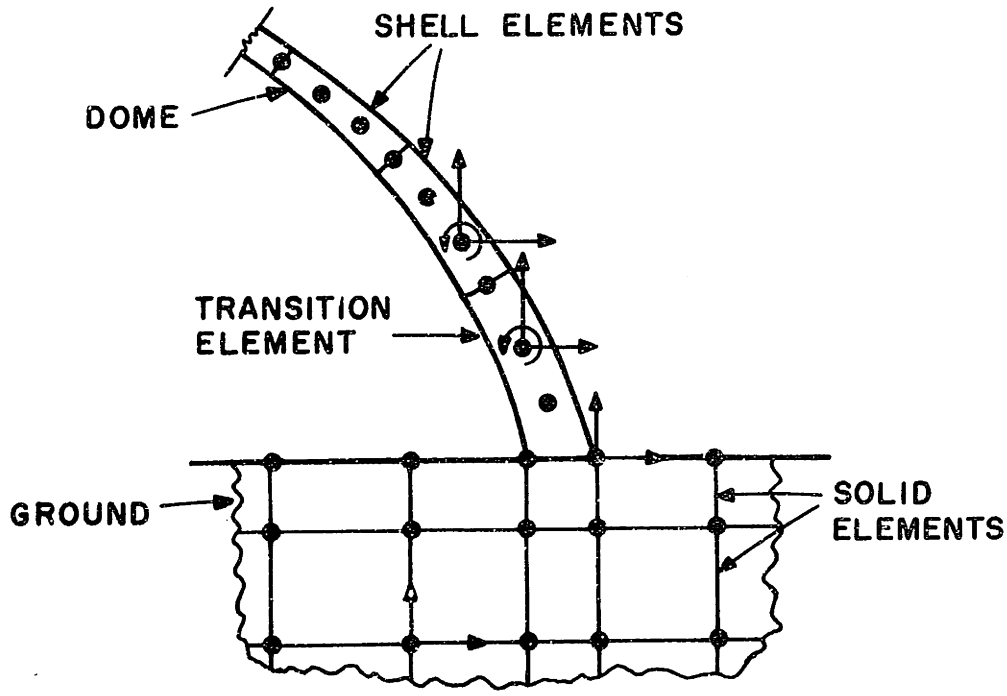

(b) SECTION OF A DOME AND ITS FOUNDATION

FIGURE 7.3 MODELING OF SHELL-TO-SOLID TRANSITIONAL REGIONS

as the two rotational degrees-of-freedom associated with the shell element are those about the body axes. Hence, when modeling a shell structure with eccentric stiffeners, the degrees-of-freedom of the stiffener elements have to be constrained to the shell elements degrees-of-freedom [39]. When shells with non-eccentric stiffeners are studied, either the constraint equation method can be employed, or the matrices of the bending element can be transformed to correspond to the directions of the shell element degrees-of-freedom. Further research is needed to study the large deflection behavior of stiffened shells, because the rotational degrees-of-freedom of the shell element are referred to the body coordinate axes, which are not fixed axes.

7.4 Use of Global or Element Convected Coordinate System

The element is formulated in the global Cartesian coordinate system, so that the element matrices are directly obtained corresponding to the global coordinate axes. This derivation requires the use of strain-displacement transformation matrices with 6 rows (that correspond to the global strain components) and also a 6 x 6 stress-strain constitutive matrix, which is calculated as described in Section 5.3. Alternatively, an element convected coordinate system could be employed, in which the local element coordinate axes are aligned with the mid-surface of the element. In this case, the element matrices are calculated corresponding to the convected coordinate system using a 5 x 5 stress-strain matrix and strain-displacement transformation matrices with only 5 rows (corresponding to the element strains in the convected coordinate system).

However, the resulting element stiffness matrix and force vector must then be transformed to correspond to the global coordinate system prior to their assemblage into the complete structure stiffness matrix and force vector. The two methods lead to identical matrices, and the advantage of using the first method is its numerical efficiency, especially in the case of transition element.

7.5 Effects of Element Aspect Ratio

One of the most significant draw-backs of using solid elements in analyzing the shell structures is that the element performance deteriorates very rapidly when the element aspect ratio (the ratio of element length to its thickness) increases [4]. Then many solid elements are needed to analyze thin shells, and the required number of solid elements is very much dependent on the thickness rather than the complete size of the structure. However, the shell element does not display any stiffening behavior when the element aspect ratio changes. This is because the stress through the thickness is ignored and the length of the thickness is assumed to be inextensible. This important feature of the shell element is demonstrated numerically for linear analyses in sections 8.1 and 8.8, and for geometric nonlinear analysis in Section 8.8.

7.6 Important Element Nodal Layouts

For analyzing different shell structures different element nodal layouts are usually most effective. However, the elements with the following nodal layouts are usually effective in analyzing most shell problems; (a) cubic elements, 12-node and 16-node quadrilateral elements can be

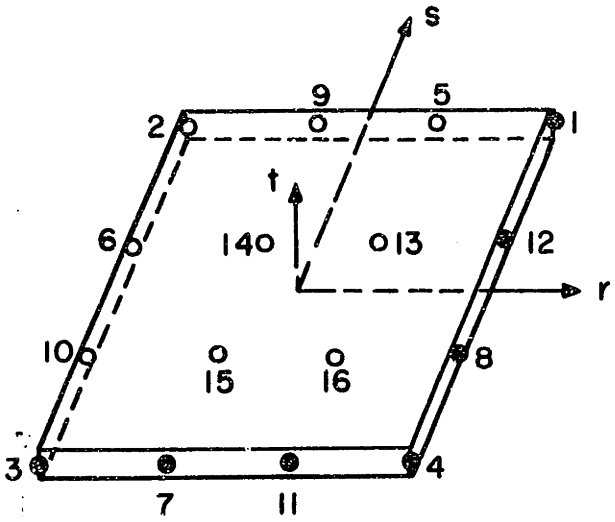

16-NODE ELEMENT

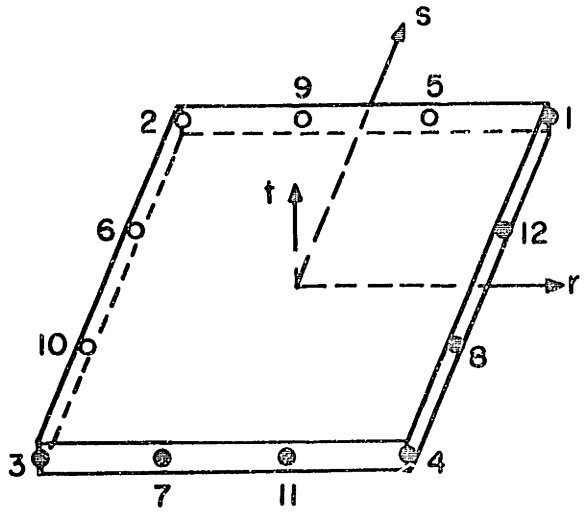

12-NODE ELEMENT

(a) CUBIC ELEMENTS

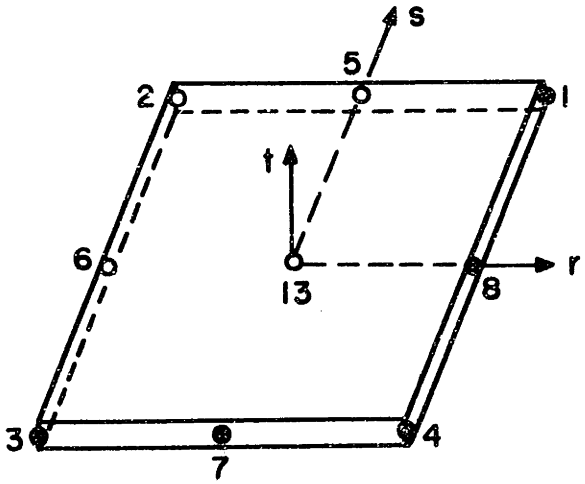

9-NODE ELEMENT

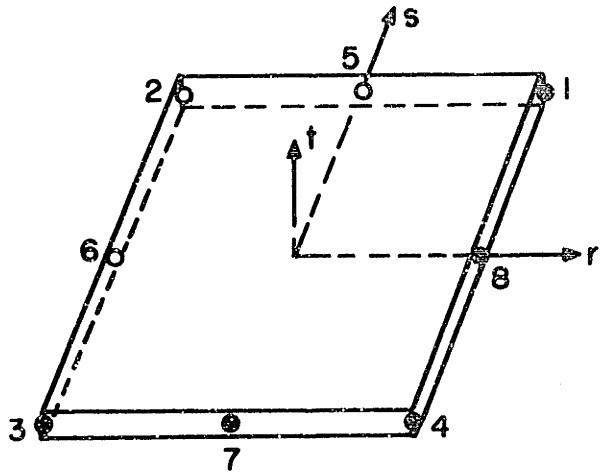

8-NODE ELEMENT

(b) QUADRATIC ELEMENTS

FIGURE 7.4 RECOMMENDED SHELL ELEMENTS

employed very effectively in linear and nonlinear analyses using high or low order numerical integration schemes as shown in Chapter 8. The cubic elements are very effective where the bending moment varies rapidly. In analyzing a shell problem it is usually required to employ less cubic elements than quadratic shell elements, an example of this is shown in Section 8.3.

(b) Quadratic elements, 8-node and 9-node quadrilateral elements with low order numerical integration (2x2x2 Gauss integration order) can be employed very effectively, but high order integrations of these elements are not recommended.

(c) Triangular elements. The quadratic and cubic traingular element usage should be confined to the region that has to be modeled with triangular elements, such as wedges and triangular sections.

(d) The transitional elements are recommended for modeling the transitional sections between the thin shells and solid sections.

The most recommended elements are shown in Fig. 7.4, and some numerical evaluations of these elements are presented in the next chapter.

7.7 Comparison of Element with Elements Based on Plate Theory

In the previous Chapter, we presented the formulation of a general shell element for large displaement and rotation analysis. Both the U.L. and the T.L. formulations reduce as usual to a linear analysis in the first step of the incremental solution.

In the linear analysis of plates and shells, the element is identical to those discussed by Ahmad et al. [24], Zienkiewicz [4], and Hughes et al.

[53]. Ahmad, Irons and Zienkiewicz used the formulation employed in this report, whereas Hughes et al. employed the Mindlin plate theory that includes shear deformations to develop the stiffness matrix of the four-node quadrilateral element of the variable-number-nodes element.

The important point is that in linear analysis of plates, the variable-number-nodes element is based on classical plate theory including shear deformations and all element matrices can also be derived using this theory. Considering large displacement analysis, the element matrices are calculated using general nonlinear continuum mechanics equations with no assumptions on the magnitude of the plate or shell displacements and rotations. This approach is equivalent to using a general nonlinear shell theory.

8. SAMPLE ANALYSES

In this chapter the results of a number of sample analyses that demonstrate the versatility and effectiveness of the variable-number-nodes shell element are presented. First solutions are presented to some simple problems merely to demonstrate some important features of the element and modelling techniques of engineering problems (such as modelling of intersecting sections and reinforced structures). Next the solution of some important linear and highly nonlinear problems are presented.

8.1 Linear Analysis of Three Cantilevers

The objective in analyzing the three cantilevers is to show: the effects of element aspect ratio, modelling of variable thickness sections, and modelling of a stiffened structure.

(A) The results of the analysis of a uniform cantilever subjected to a tip transverse load are listed in Fig. 8.1. These results show that the cubic element can be employed without selective or reduced integration with very large aspect ratios, and the element does not display the stiffening effect that is observed with the low-order elements [4].

(B) The objective in reporting on the second cantilever analysis is to demonstrate the use of the transition element between solid and shell elements. Figure 8.2 shows the tapered cantilever analyzed, the model employed and the analysis results. In this analysis, a transition element was employed to model the transition region between the relatively thick root and thin tip of the structure. The transition element can be very useful in the analysis of some practical shell structures for which

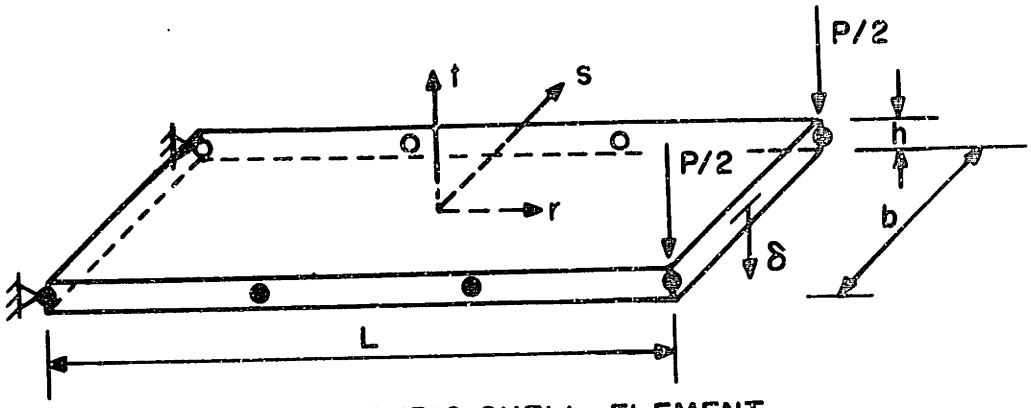

MODEL 1: ONE 8-NODE CUBIC SHELL ELEMENT, WITH 4x2x2 GAUSS INTEGRATION

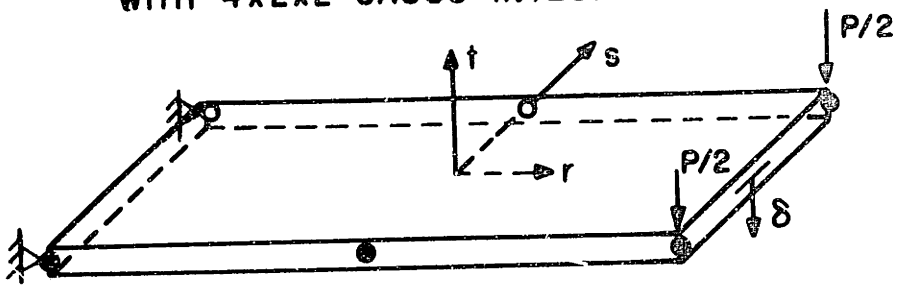

MODEL 2: ONE 6-NODE QUADRATIC SHELL ELEMENT, WITH 3x2x2 GAUSS INTEGRATION

ASPECT RATIO L/h	$(\delta-\delta_{Th})/\delta_{Th}$	
	MODEL 1	MODEL 2
10	.00500	-.22227
100	.00005	-.24970
1,000	.00000	-.25000
10,000	-.00001	-.25001

$$\delta_{Th} = \frac{PL^3}{3EI} \quad ; \quad I = \frac{bh^3}{12} \quad ; \quad E = \text{YOUNG'S MODULUS}$$

FIGURE 8.1 EFFECTS OF ASPECT RATIO IN LINEAR ANALYSIS OF A UNIFORM CANTILEVER

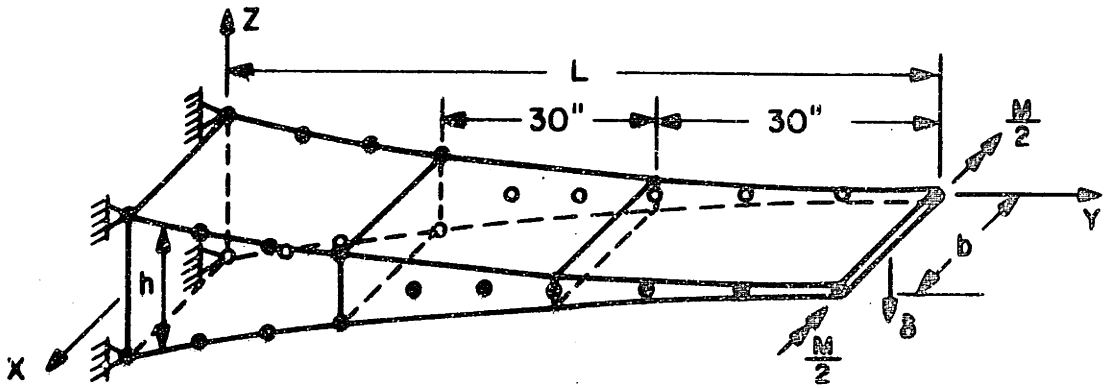

$E = 3.0 \times 10^7$ PSI

$\nu = 0$

L = 100 IN

b = 10 IN

$h = 10/(1 + 9\frac{Y}{L})$ IN

δ = CALCULATED TIP DEFLECTION

δ_{TH} = THEORETICAL TIP DEFLECTION
(NO SHEAR DEFORMATION INCLUDED)

M = CONCENTRATED END MOMENT

GAUSS INTEGRATION ORDER = 3x2x2

STRESSES (AT INTEGRATION POINTS)

LOCATION		$\frac{\sigma_{Th}-\sigma}{\sigma_{Th}}$
Y	Z	
3.3811	2.2133	0.0375
15.0	1.2284	-0.0044
26.6190	0.8501	0.0375
33.3811	0.7209	0.0013
45.0	0.5716	-0.0001
56.6190	0.4736	0.0013
64.5081	0.4242	0.0006
80.0	0.3520	-0.0001
95.4919	0.3008	0.0005

$$\frac{\delta_{Th}-\delta}{\delta_{Th}} = 0.0022$$

FIGURE 8.2 LINEAR ANALYSIS OF A TAPERED CANTILEVER

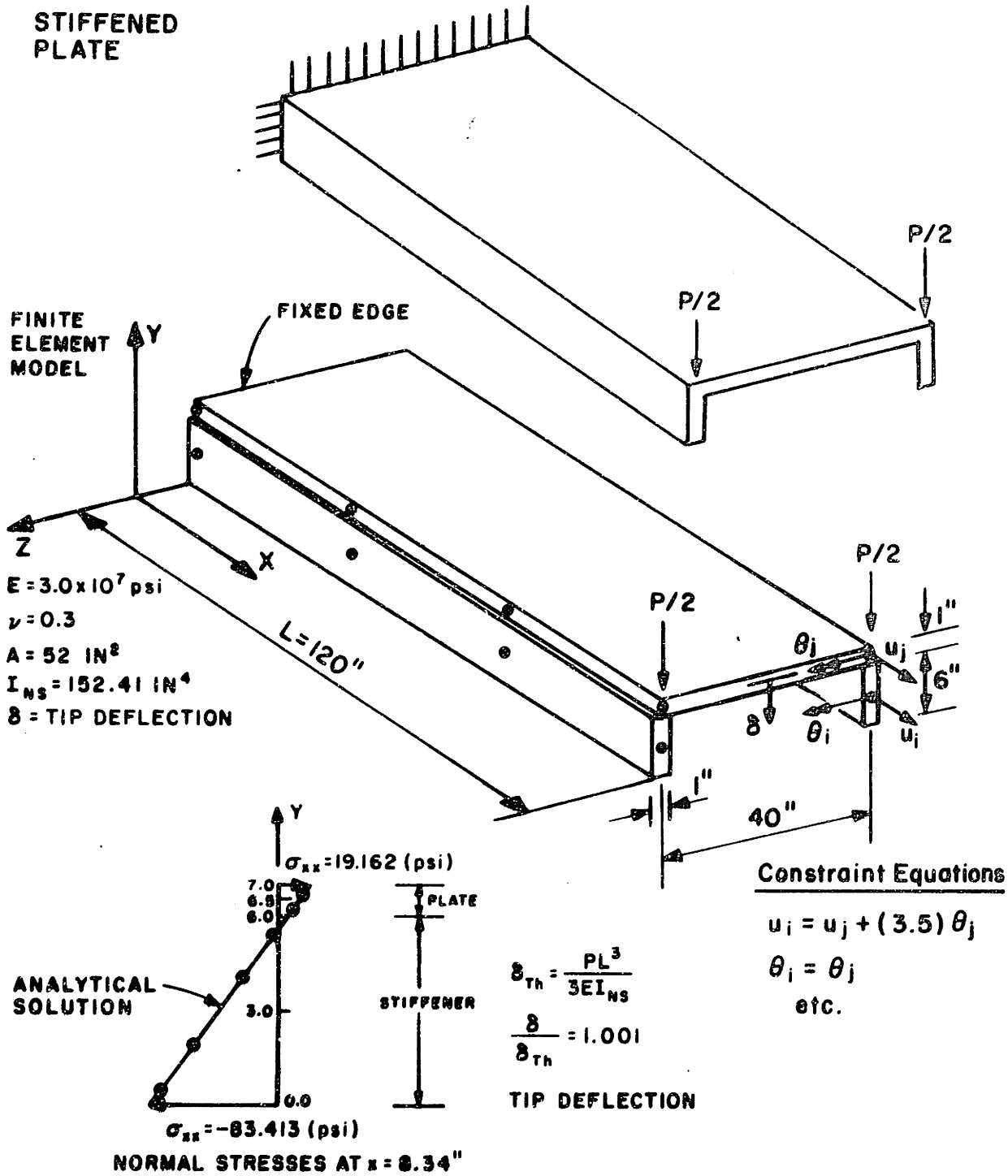

FIGURE 8.3 LINEAR ANALYSIS OF A STIFFENED PLATE

shell-solid regions must be included in the analysis (e.g. analysis of arch dams and foundations, turbine blades mounted on a shaft) and in the modeling of shell intersections and branches.

(C) The third cantilever analysis illustrates the use of the shell element in conjunction with the three-dimensional bending element in the analysis of stiffened plates and shells. Figure 8.3 shows the cantilever plate model used and the response predicted. The analysis results compare well with the solution calculated using elementary beam theory.

8.2 Linear Analysis of Folded Plates

A folded plate is analyzed using shell elements. The intersecting region is idealized by the following three models (a) transition element, i.e., using top and bottom surface nodes at the intersecting boundary, (b) defining a single node at the boundary common to the both plates and assigning an average normal to this node. (c) assigning one node to each plate at the intersecting boundary, and the normal vector at each node is normal to the plate that contains that node. The constraint equations are used to represent the common nodal point rotations and displacements at the intersecting boundary, Fig. 8.4.

In this figure the tip deflection of the structure using all three models are shown. It is seen that the constraint equation technique is most effective in this case. It should be mentioned that the above techniques can be applied directly to the intersection region of shells.

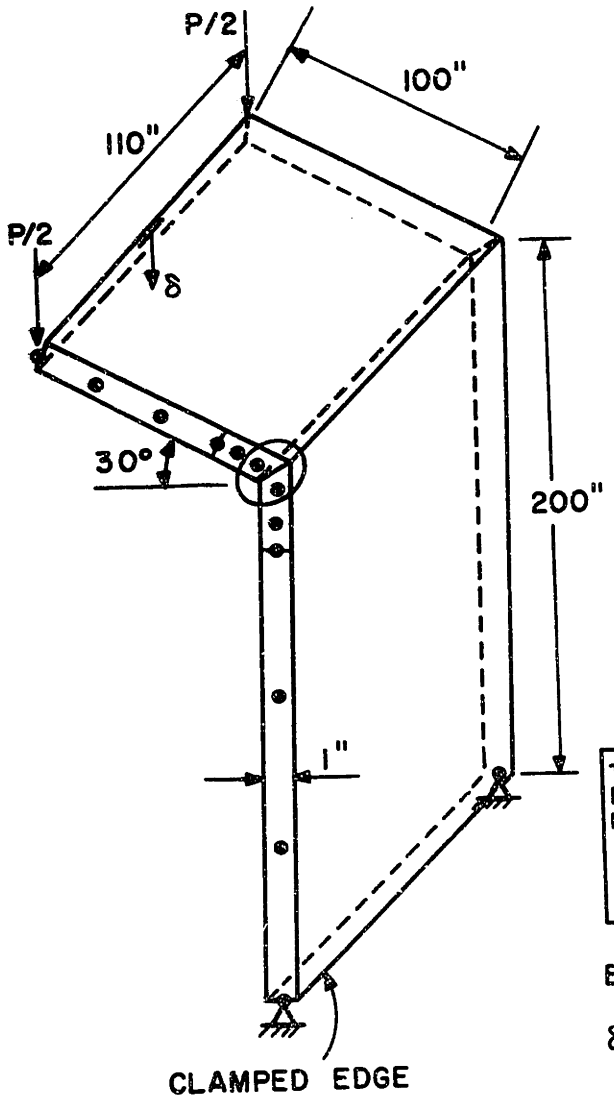

MODELING OF SHELL INTERSECTIONS			
	MODEL (a)	MODEL (b)	MODEL (c)
	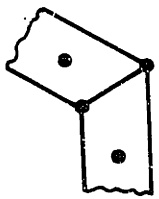	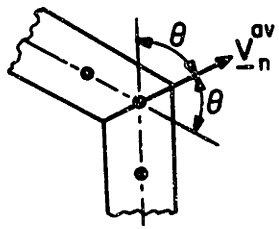	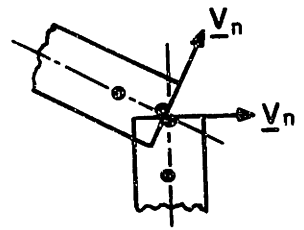
	USE OF TRANSITION ELEMENTS	USE OF AVERAGE NORMAL	USE OF CONSTRAINT EQUATIONS
TIP DEFLECTION RATIO δ/δ^{Th}	1.0176	0.9970	1.0000

$E = 10^6$ psi , $\nu = 0$

δ^{Th} = TIP DEFLECTION , USING BEAM THEORY

FIGURE 8.4 ANALYSIS OF FOLDED PLATES

8.3 Linear Analysis of a Cylindrical Shell

The thin cylindrical shell shown in Fig. 8.5 was analyzed for its static response. The cylinder is freely supported at its ends and is loaded by two centrally located and diametrically opposed concentrated forces. Using the double symmetry of the structure and the loading, only one-eigth of the cylinder was analyzed.

This structural problem was employed to study the convergence of the shell element when using different element nodal configurations and increasing the number of elements. The different element assemblages considered in this study are: (i) quadratic elements, with 8 and 9-node quadrilaterals and 6-node triangular shape and, (ii) cubic elements with 12- and 16-nodes quadrilaterals, Fig. 8.6. Also the effects of integration order on the rate of convergence of displacements predicted using the different element asemblies were examined.

The predicted numerical values of the lateral displacements at point C, w_C, and axial displacements at point D, u_D, (see Fig. 8.5) are given in Fig. 8.7. The ratio of the computed displacements w_C and u_D to the theoretical values reported by Lindberg [48] are shown in Fig. 8.8. It is seen that as expected, using the lower-order integration in the finite element analysis, in general, improves the predicted displacements. However, Fig. 8.8 also shows that using cubic elements (12-nodes and 16-nodes) with high-order integration the displacements converge rapidly as the number of elements used in the idealization is increased. Figure 8.9 shows that for the 6 x 6 element idealizations, the

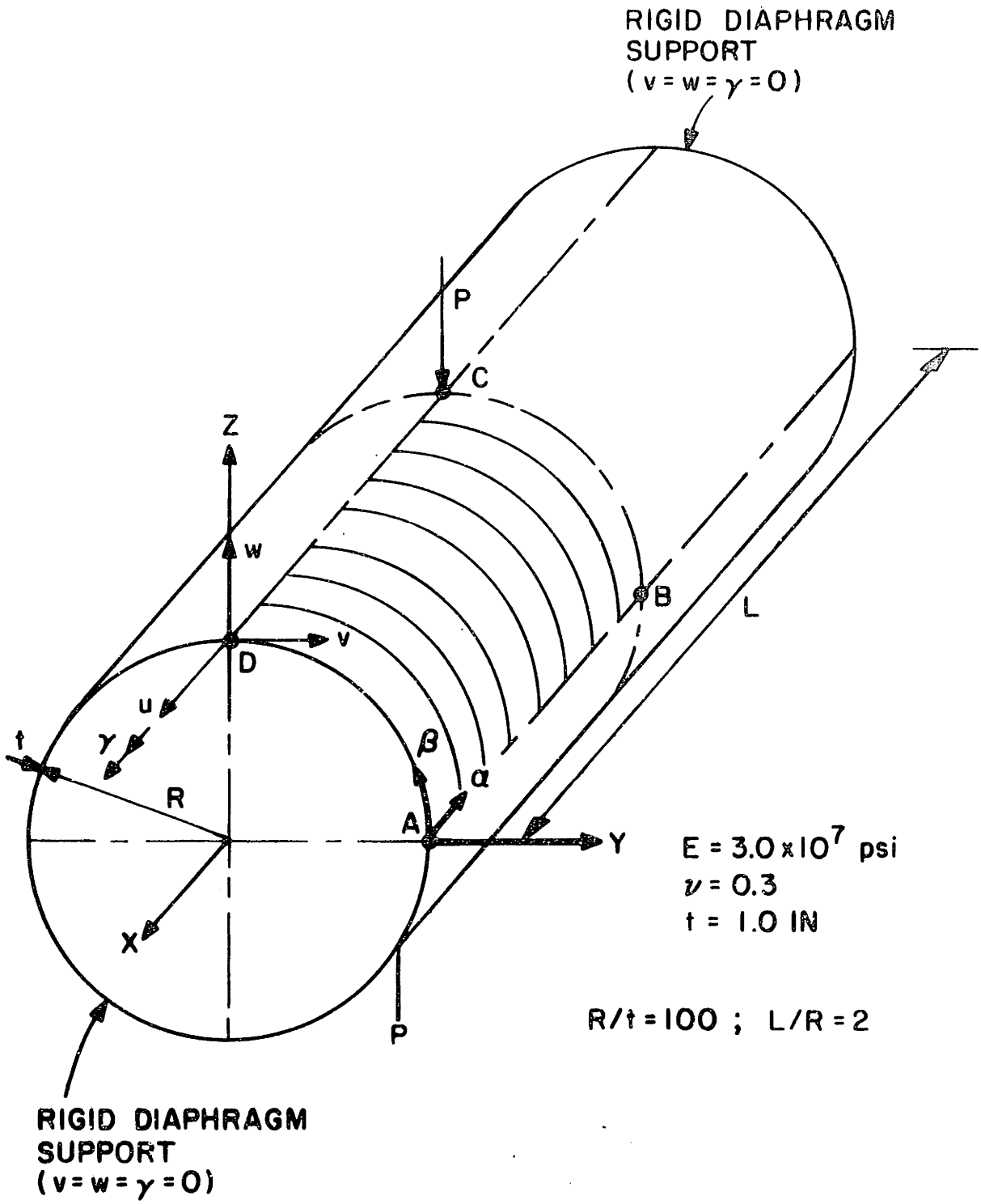

FIGURE 8.5 PINCHED CYLINDRICAL SHELL

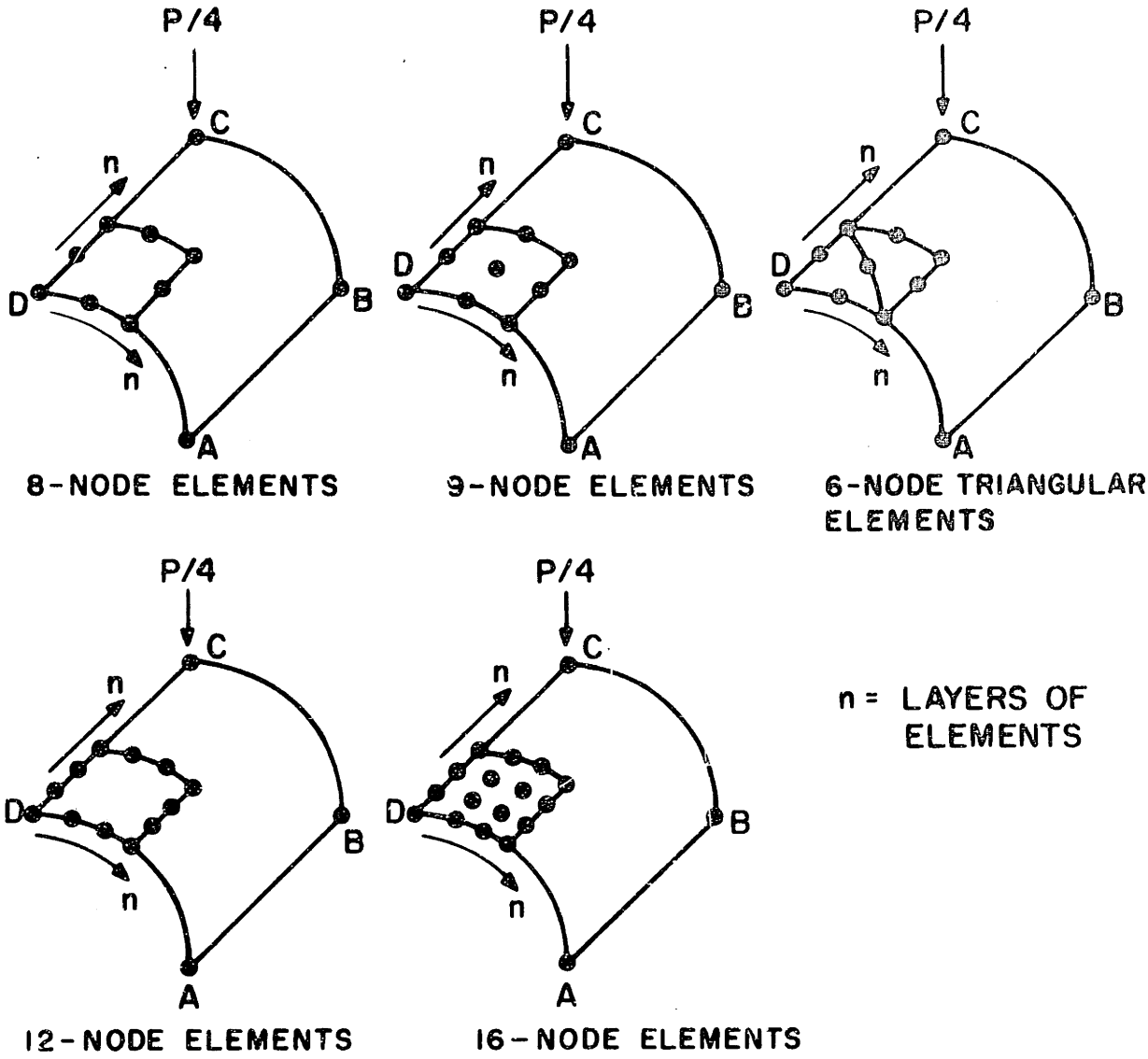

FIGURE 8.6 FINITE ELEMENT MODELS OF A PINCHED CYLINDRICAL SHELL

F.E.Grid	8-Node		9-Node		6-Node Triangle	12-Node		16-Node		Element
	3x3x2	2x2x2	3x3x2	2x2x2	7x2	4x4x2	3x3x2	4x4x2	3x3x2	Integ. Order
2x2	-	-	-	-	-	-16.83	-72.75	-20.05	-152.32	$\frac{EtW_c}{P}$
3x3	-12.92	-135.15	-13.86	-153.20	-12.82	-	-	-	-	
4x4	-24.01	-146.44	-25.69	-161.19	-22.38	-83.01	-138.73	-92.46	-163.93	
5x5	-39.08	-154.85	-41.62	-164.32	-35.52	-	-	-	-	
6x6	-55.77	-158.01	-58.99	-165.23	-	-	-	-138.98	-166.44	

Analytical value; $\left(\frac{EtW_c}{P}\right)_{analytical} = -164.24$

FIGURE 8.7. Numerical Value of W_c and U_D

F.E. Grid	8 - Node		9 - Node		6 - Node Triangle	12 - Node		16 - Node		Element
	3x3x2	2x2x2	3x3x2	2x2x2	7X2	4x4x2	3x3x2	4x4x2	3x3x2	Integ. Order
2 x 2	—	—	—	—	—	.917	2.957	.902	2.170	$\frac{EtU_D}{P}$
3 x 3	.734	4.111	.728	2.665	.691	—	—	—	—	
4 x 4	1.242	3.775	1.238	2.599	1.137	3.265	4.118	3.372	2.900	
5 x 5	1.838	3.974	1.826	2.784	1.703	—	—	—	—	
6 x 6	2.361	4.089	2.353	2.843	—	—	—	3.979	2.979	

Analytical value ; $\left(\frac{EtU_D}{P}\right) = 4.114$

FIGURE 8.7. (continued)

TYPE OF ELEMENTS	INTEGRATION ORDER	SYMBOL
8 NODES	3 x 3 x 2 2 x 2 x 2	—○— —●—
9 NODES	3 x 3 x 2 2 x 2 x 2	---□--- ---■---
6 NODES (TRIANGLE)	7 x 2	—×—

TYPE OF ELEMENTS	INTEGRATION ORDER	SYMBOL
12 NODES	4 x 4 x 2 3 x 3 x 2	-·-▽·-· -·-▼·-·
16 NODES	4 x 4 x 2 3 x 3 x 2	- -◇- - - -◆- -

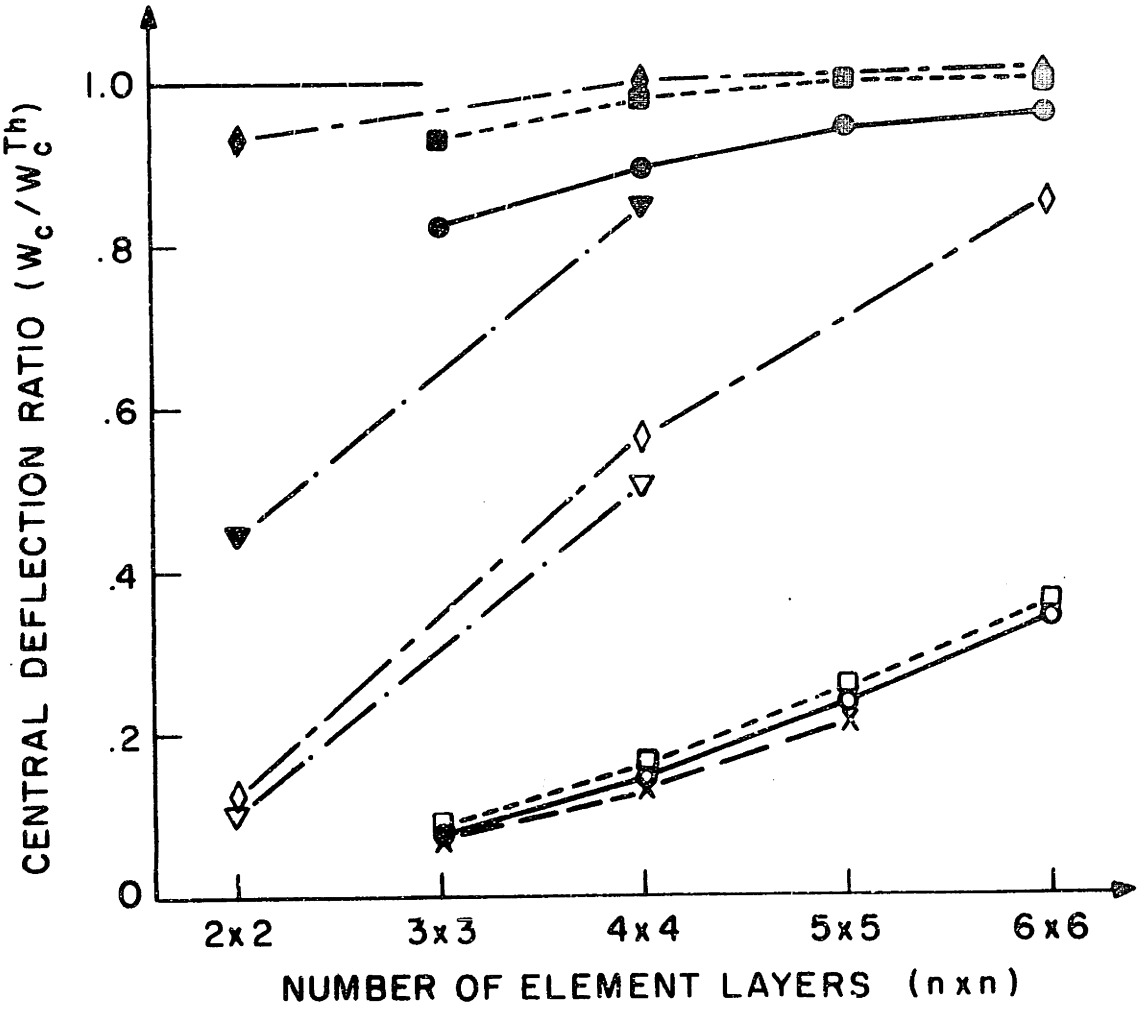

FIGURE 8.8 DISPLACEMENTS CONVERGENCE STUDY OF A PINCHED CYLINDRICAL SHELL

TYPE OF ELEMENTS	INTEGRATION ORDER	SYMBOL
8 NODES	3 x 3 x 2 2 x 2 x 2	—○— —●—
9 NODES	3 x 3 x 2 2 x 2 x 2	---□--- ---■---
6 NODES (TRIANGLE)	7 x 2	— —X— —

TYPE OF ELEMENTS	INTEGRATION ORDER	SYMBOL
12 NODES	4 x 4 x 2 3 x 3 x 2	—·—▽—·— —·—▼—·—
16 NODES	4 x 4 x 2 3 x 3 x 2	— - ◊ — - — - ◆ — -

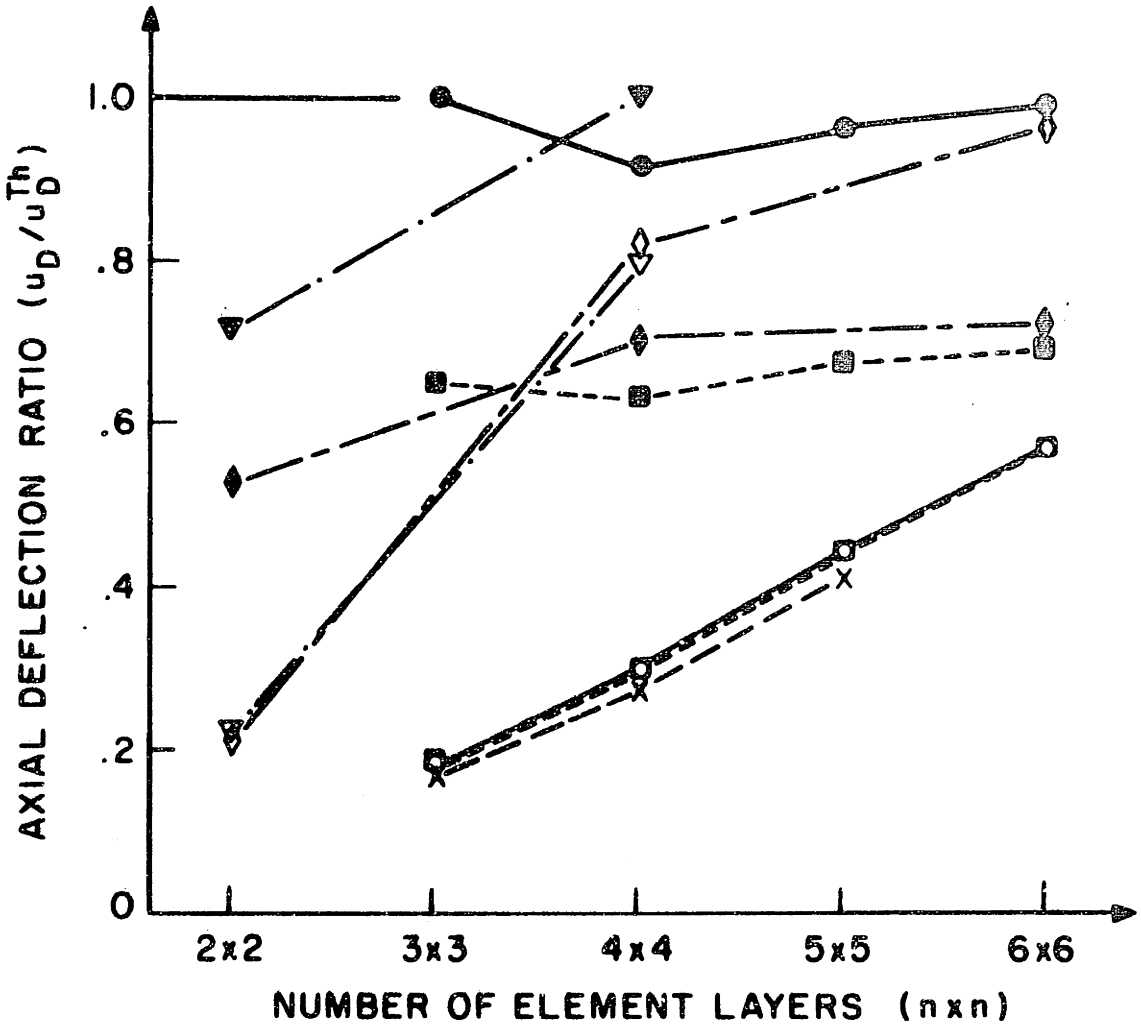

FIGURE 8.8 (Continued)

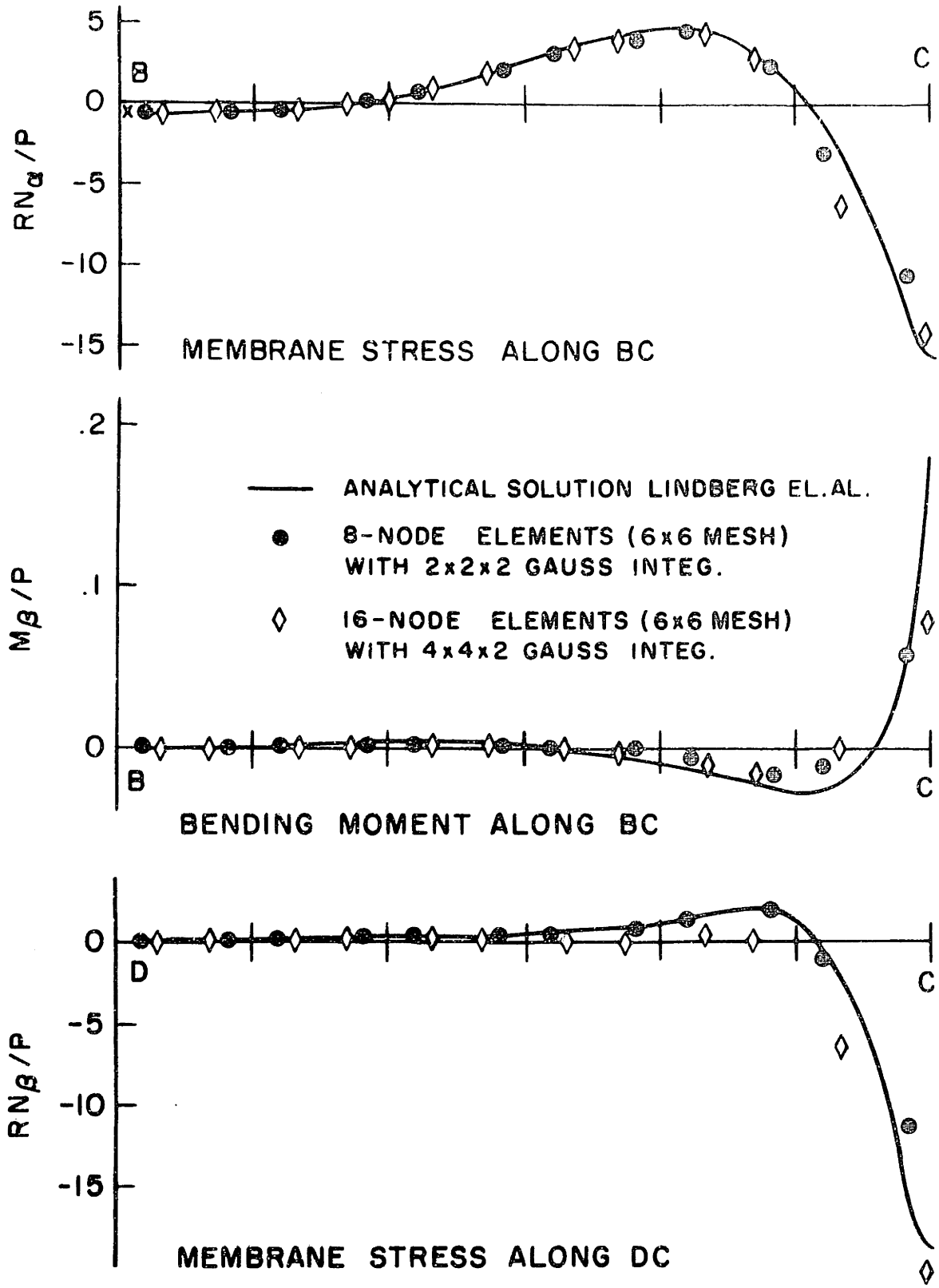

FIGURE 8.9 STRESS DISTRIBUTIONS OF A PINCHED CYLINDRICAL SHELL

(the element stresses have been calculated in the finite element solutions at the integration points that are closest to the section considered)

stress distributions are predicted accurately compared to analytical values using the 8 node element with 2 x 2 x 2 Gauss integration and the 16-node element with 4 x 4 x 2 Gauss integration.

8.4 Elastic-Plastic Dynamic Analysis of a Simply Supported Plate

A dynamic analysis of a simply supported square plate subjected to lateral pressure loading was carried out. The Newmark time integration method was used with the time step increment $\Delta t = \frac{T_f}{48}$, where T_f is the fundamental period of the linear elastic plate. Nine 8-node quadratic shell elements were used to model a quarter of the plate. In a first analysis an elastic and in a second analysis an elastic-perfectly plastic material was assumed.

Figure 8.10 shows the predicted response for both material property assumptions, and compares the calculated response with a solution given by Liu and Lin [49].

8.5 Large Displacement/Rotation Analysis of a Cantilever

A cantilever subjected to a concentrated end moment was idealized using one 8-node cubic element. Figure 8.11 shows the load deflection curves for different displacemnt/rotation variables. The predicted response shows excellent agreement with the analytical solution [28].

8.6 Elastic-Plastic Instability Analysis of a Column

The column shown in Fig. 8.12 was analyzed for its large displacement elastic-plastic response. Two different finite element idealizations were employed in the study. Namely, one model using six quadratic shell elements (using 2 x 2 x 2 Gauss integration) and another model using

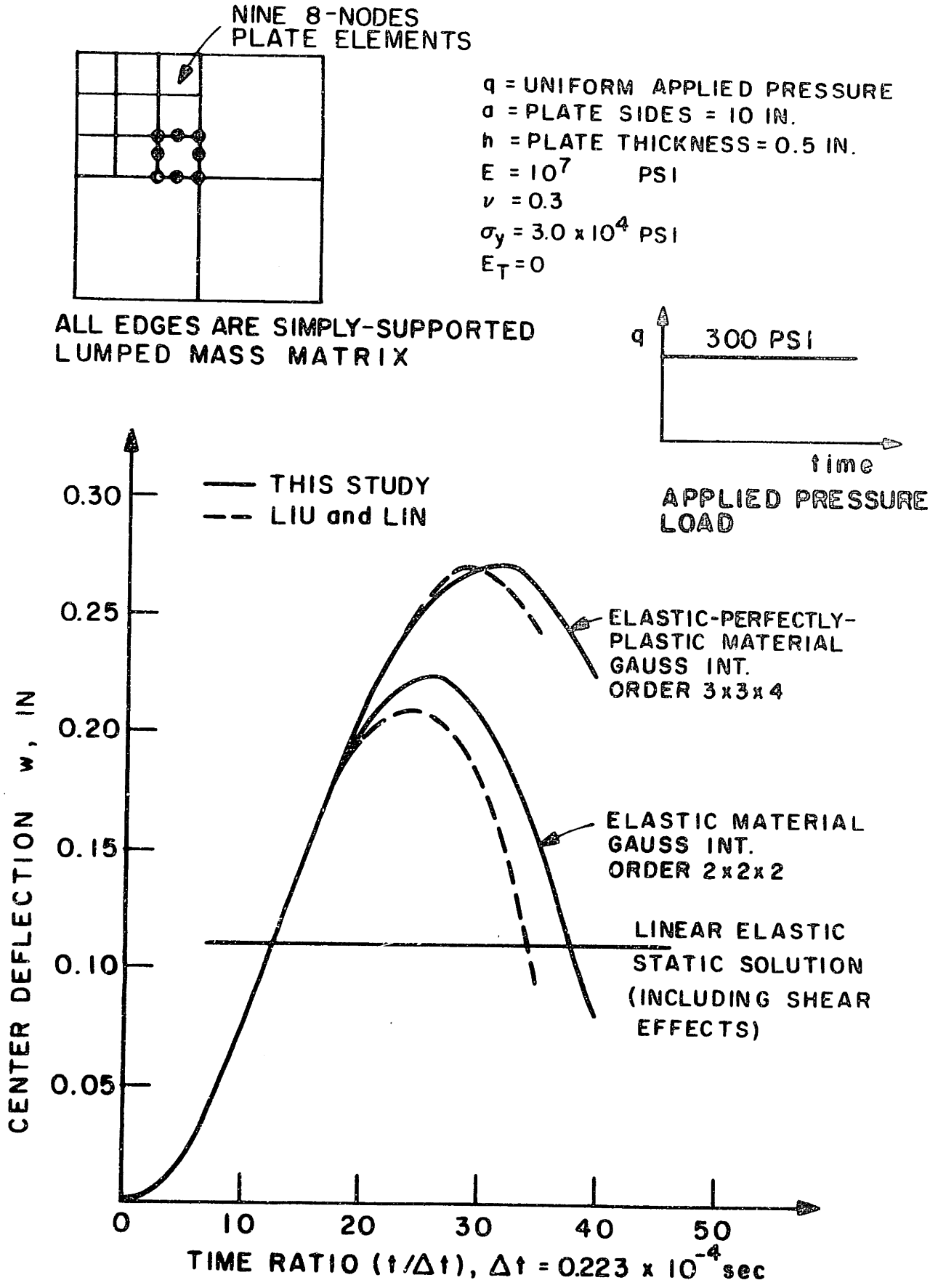

FIGURE 8.10 ELASTIC AND ELASTIC-PLASTIC DYNAMIC RESPONSE OF A SIMPLY SUPPORTED SQUARE PLATE

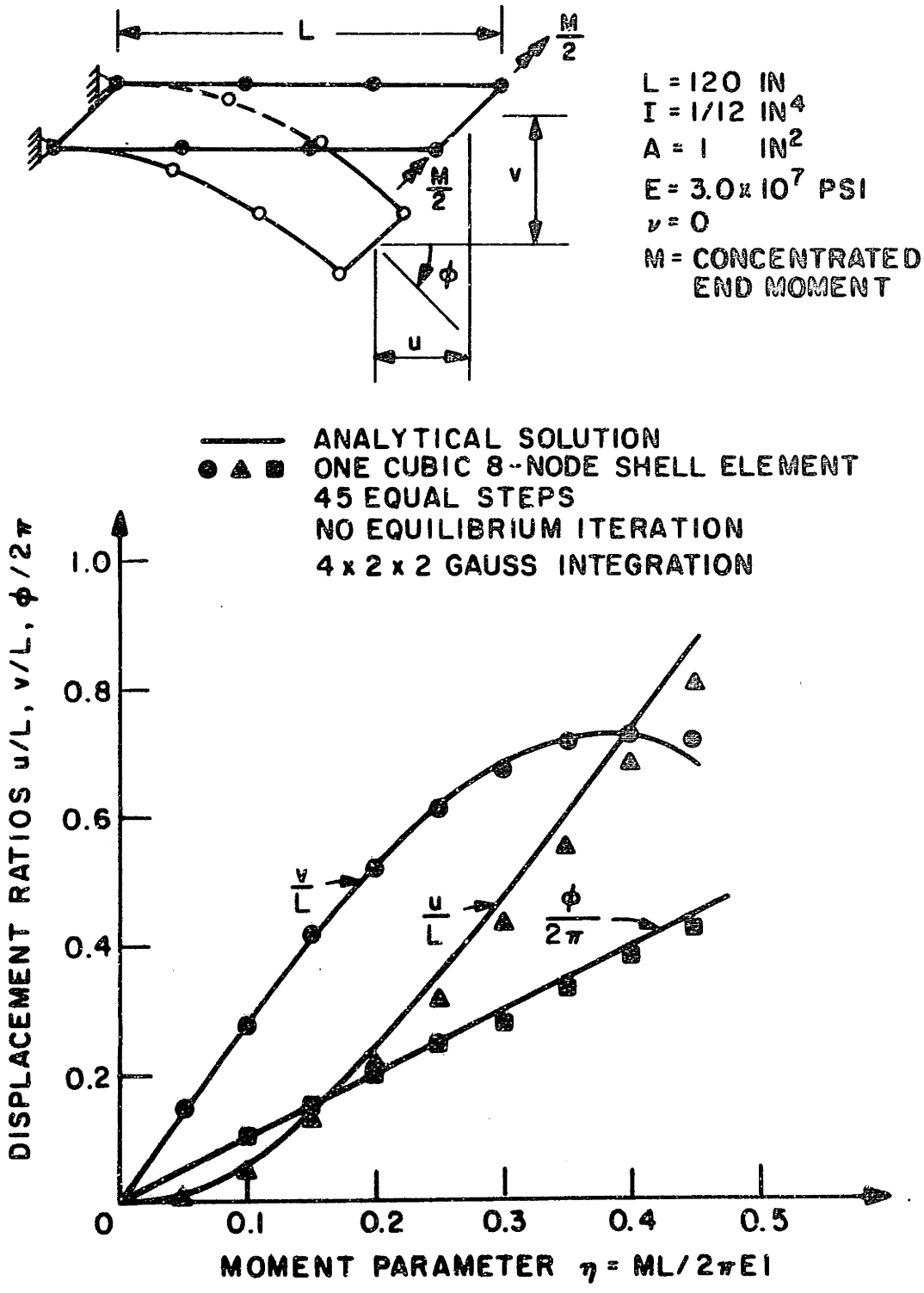

FIGURE 8.11 LARGE DEFLECTION RESPONSE OF A CANTILEVER SUBJECTED TO AN END MOMENT

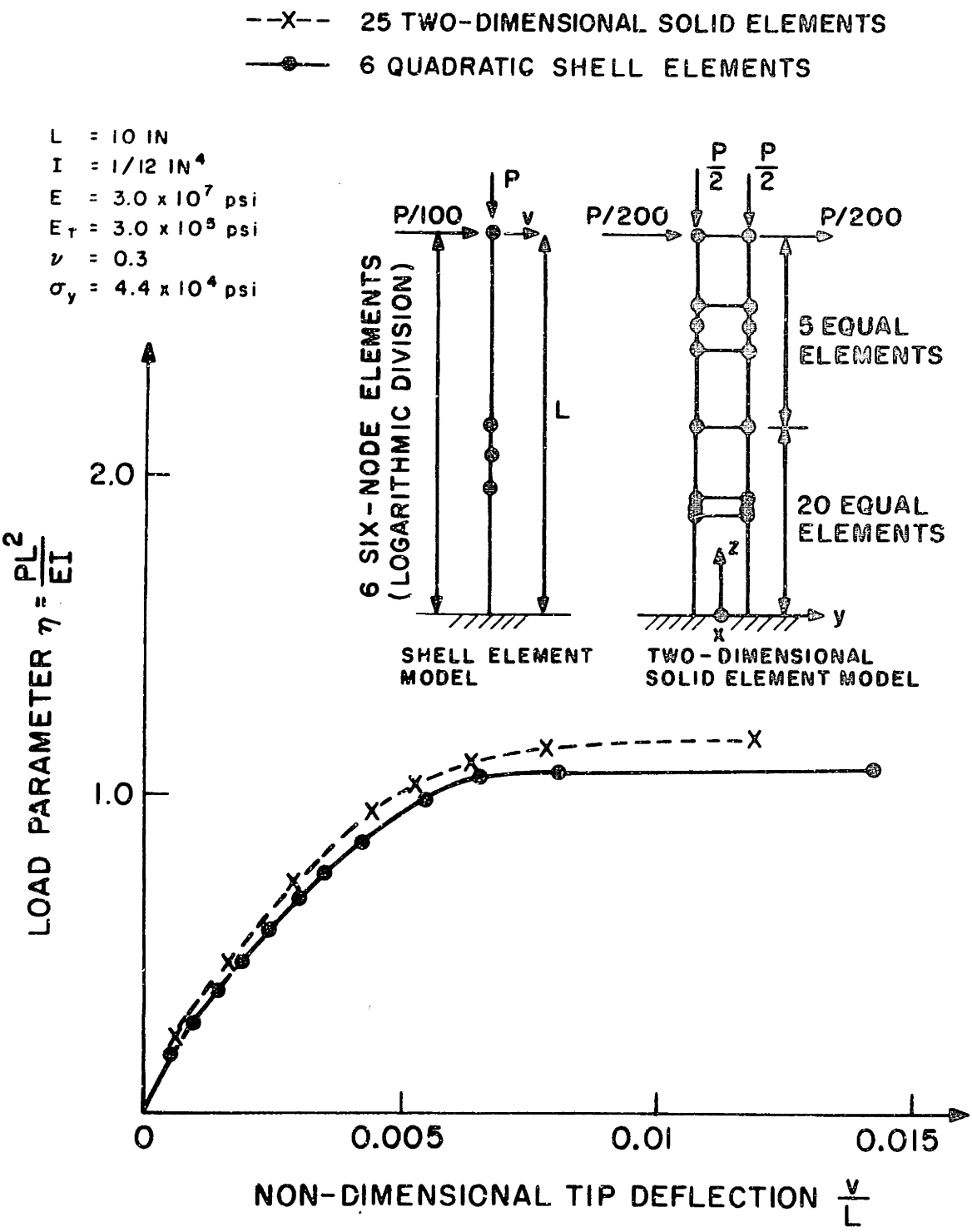

FIGURE 8.12 ELASTIC-PLASTIC INSTABILITY ANALYSIS OF A COLUMN

twenty-five 6-node isoparametric two-dimensional elements (with 4 x 4 Gauss integration).

Figure 8.12 shows the calculated response of the column using the two finite element idealizations. It is seen that the predicted collapse load is slightly higher using the two-dimensional element model.

8.7 Large Deflection Analysis of a Diamond Structure

A diamond structure constructed of four equal length bars and loaded as shown in Fig. 8.13 was analyzed using five 6-node quadratic shell elements. Using the symmetry of the structure and its loading only one quarter of the structure (one of the beams) was modeled. The finite element model used and the predicted load deflection response of the structure are shown in Fig. 8.13. The predicted response shows excellent agreement with the analytical solution [50].

Figure 8.14 shows various equilibrium positions of the structure at different load levels. The deformed shapes of the structure compare very closely to the analytically calculated shapes.

8.8 Large Displacement Analysis of an Elastic Simply-Supported Plate

The simply supported square plate subjected to a uniformly distributed pressure shown in Fig. 8.15 was analyzed for its large deflection response. One single 16-node shell element was used to model one quarter of the plate. The total Lagrangian formulation was employed.

Figure 8.15 shows the displacement response predicted in the finite element analysis. The computed displacement response is very close to the solutions given by Levy [51], where the effect of using

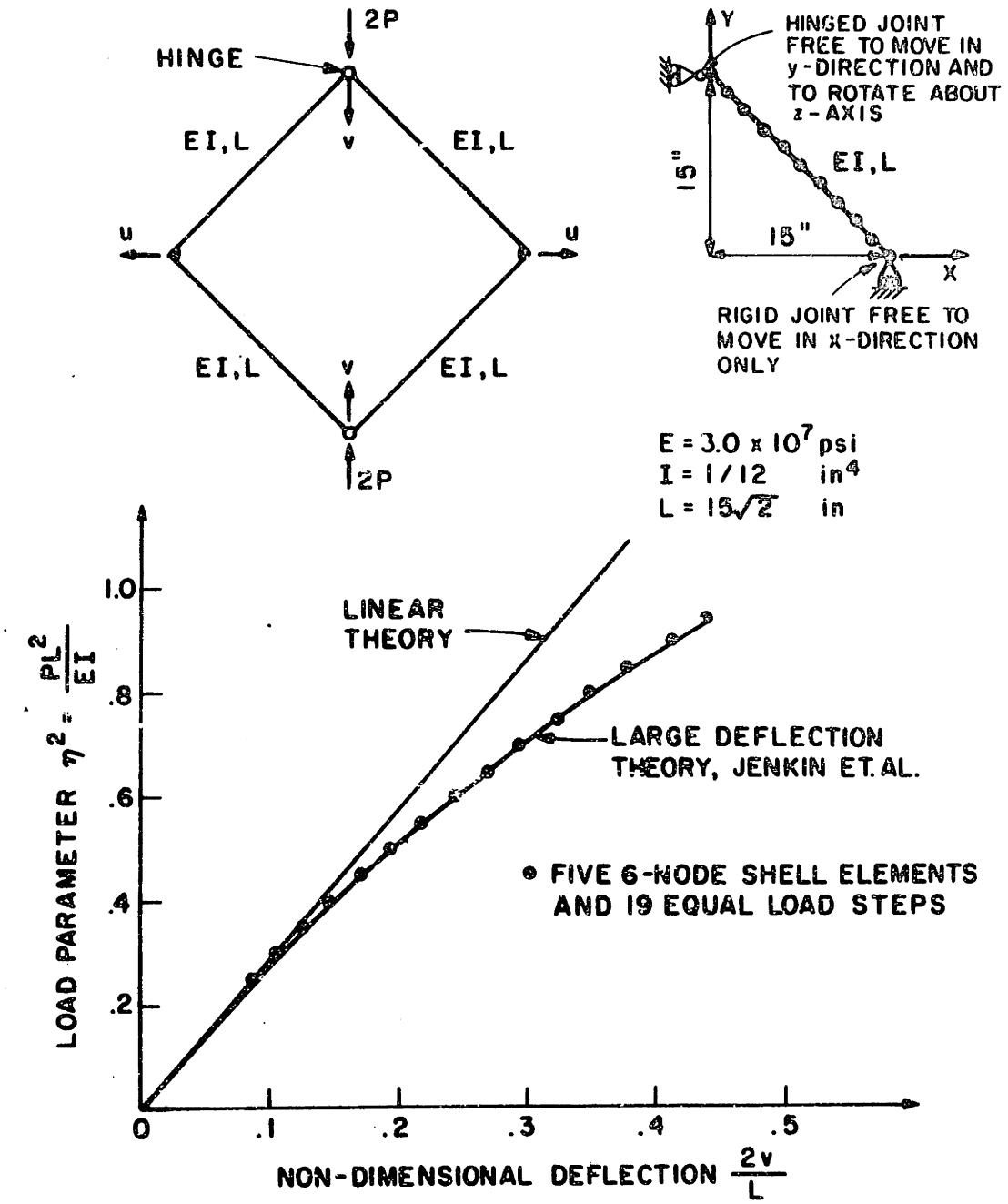

FIGURE 8.13 LOAD DEFLECTION CURVE FOR A DIAMOND STRUCTURE

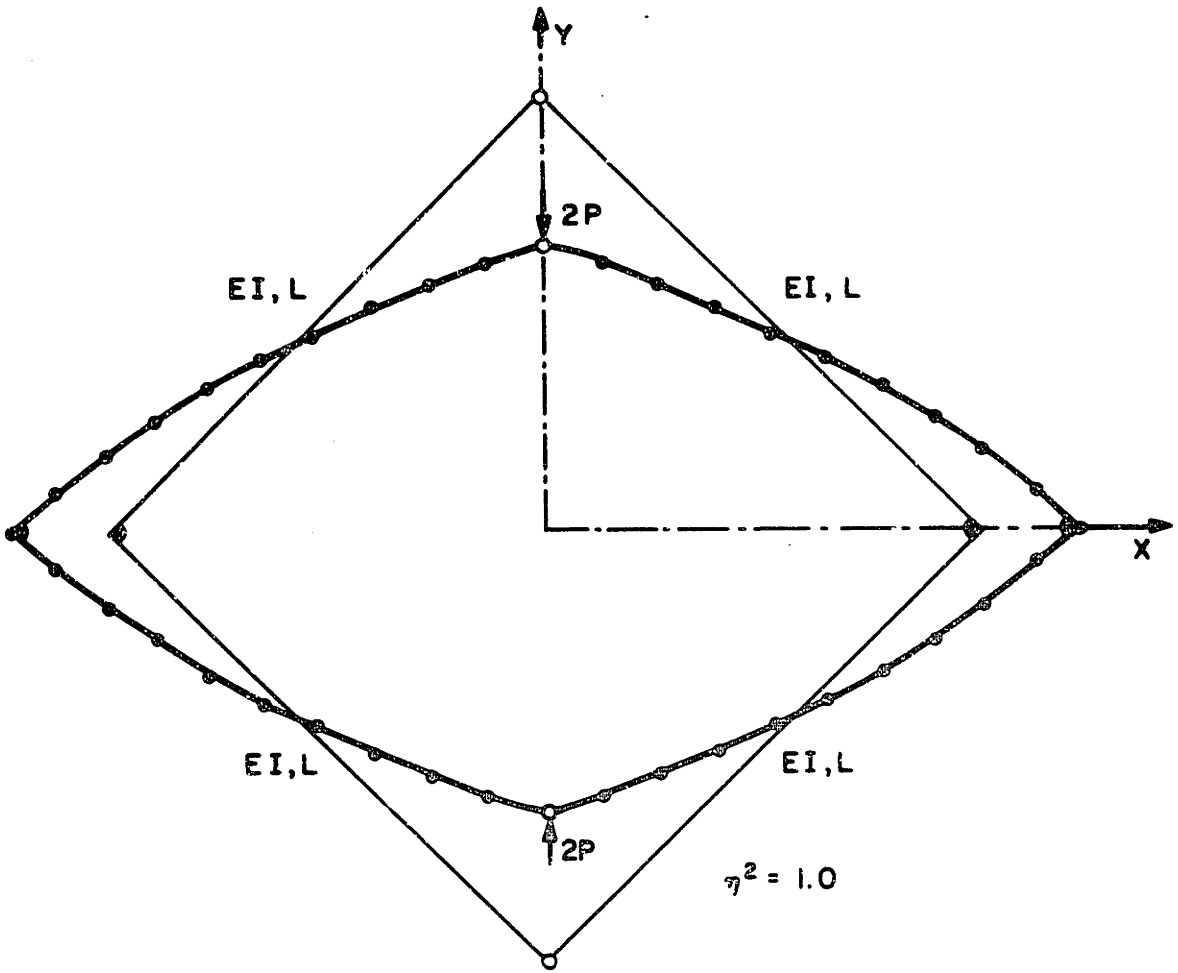

FIGURE 8.14 DEFORMED SHAPES OF THE DIAMOND STRUCTURE FOR DIFFERENT VALUES OF THE LOADING PARAMETER $\eta^2 = PL^2/EI$

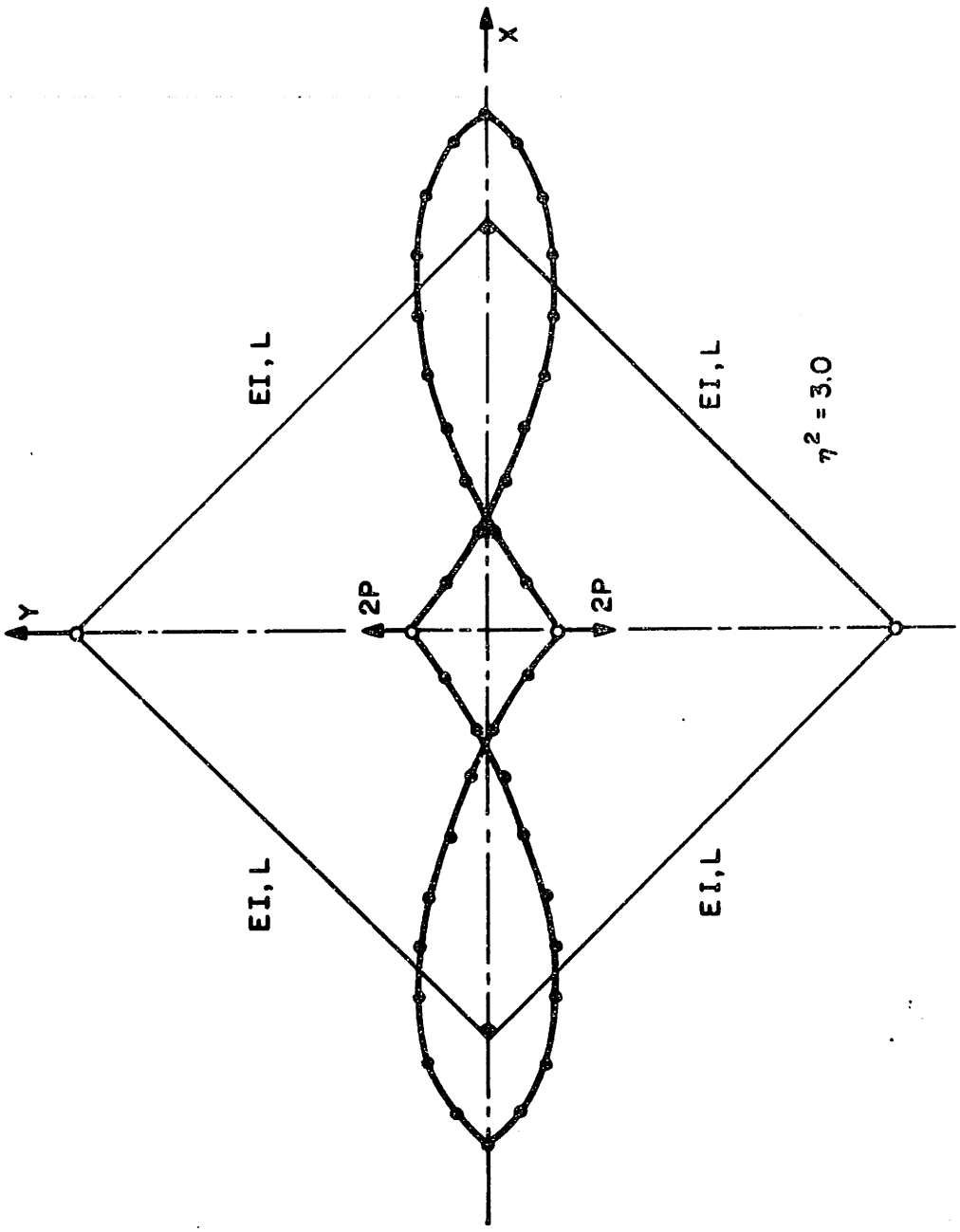

FIGURE 8.14 (Continued)

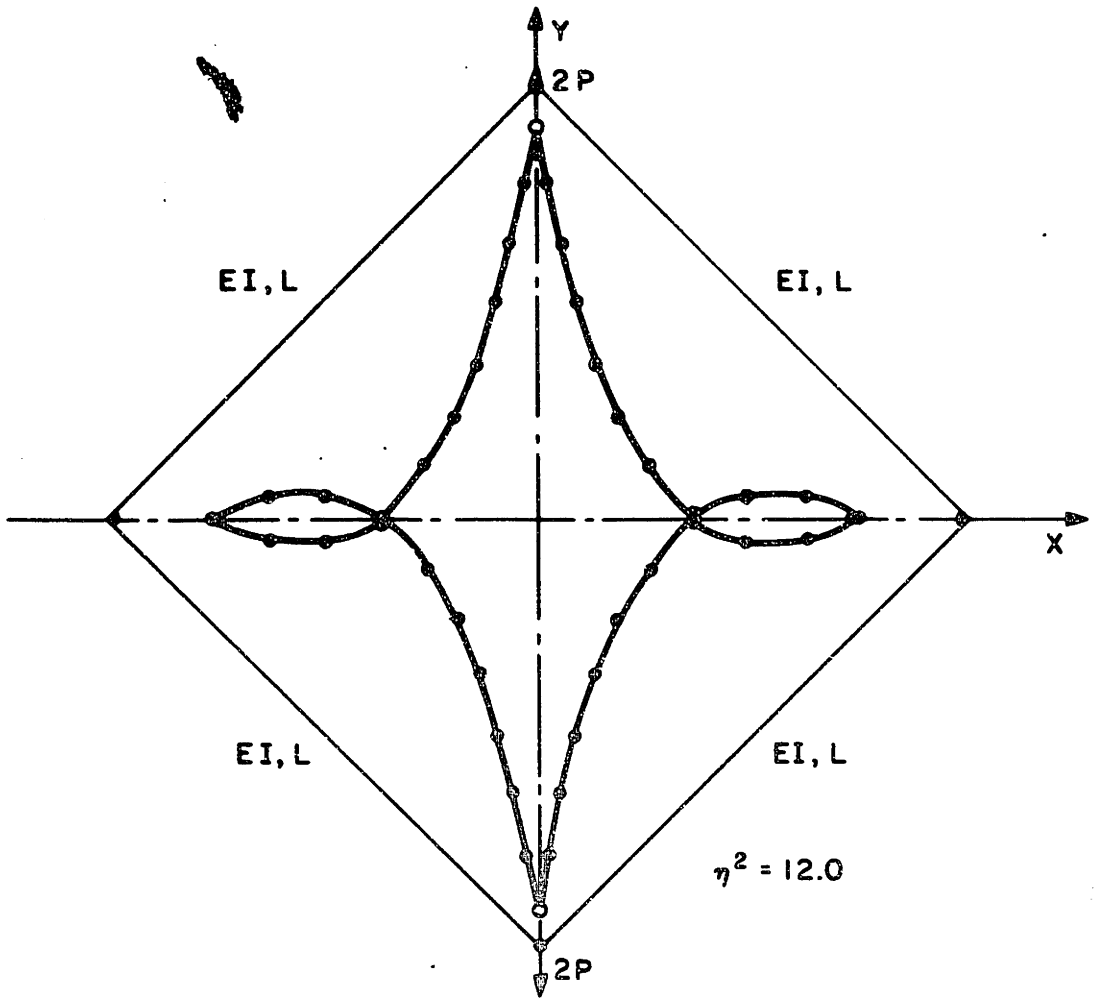

FIGURE 8.14 (Continued)

different assumptions on the plate edge in-plane displacements should be noted. The predicted stresses are shown in Fig. 8.16, which is very close to the analytical values given by Levy.

It should be noted that the predicted non-dimensional displacements and stresses are identical for plate aspect ratios of 200 and 2000.

The effect of the element aspect ratio on the performance of the 16-node element was investigated by considering the linear analysis of the same plate. The results shown in the table below shows that the cubic Lagrangian element can be employed with very large aspect ratios a/h. It is observed that the predicted response is higher than theoretical values at low element aspect ratio. This is because the reference analytical value does not allow for shear deflection [2, pp. 108-110]. However, the predicted value is very close to the analytical displacement value when shear effects are considered [58].

Aspect ratio a/h	$(w-w_{Th})/w_{Th}$
10	.10019
20	.03726
50	.01811
100	.01536
1000	.01445
10000	.01445

$$w_{Th} = .00416 \frac{q a^4}{D}$$

$$D = \frac{Eh^3}{12(1-\nu^2)}$$

w = central deflection of the plate

Effect of Aspect Ratio on the Performance of Cubic Lagrangian Element

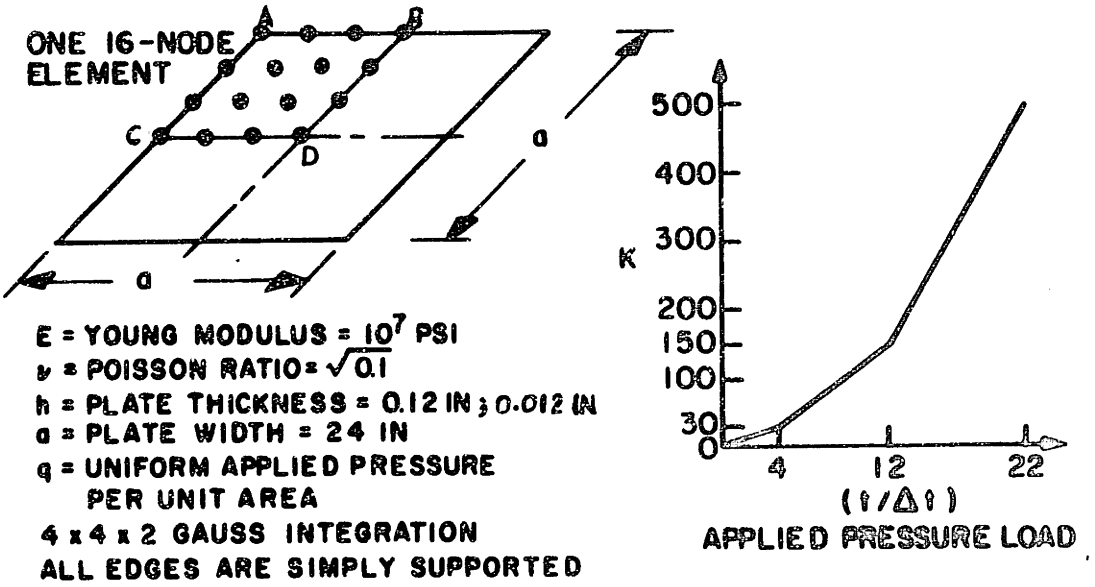

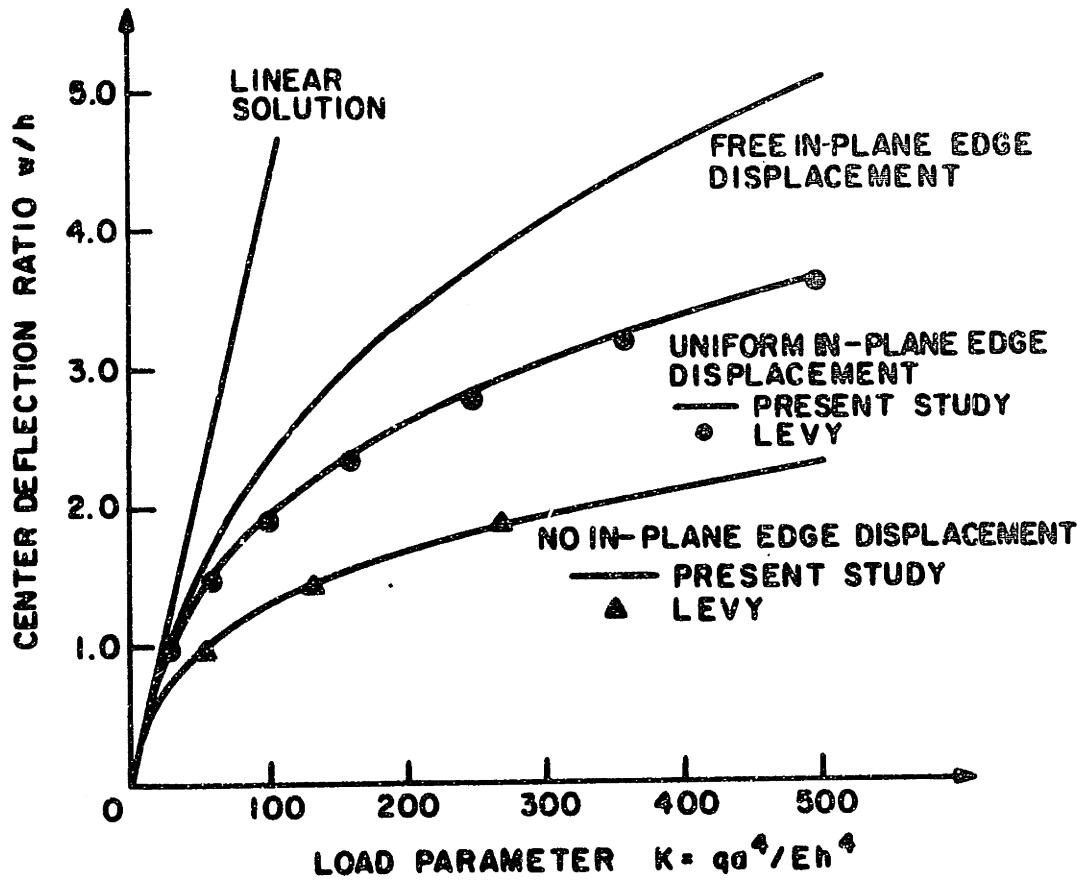

FIGURE 8.15 LARGE DEFLECTION ANALYSIS OF A SIMPLY-SUPPORTED SQUARE PLATE SUBJECTED TO PRESSURE LOADING

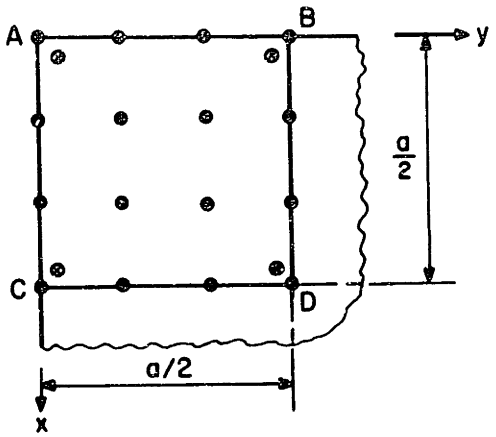

ONE 16-NODE ELEMENT TO MODEL 1/4 OF THE PLATE

E = YOUNG MODULUS = 10^7 PSI
ν = POISSON RATIO = $\sqrt{0.1}$
h = PLATE THICKNESS = 0.12 IN, 0.012 IN
a = PLATE WIDTH = 24 IN
q = UNIFORM APPLIED PRESSURE PER UNIT AREA
4 x 4 x 2 GAUSS INTEGRATION
ALL EDGES ARE SIMPLY SUPPORTED WITH UNIFORM IN-PLANE EDGE DISPLACEMENT

$\frac{a}{h}$ = 200, 2000

$\sigma_r = E(\frac{h}{a})^2$

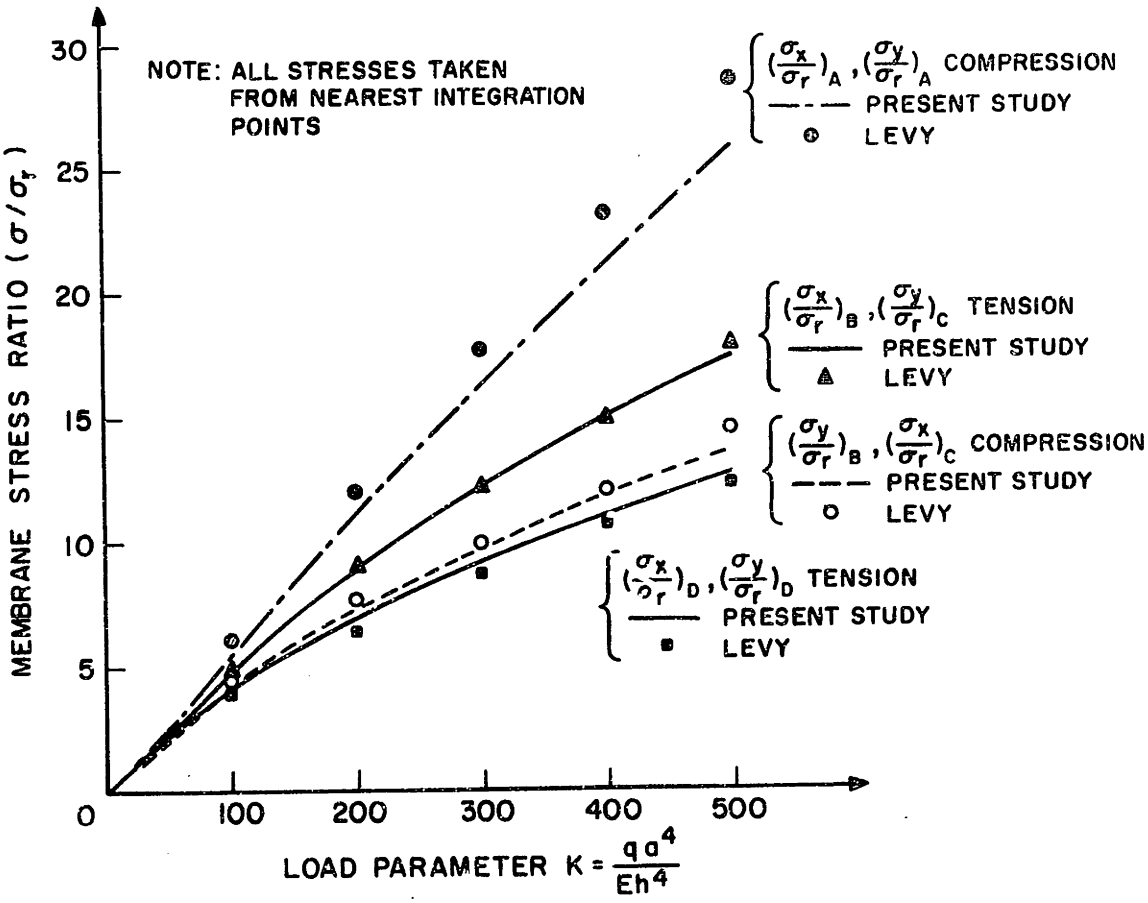

FIGURE 8.16 MEMBRANE STRESSES OF THE SIMPLY-SUPPORTED SQUARE PLATE (UNIFORM IN-PLANE EDGE DISPLACEMENT)

8.9 Large Deflection Analysis of a Shallow Cylindrical Shell

A shallow cylindrical shell with a concentrated central load was analyzed for its large deflection behavior. The longitudinal boundaries are hinged and immovable whereas the curved edges are completely free, Fig. 8.17. The material of the shell is assumed to remain elastic.

One 16-node shell element was used to idealize a quarter of the shell because of its geometrical and loading symmetry. The subtended angle by the element is 0.1 radian. Gauss integration order of 4x4x2 was used to evaluate element matrices and force vector. The same shell was analyzed by Horrigmoe [15] using 3x3 meshes of quadrilateral and triangular elements. The predicted central deflection response, using one shell element shown in Fig. 8.17. It is seen that the predicted response is in good agreement with Horrigmoe results and also response reported by Sabir and Lock [54]. The predicted maximum load (before the shell snap-through) is P_{max} = 2.24 (KN), which compares very closely to the value P_{max} = 2.22 (KN) reported by Horrigmoe.

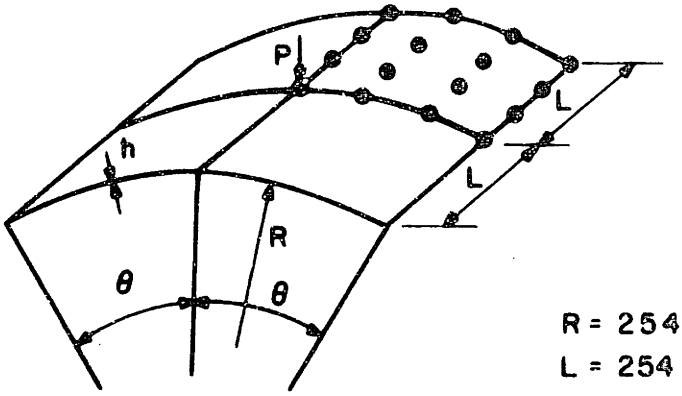

R = 2540 mm
L = 254 mm
h = 12.7 mm
θ = 0.1 rad.
E = 3102.75 N/mm^2
ν = 0.3

STRAIGHT EDGES ARE HINGED
AND IMMOVEABLE
CURVED EDGES ARE FREE

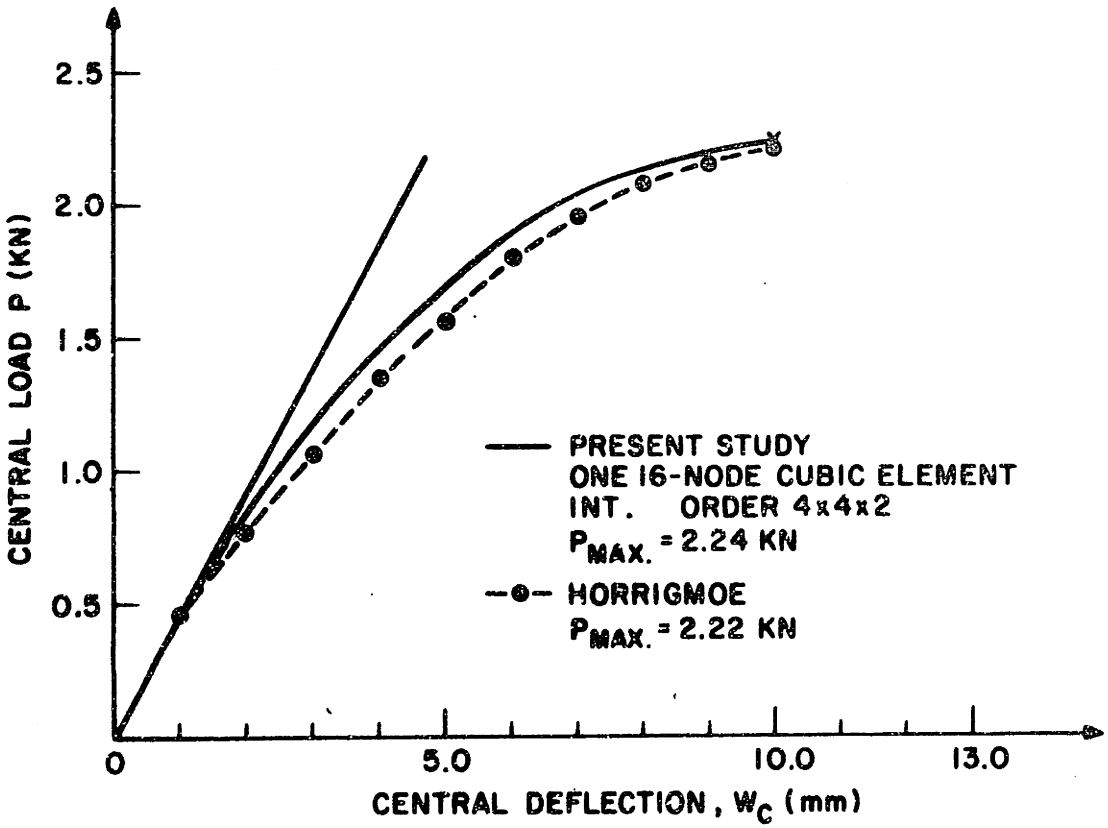

FIGURE 8.17 CENTRAL DEFLECTION OF A HINGED SHALLOW CYLINDRICAL SHELL

8.10 Large Deflection Analysis of a Spherical Shell

The spherical shell shown in Fig. 8.18 subjected to a concentrated load P is analyzed for its large deflection behavior. All edges of the shell are hinged and immovable. The geometrical and physical properties of the shell are given in Fig. 8.18.

One quarter of the shell was modeled by one 16-node cubic shell element with 4x4x2 Gauss integration order. The same shell was analyzed by Horrigmoe [15], who used 5x5 mesh, and Dhatt [55], and Leicester [56] employed series solution. Thomas and Gallagher [57] have reported a solution to this problem using elements based on deep shells. The predicted displacement response using this study is shown in Fig. 8.18. This figure shows that the response predicted using one cubic element compares very closely to the responses reported by other researchers.

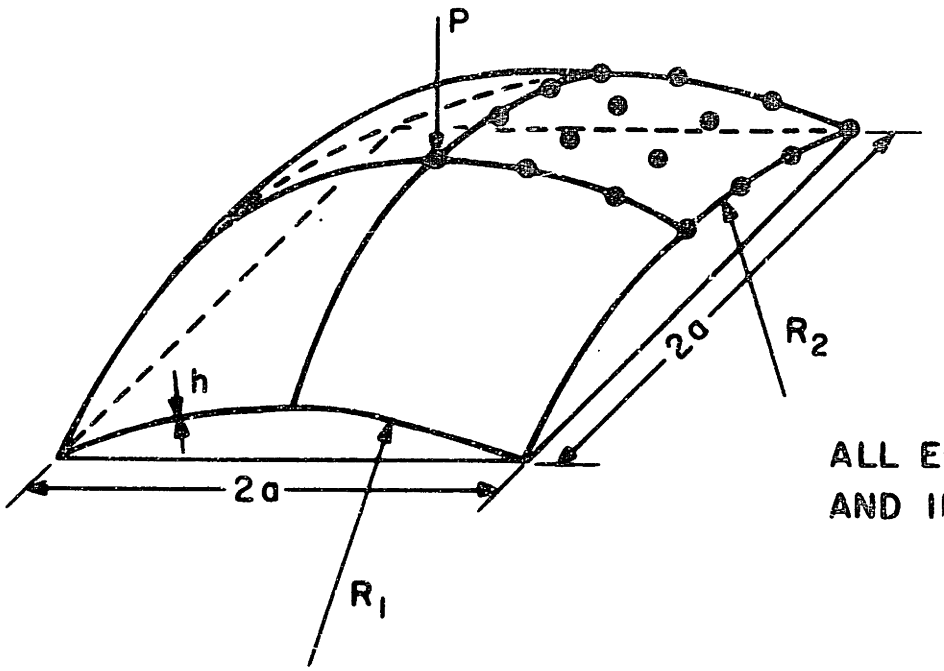

$R_1 = R_2 = 2540$ mm
$a = 784.90$ mm
$h = 99.45$ mm
$E = 68.95$ N/mm^2
$\nu = 0.3$

ALL EDGES ARE HINGED
AND IMMOVEABLE

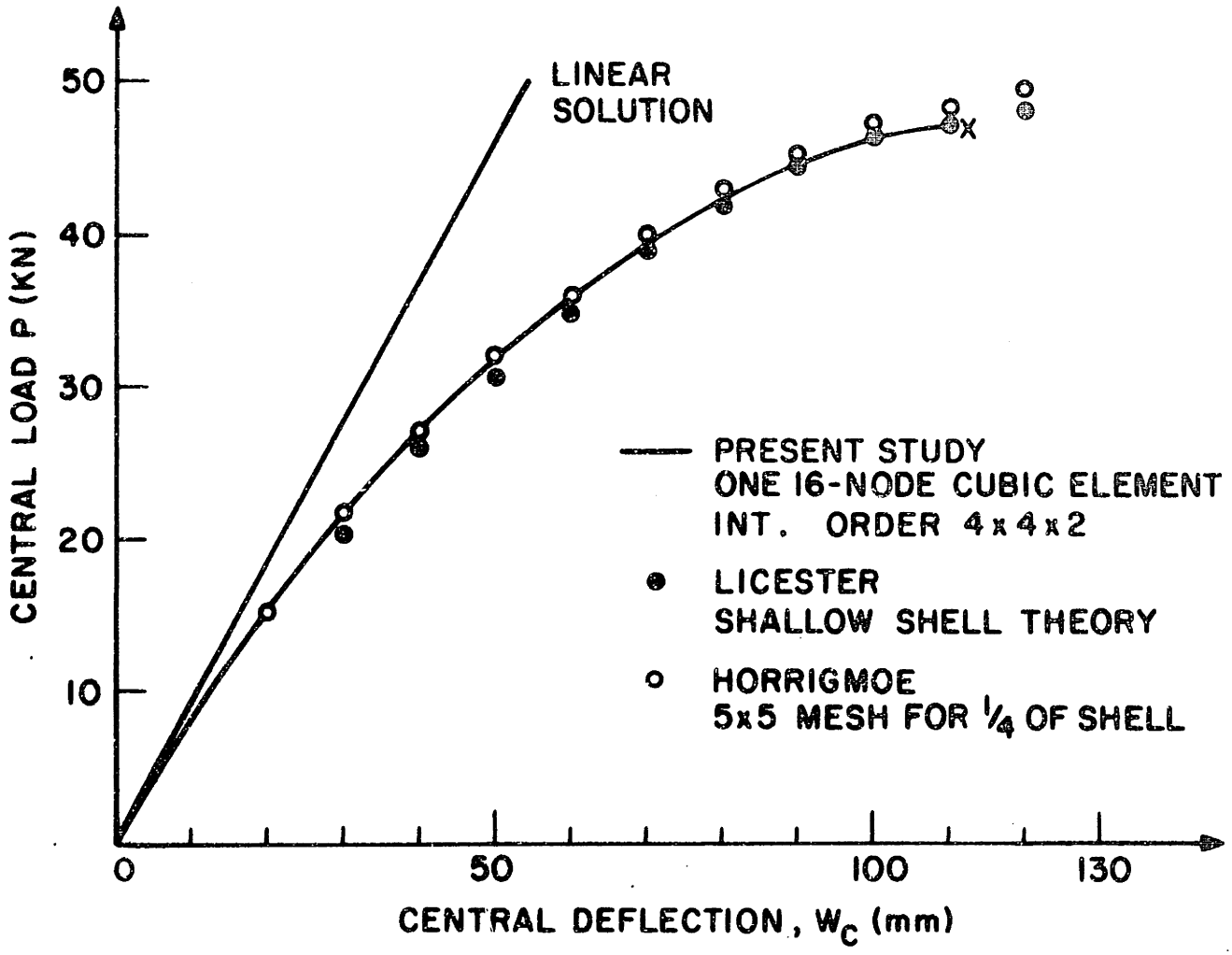

FIGURE 8.18 LARGE DEFLECTION ANALYSIS OF A HINGED SPHERICAL SHELL

9. CONCLUSIONS

The objective in this study was to develop finite element procedure for analyzing general shell structures. An effective nonlinear analysis of a general shell structure requires the use of shell and beam elements that are accurate, reliable and versatile.

In this thesis, two general continuum-mechanics-based incremental formulation, namely, a total Lagrangian (T.L.) formulation and an updated Lagrangian (U.L.) formulation, for formulating displacement-based structural elements have been summarized.

A straight beam element has been developed based on the T.L. and the U.L. formulations. The displacement field inside the element was interpolated from the nodal point displacements and rotations using Hermitian polynomials. It was shown that the use of Hermitian interpolating functions introduces interpolation directionality which poses special problems and necessitates additional computational effort in the T.L. formulation. However, it was shown that consistent T.L. and U.L. formulations yield identical element matrices and force vectors. It was, further, concluded that the updated Lagrangian formulation is computationally more effective than the T.L. formulation in the case of the straight beam element.

Difficulties in the formulation of the straight Hermitian-based beam element (namely, the interpolation directionality and the approximation of the geometry with functions that are of lower order than the displacement interpolation functions) showed the need for a different

procedure for interpolating the displacement field and the geometry of a bending element. Therefore, an effective isoparametric displacemnt/rotation bending element was proposed for large displacement and rotation analysis, using the T.L. and U.L. formulations. The geometry and the displacement field of the element are interpolated using the same Lagrangian interpolation. The interpolation directionality is not present in this element, because all displacements are interpolated with identical functions. Considering the formulation and performance of the bending element it was concluded that it is more effective to employ the isoparametric displacement/rotation procedure for formulating effective and reliable structural elements.

The displacment/rotation isoparametric formulation was employed to develop a versatile shell element. The element can have a variable number of nodes, and can have a quadrilateral or a triangular shape. It also can be used as a transition element (by having both top and bottom nodes, and mid-surface nodes) to model shell to solid transition regions or shell intersections. The element can be used with a compatible bending element to model shell structures with eccentric and non-eccentric stiffeners. This element can be employed in linear material and/or geometric nonlinear analysis of plates and shells with complex geometries. The shell element can be employed in analyzing shell structures of general radii and curvatures because no specific shell theory was assumed in the formulation of the element.

The analysis results of various linear and highly nonlinear

structural problems have been presented to indicate the accuracy and versatility of the shell element. It is concluded that the element presented in this report is very effective for practical analysis of general shell structures. It is also concluded that, although the reduced integration, in general, improves the performance of the element, the cubic element yields accurate response predictions with high-order integration, both in linear and nonlinear analyses. It is noted that the increase of the element aspect ratio does not necessarily deteriorate the shell element performance in linear and nonlinear analyses.

Considering further work on the element, it is desirable that possibilities of improving the element performance using special numerical integration schemes be investigated. The difficulties lie in that such schemes must be put on a firm theoretical foundation and must be generally applicable and reliable in linear and geometric and material nonlinear analysis.

In modeling many structures using finite element techniques, it is required to distorte the geometry of the isoparametric elements to approximate the initial geometry of the structure. In geometric nonlinear analysis, however, every element distorts (even the element that was undistorted initially) due to the large deflection of the structure. Thus in incremental geometric nonlinear analysis the presence of distorted elements are unavoidable. It is known that the performance of an element is dependent on the distortion of both its geometry and its nodal point positions. It is desirable to investigate both theoretically

and numerically the effects of the element distortion on its performance, and if possible, by developing special numerical integration technique or methods of modifying the interpolation function, the undesirable effects of the element distortion may be eliminated.

In many practical structures the loading is dependent on the deformed geometry of the structures. This is especially observed in structures subjected to pressure load (live load) which undergoes large deflection and rotation both in statics and dynamics response. Thus, it is desirable to include the path dependent loading in the analysis of general shell structures.

TABLE 1 UPDATED LAGRANGIAN FORMULATION

1. Equation of Motion

$$\int_{{}^{t}V}{}^{t+\Delta t}_{\ t}S_{ij}\ \delta\,{}^{t+\Delta t}_{\ t}\varepsilon_{ij}\ {}^{t}dv = {}^{t+\Delta t}R$$

where

$$^{t+\Delta t}_{\ t}S_{ij} = \frac{^{t}\rho}{^{t+\Delta t}\rho}\ ^{t}_{t+\Delta t}x_{i,s}\ ^{t+\Delta t}\tau_{sr}\ ^{t}_{t+\Delta t}x_{j,r}$$

$$^{t+\Delta t}_{\ t}\varepsilon_{ij} = \frac{1}{2}(^{t}u_{i,j} + {}^{t}u_{j,i} + {}^{t}u_{k,i}\ {}^{t}u_{k,j})$$

Notation

$$^{t+\Delta t}x_i = {}^{t}x_i + u_i$$

$$^{t}_{t+\Delta t}x_{i,s} = \frac{\partial\,{}^{t}x_i}{\partial\,{}^{t+\Delta t}x_s}$$

$$^{t}u_{i,j} = \frac{\partial u_i}{\partial\,{}^{t}x_j}$$

2. Incremental Decompositions

a. stresses

$$^{t+\Delta t}_{\ t}S_{ij} = {}^{t}\tau_{ij} + {}^{t}S_{ij}$$

b. strains

$$^{t+\Delta t}_{\ t}\varepsilon_{ij} = {}^{t}\varepsilon_{ij}\ ;\quad {}^{t}\varepsilon_{ij} = {}^{t}e_{ij} + {}^{t}\eta_{ij}$$

TABLE 1 UPDATED LAGRANGIAN FORMULATION (CONTINUED)

$$ {}^{t}e_{ij} = \frac{1}{2}\left({}^{t}u_{i,j} + {}^{t}u_{j,i}\right); \quad {}^{t}\eta_{ij} = \frac{1}{2}\, {}^{t}u_{k,i}\ {}^{t}u_{k,j} $$

3. Equation of Motion with Incremental Decompositions

Noting that ${}^{t}S_{ij} = {}^{t}C_{ijrs}\ {}^{t}\varepsilon_{rs}$ the equation of motion is

$$ \int_{{}^{t}V} {}^{t}C_{ijrs}\ {}^{t}\varepsilon_{rs}\ \delta\, {}^{t}\varepsilon_{ij}\ {}^{t}dv + \int_{{}^{t}V} {}^{t}\tau_{ij}\ \delta\, {}^{t}\eta_{ij}\ {}^{t}dv = {}^{t+\Delta t}R - \int_{{}^{t}V} {}^{t}\tau_{ij}\ \delta\, {}^{t}e_{ij}\ {}^{t}dv $$

4. Linearization of Equation of Motion

Using the approximations ${}^{t}S_{ij} = {}^{t}C_{ijrs}\ {}^{t}e_{rs}$, $\delta\, {}^{t}\varepsilon_{ij} = \delta\, {}^{t}e_{ij}$

we obtain as approximate equation of motion

$$ \int_{{}^{t}V} {}^{t}C_{ijrs}\ {}^{t}e_{rs}\ \delta\, {}^{t}e_{ij}\ {}^{t}dv + \int_{{}^{t}V} {}^{t}\tau_{ij}\ \delta\, {}^{t}\eta_{ij}\ {}^{t}dv = {}^{t+\Delta t}R - \int_{{}^{t}V} {}^{t}\tau_{ij}\ \delta\, {}^{t}e_{ij}\ {}^{t}dv $$

TABLE 1 UPDATED LAGRANGIAN FORMULATION (CONTINUED)

5. Equilibrium Iteration (Modified Newton-Raphson Iteration)

$$\int_{t_V} {}^{t}C_{ijrs}\, {}^{\Delta}{}_{t}e_{rs}\, {}^{\delta\Delta}{}_{t}e_{ij}\ {}^{t}dv + \int_{t_V} {}^{t}\tau_{ij}\, {}^{\delta\Delta}{}_{t}\eta_{ij}\ {}^{t}dv = {}^{t+\Delta t}R - \int_{t+\Delta t_V(i-1)} {}^{t+\Delta t}\tau_{ij}^{(i-1)}\, {}^{\delta}{}_{t+\Delta t}e_{ij}^{(i-1)}\ {}^{t+\Delta t}dv^{(i-1)}$$

6. Finite Element Discretization (for a single element)

$$\left\{\int_{t_V} {}^{t}\underline{B}_L^{T}\, {}^{t}\underline{C}\, {}^{t}\underline{B}_L\ {}^{t}dv + \int_{t_V} {}^{t}\underline{B}_{NL}^{T}\, {}^{t}\underline{\tau}\, {}^{t}\underline{B}_{NL}\ {}^{t}dv\right\}\ {}^{\Delta}\underline{u}^{(i)} = {}^{t+\Delta t}\underline{R} - \int_{t+\Delta t_V(i-1)} {}^{t+\Delta t}\underline{B}_L^{(i-1)T}\ {}^{t+\Delta t}\hat{\underline{\tau}}^{(i-1)}\ {}^{t+\Delta t}dv^{(i-1)}$$

$${}^{t+\Delta t}\underline{u}^{(i)} = {}^{t+\Delta t}\underline{u}^{(i-1)} + {}^{\Delta}\underline{u}^{(i)}$$

TABLE 2 TOTAL LAGRANGIAN FORMULATION

1. Equation of Motion

$$\int_{{}^0V} {}^{t+\Delta t}_{\ 0}S_{ij}\ \delta\, {}^{t+\Delta t}_{\ 0}\varepsilon_{ij}\ {}^0dv = {}^{t+\Delta t}R$$

where

$${}^{t+\Delta t}_{\ 0}S_{ij} = \frac{{}^0\rho}{{}^{t+\Delta t}\rho}\ {}^0_{t+\Delta t}x_{i,s}\ {}^{t+\Delta t}\tau_{sr}\ {}^0_{t+\Delta t}x_{j,r}\ ;$$

$${}^{t+\Delta t}_{\ 0}\varepsilon_{ij} = \frac{1}{2}({}^{t+\Delta t}_{\ 0}u_{i,j} + {}^{t+\Delta t}_{\ 0}u_{j,i} + {}^{t+\Delta t}_{\ 0}u_{k,i}\ {}^{t+\Delta t}_{\ 0}u_{k,j})$$

Notation

$${}^{t+\Delta t}x_i = {}^0x_i + {}^{t+\Delta t}u_i$$

$${}^0_{t+\Delta t}x_{j,r} = \frac{\partial\, {}^0x_j}{\partial\, {}^{t+\Delta t}x_r}$$

$${}^{t+\Delta t}_{\ 0}u_{i,j} = \frac{\partial\, {}^{t+\Delta t}u_i}{\partial\, {}^0x_j}$$

2. Incremental Decompositions

a. stresses

$${}^{t+\Delta t}_{\ 0}S_{ij} = {}^t_0S_{ij} + {}^0S_{ij}$$

b. strains

$${}^{t+\Delta t}_{\ 0}\varepsilon_{ij} = {}^t_0\varepsilon_{ij} + {}^0\varepsilon_{ij}\ ;\quad {}^0\varepsilon_{ij} = {}^0e_{ij} + {}^0\eta_{ij}$$

TABLE 2 TOTAL LAGRANGIAN FORMULATION (CONTINUED)

$$ {}_0^t e_{ij} = \frac{1}{2}\left({}_0u_{i,j} + {}_0u_{j,i} + {}_0^t u_{k,i}\,{}_0u_{k,j} + {}_0u_{k,i}\,{}_0^t u_{k,j}\right);\quad {}_0^t \eta_{ij} = \frac{1}{2}\,{}_0u_{k,i}\,{}_0u_{k,j} $$

3. Equation of Motion with Incremental Decompositions

Noting that $\delta\,{}_0^{t+\Delta t}\varepsilon_{ij} = \delta\,{}_0\varepsilon_{ij}$ and ${}_0^t S_{ij} = {}_0C_{ijrs}\,{}_0^t\varepsilon_{rs}$

the equation of motion is

$$ \int_{{}_0V} {}_0C_{ijrs}\,{}_0\varepsilon_{rs}\,\delta\,{}_0\varepsilon_{ij}\,{}_0dv + \int_{{}_0V} {}_0^t S_{ij}\,\delta\,{}_0\eta_{ij}\,{}_0dv = {}^{t+\Delta t}R - \int_{{}_0V} {}_0^t S_{ij}\,\delta\,{}_0e_{ij}\,{}_0dv $$

4. Linearization of Equation of Motion

Using the approximations ${}_0S_{ij} = {}_0C_{ijrs}\,{}_0e_{rs}$, $\delta\,{}_0\varepsilon_{ij} = \delta\,{}_0e_{ij}$

we obtain as approximate equation of motion

$$ \int_{{}_0V} {}_0C_{ijrs}\,{}_0e_{rs}\,\delta\,{}_0e_{ij}\,{}_0dv + \int_{{}_0V} {}_0^t S_{ij}\,\delta\,{}_0\eta_{ij}\,{}_0dv = {}^{t+\Delta t}R - \int_{{}_0V} {}_0^t S_{ij}\,\delta\,{}_0e_{ij}\,{}_0dv $$

TABLE 2 TOTAL LAGRANGIAN FORMULATION (CONTINUED)

5. Equilibrium Iteration (Modified Newton-Raphson Iteration)

$$\int_{{}^0V} {}^0C_{ijrs}\ {}^{\Delta}{}_0e_{rs}\ \delta{}^{\Delta}{}_0e_{ij}\ {}^0dv + \int_{{}^0V} {}^{t}_{0}S_{ij}\ \delta{}^{\Delta}{}_0\eta_{ij}\ {}^0dv = {}^{t+t\Delta}R - \int_{{}^0V} {}^{t+\Delta t}_{0}S^{(i-1)}_{ij}\ \delta\,{}^{t+\Delta t}_{0}\epsilon^{(i-1)}_{ij}\ {}^0dv$$

6. Finite Element Discretization (for a Single Element)

$$\left\{ \int_{{}^0V} {}^{t}_{0}\underline{B}_L^T\ {}^0\underline{C}\ {}^{t}_{0}\underline{B}_L\ {}^0dv + \int_{{}^0V} {}^{t}_{0}\underline{B}_{NL}\ {}^{t}_{0}\underline{S}\ {}^{t}_{0}\underline{B}_{NL}\ {}^0dv \right\} \underline{\Delta u}^{(i)} = {}^{t+\Delta t}\underline{R} - \int_{{}^0V} {}^{t+\Delta t}_{0}\underline{B}_L^{(i-1)T}\ {}^{t+\Delta t}_{0}\underline{\hat{S}}^{(i-1)}\ {}^0dv$$

$${}^{t+\Delta t}\underline{u}^{(i)} = {}^{t+\Delta t}\underline{u}^{(i-1)} + \underline{\Delta u}^{(i)}$$

TABLE 3. FINITE ELEMENT MATRICES IN ALL ANALYSIS

INTEGRAL	MATRIX EVALUATION
$\int_{{}^0V} {}^0\rho \; {}^{t+\Delta t}\ddot{u}_k \; \delta u_k \; {}^0dv$	$\underline{M} \; {}^{t+\Delta t}\underline{\ddot{u}} = {}^0\rho \left(\int_{{}^0V} {}^0\underline{H}^T \; {}^0\underline{H} \; {}^0dv \right) \; {}^{t+\Delta t}\underline{\ddot{u}}$
${}^{t+\Delta t}R = \int_{{}^0V} {}^{t+\Delta t}_{\;\;0}t_k \; \delta u_k \; {}^0da$	${}^{t+\Delta t}\underline{R} = \int_{{}^0V} {}^0\underline{H}_S^T \; {}^{t+\Delta t}_{\;\;0}\underline{t} \; {}^0da$
$+ \int_{{}^0V} {}^0\rho \; {}^{t+\Delta t}_{\;\;0}f_k \; \delta u_k \; {}^0dv$	$+ \int_{{}^0V} {}^0\rho \; {}^0\underline{H}^T \; {}^0\underline{H}^T \; {}^{t+\Delta t}_{\;\;0}\underline{f} \; {}^0dv$

A. Linear Analysis

INTEGRAL	MATRIX EVALUATION
$\int_{{}^0V} {}^0C_{ijrs} \; {}^{t+\Delta t}e_{rs} \; \delta e_{ij} \; {}^0dv$	$\underline{K} \; {}^{t+\Delta t}\underline{u} = \left(\int_{{}^0V} \underline{B_L}^T \; \underline{C} \; \underline{B_L} \; {}^0dv \right) \; {}^{t+\Delta t}\underline{u}$

B. Material Nonlinear Only Analysis

INTEGRAL	MATRIX EVALUATION
$\int_{{}^0V} {}^0C_{ijrs} \; e_{rs} \; \delta e_{ij} \; {}^0dv$	${}^t\underline{k} \; \underline{u} = \left(\int_{{}^0V} \underline{B_L}^T \; \underline{C} \; \underline{B_L} \; {}^0dv \right) \; \underline{u}$
$\int_{{}^0V} {}^t\sigma_{ij} \; \delta e_{ij} \; {}^0dv$	${}^t\underline{F} = \int_{{}^0V} \underline{B_L}^T \; {}^t\underline{\Sigma} \; {}^0dv$

TABLE 3 (continued)

C. Updated Lagrangian Formulation

INTEGRAL	MATRIX EVALUATION
$\int_{t_V} {}^{t}C_{ijrs}\ {}^{t}e_{rs}\ \delta\,{}^{t}e_{ij}\ {}^{t}dv$	${}^{t}_{t}\underline{K}_{L}\ \underline{u} = \int_{t_V} {}^{t}_{t}\underline{B}_{L}^{T}\ {}^{t}\underline{C}\ {}^{t}_{t}\underline{B}_{L}\ {}^{t}dv\ \underline{u}$
$\int_{t_V} {}^{t}\tau_{ij}\ \delta\,{}^{t}\eta_{ij}\ {}^{t}dv$	${}^{t}_{t}\underline{K}_{NL}\ \underline{u} = \int_{t_V} {}^{t}_{t}\underline{B}_{NL}^{T}\ {}^{t}\underline{\hat{\tau}}\ {}^{t}_{t}\underline{B}_{NL}\ {}^{t}dv\ \underline{u}$
$\int_{t_V} {}^{t}\tau_{ij}\ \delta\,{}^{t}e_{ij}\ {}^{t}dv$	${}^{t}_{t}\underline{F} = \int_{t_V} {}^{t}_{t}\underline{B}_{L}^{T}\ {}^{t}\underline{\hat{\tau}}\ {}^{t}dv$

D. Total Lagrangian Formulation

INTEGRAL	MATRIX EVALUATION
$\int_{0_V} {}^{0}C_{ijrs}\ {}^{0}e_{rs}\ \delta\,{}^{0}e_{ij}\ {}^{0}dv$	${}^{t}_{0}\underline{K}_{L}\ \underline{u} = \int_{0_V} {}^{t}_{0}\underline{B}_{L}^{T}\ {}^{0}\underline{C}\ {}^{t}_{0}\underline{B}_{L}\ {}^{0}dv\ \underline{u}$
$\int_{0_V} {}^{t}S_{ij}\ \delta\,{}^{0}\eta_{ij}\ {}^{0}dv$	${}^{t}_{0}\underline{K}_{NL}\ \underline{u} = \int_{0_V} {}^{t}_{0}\underline{B}_{NL}^{T}\ {}^{t}\underline{S}\ {}^{t}_{0}\underline{B}_{NL}\ {}^{0}dv\ \underline{u}$
$\int_{0_V} {}^{t}S_{ij}\ \delta\,{}^{0}e_{ij}\ {}^{0}dv$	${}^{t}_{0}\underline{F} = \int_{0_V} {}^{t}_{0}\underline{B}_{L}^{T}\ {}^{t}\underline{S}\ {}^{0}dv$

TABLE 4 MATRICES USED IN STRAIGHT HERMITIAN-BASED BEAM ELEMENT FORMULATION

A. HERMITIAN INTERPOLATION FUNCTIONS

We define: $\psi_1 = \frac{r}{L} - \left(\frac{r}{L}\right)^2$; $\psi_2 = 1 - 4\frac{r}{L} + 3\left(\frac{r}{L}\right)^2$; $\psi_3 = 2\frac{r}{L} - 3\left(\frac{r}{L}\right)^2$

$\psi_4 = 1 - 3\left(\frac{r}{L}\right)^2 + 2\left(\frac{r}{L}\right)^3$; $\psi_5 = \frac{r}{L} - 2\left(\frac{r}{L}\right)^2 + \left(\frac{r}{L}\right)^3$; $\psi_6 = 1 - \psi_4$

Incremental Displacement Hermitian Interpolation Matrix

$$ {}^t\underline{B} = \begin{bmatrix} {}^t\underline{h}^1 \\ {}^t\underline{h}^2 \\ {}^t\underline{h}^3 \end{bmatrix} = \begin{bmatrix} 1-\frac{r}{L} & 6\psi_1\frac{s}{L} & 6\psi_1\frac{t}{L} & 0 & \psi_2 t & -\psi_2 s & \frac{r}{L} & -6\psi_1\frac{s}{L} & -6\psi_1\frac{t}{L} & 0 & -\psi_3 t & \psi_3 s \\ 0 & \psi_4 & 0 & -\left(1-\frac{r}{L}\right)t & 0 & \psi_5 L & 0 & \psi_6 & 0 & -\frac{r}{L}t & 0 & -\psi_1 r \\ 0 & 0 & \psi_4 & \left(1-\frac{r}{L}\right)s & -\psi_5 L & 0 & 0 & 0 & \psi_6 & \frac{r}{L}s & \psi_1 r & 0 \end{bmatrix} $$

where L = length of the beam element

${}^t\underline{h}^i$ = vector of interpolation functions in ${}^t\bar{x}_i$ direction

r,s,t = beam convective coordinate axes (see Fig. 3.2)

The incremental displacement vector is ${}^t\underline{\bar{u}}^T = \begin{bmatrix} {}^t\bar{u}^1 & {}^t\bar{u}^2 & \dots & {}^t\bar{u}^{12} \end{bmatrix}$

TABLE 4 (Continued)

B. UPDATED LAGRANGIAN FORMULATION

1. Incremental Strains

$$ {}^t\bar{\epsilon}_{ij} = {}^t\bar{e}_{ij} + {}^t\bar{\eta}_{ij} $$

$$ {}^t\bar{e}_{11} = {}^t\bar{u}_{1,1} + \frac{1}{2}\left[({}^t\bar{u}_{1,1})^2 + ({}^t\bar{u}_{2,1})^2 + ({}^t\bar{u}_{3,1})^2\right] $$

$$ {}^t\bar{e}_{12} = \frac{1}{2}\left[{}^t\bar{u}_{1,2} + {}^t\bar{u}_{2,1}\right] + \frac{1}{2}\left[{}^t\bar{u}_{1,1}\,{}^t\bar{u}_{1,2} + {}^t\bar{u}_{3,1}\,{}^t\bar{u}_{3,2}\right] $$

$$ {}^t\bar{e}_{13} = \frac{1}{2}\left[{}^t\bar{u}_{1,3} + {}^t\bar{u}_{3,1}\right] + \frac{1}{2}\left[{}^t\bar{u}_{1,1}\,{}^t\bar{u}_{1,3} + {}^t\bar{u}_{2,1}\,{}^t\bar{u}_{2,3}\right] $$

where $ {}^t\bar{u}_{i,j} = \dfrac{\partial\, {}^t\bar{u}_i}{\partial\, {}^t\bar{x}_j} $; ${}^t\bar{x}_j$ (j=1,2,3) ≡ r,s,t

2. Linear Strain-Displacement Transformation Matrix

Using $ {}^t\bar{\underline{e}} = {}^t_t\bar{\underline{B}}_L\, {}^t\bar{\underline{u}} $

where $ {}^t\bar{\underline{e}}^T = \left[{}^t\bar{e}_{11} \quad 2\,{}^t\bar{e}_{12} \quad 2\,{}^t\bar{e}_{13}\right] $

and $ {}^t\bar{\underline{u}} = {}^t\underline{R}\, \underline{u} $

where ${}^t\bar{\underline{u}}$ = vector of incremental nodal displacements measured in the ${}^t\bar{x}_i$ (i=1,2,3) coordinate system

$\underline{u}$ = vector of incremental nodal displacements in the global coordinate system

${}^t\underline{R}$ = transformation matrix between the local coordinate system at time t and the global coordinate system

TABLE 4 (Continued)

$$
{}^{t}_{t}\underline{B}_{L} = \begin{bmatrix}
{}^{t}h^{1}_{1,1} & {}^{t}h^{1}_{2,1} & {}^{t}h^{1}_{3,1} & \cdots & {}^{t}h^{1}_{I2,1} \\
({}^{t}h^{1}_{1,2} + {}^{t}h^{2}_{1,1}) & ({}^{t}h^{1}_{2,2} + {}^{t}h^{2}_{2,1}) & ({}^{t}h^{1}_{3,2} + {}^{t}h^{2}_{3,1}) & \cdots & ({}^{t}h^{1}_{12,2} + {}^{t}h^{2}_{12,2}) \\
({}^{t}h^{1}_{1,3} + {}^{t}h^{3}_{1,1}) & ({}^{t}h^{1}_{2,3} + {}^{t}h^{3}_{2,1}) & ({}^{t}h^{1}_{3,3} + {}^{t}h^{3}_{3,1}) & \cdots & ({}^{t}h^{1}_{12,3} + {}^{t}h^{3}_{12,1})
\end{bmatrix}
$$

where ${}^{t}h^{1}_{k,j} = \dfrac{\partial\, {}^{t}h^{1}_{k}}{\partial\, {}^{t}x_{j}}$

3. Nonlinear Strain-Displacement Transformation Matrix

$$
{}^{t}_{t}\underline{B}_{NL} = \begin{bmatrix}
{}^{t}h^{1}_{1,1} & {}^{t}h^{1}_{2,1} & {}^{t}h^{1}_{3,1} & \cdots & {}^{t}h^{1}_{12,1} \\
{}^{t}h^{2}_{1,1} & {}^{t}h^{2}_{2,1} & {}^{t}h^{2}_{3,1} & \cdots & {}^{t}h^{2}_{12,1} \\
{}^{t}h^{3}_{1,1} & {}^{t}h^{3}_{2,1} & {}^{t}h^{3}_{3,1} & \cdots & {}^{t}h^{3}_{12,1} \\
{}^{t}h^{1}_{1,2} & {}^{t}h^{1}_{2,2} & {}^{t}h^{1}_{3,2} & \cdots & {}^{t}h^{1}_{12,2} \\
{}^{t}h^{3}_{1,2} & {}^{t}h^{3}_{2,2} & {}^{t}h^{3}_{3,2} & \cdots & {}^{t}h^{3}_{12,2} \\
{}^{t}h^{1}_{1,3} & {}^{t}h^{1}_{2,3} & {}^{t}h^{1}_{3,3} & \cdots & {}^{t}h^{1}_{12,3} \\
{}^{t}h^{2}_{1,3} & {}^{t}h^{2}_{2,3} & {}^{t}h^{2}_{3,3} & \cdots & {}^{t}h^{2}_{12,3}
\end{bmatrix}
$$

TABLE 4 (Continued)

4. Cauchy Stress Matrix and Stress Vector

$$\underline{\underline{{}^{t}\tau}} = \begin{bmatrix} {}^{t}\tau_{11} & & & & & & \\ 0 & {}^{t}\tau_{11} & & \text{symmetric} & & & \\ 0 & 0 & {}^{t}\tau_{11} & & & & \\ {}^{t}\tau_{12} & 0 & 0 & 0 & & & \\ 0 & 0 & {}^{t}\tau_{12} & 0 & 0 & & \\ {}^{t}\tau_{13} & 0 & 0 & 0 & 0 & 0 & \\ 0 & {}^{t}\tau_{13} & 0 & 0 & 0 & 0 & 0 \end{bmatrix} ; \quad \underline{{}^{t}s} = \begin{bmatrix} {}^{t}\tau_{11} \\ {}^{t}\tau_{12} \\ {}^{t}\tau_{13} \end{bmatrix}$$

TABLE 4 (Continued)

C. TOTAL LAGRANGIAN FORMULATION

1. Incremental Strains

$$ {}_0^t\bar{\varepsilon}_{ij} = {}_0\bar{e}_{ij} + {}_0\bar{\eta}_{ij} $$

$$ {}_0\bar{e}_{11} = {}_0\bar{u}_{1,1} + {}_0^t\bar{u}_{1,1}\,{}_0\bar{u}_{1,1} + {}_0^t\bar{u}_{2,1}\,{}_0\bar{u}_{2,1} + {}_0^t\bar{u}_{3,1}\,{}_0\bar{u}_{3,1} + \frac{1}{2}\left[({}_0\bar{u}_{1,1})^2 + ({}_0\bar{u}_{2,1})^2 + ({}_0\bar{u}_{3,1})^2\right] $$

$$ {}_0\bar{e}_{12} = \frac{1}{2}\left\{\left[{}_0\bar{u}_{1,2} + {}_0\bar{u}_{2,1}\right] + \left[{}_0^t\bar{u}_{1,1}\,{}_0\bar{u}_{1,2} + {}_0^t\bar{u}_{2,1}\,{}_0\bar{u}_{2,2} + {}_0^t\bar{u}_{3,1}\,{}_0\bar{u}_{3,2} + {}_0^t\bar{u}_{1,2}\,{}_0\bar{u}_{1,1} + {}_0^t\bar{u}_{2,2}\,{}_0\bar{u}_{2,1} + {}_0^t\bar{u}_{3,2}\,{}_0\bar{u}_{3,1}\right]\right\} + \frac{1}{2}\left[{}_0\bar{u}_{1,1}\,{}_0\bar{u}_{1,2} + {}_0\bar{u}_{2,1}\,{}_0\bar{u}_{2,2} + {}_0\bar{u}_{3,1}\,{}_0\bar{u}_{3,2}\right] $$

$$ {}_0\bar{e}_{13} = \frac{1}{2}\left\{\left[{}_0\bar{u}_{1,3} + {}_0\bar{u}_{3,1}\right] + \left[{}_0^t\bar{u}_{1,1}\,{}_0\bar{u}_{1,3} + {}_0^t\bar{u}_{2,1}\,{}_0\bar{u}_{2,3} + {}_0^t\bar{u}_{3,1}\,{}_0\bar{u}_{3,3} + {}_0^t\bar{u}_{1,3}\,{}_0\bar{u}_{1,1} + {}_0^t\bar{u}_{2,3}\,{}_0\bar{u}_{2,1} + {}_0^t\bar{u}_{3,3}\,{}_0\bar{u}_{3,1}\right]\right\} + \frac{1}{2}\left[{}_0\bar{u}_{1,1}\,{}_0\bar{u}_{1,3} + {}_0\bar{u}_{2,1}\,{}_0\bar{u}_{2,3} + {}_0\bar{u}_{3,1}\,{}_0\bar{u}_{3,3}\right] $$

where $ {}_0\bar{u}_{i,j} = \dfrac{\partial\,{}_0\bar{u}_i}{\partial\,{}_0\bar{x}_j} $; $ {}_0^t\bar{u}_{i,j} = \dfrac{\partial\,{}_0^t\bar{u}_i}{\partial\,{}_0\bar{x}_j} $; $ {}_0\bar{x}_1 \equiv r $, $ {}_0\bar{x}_2 \equiv s $, $ {}_0\bar{x}_3 \equiv t $.

2. Linear Strain-Displacement Transformation Matrix

Using $ {}_0\underline{\bar{e}} = {}_0^t\underline{\bar{B}}_L\,{}_0\underline{\bar{u}} $

where $ {}_0\underline{\bar{u}} = {}_0\underline{R}\,\underline{u} $; $ {}_0\underline{\bar{u}} $ = vector of incremental nodal displacements measured in ${}_0\bar{x}_i$ $(i=1,2,3)$ coordinate system

$ \underline{u} $ = vector of incremental nodal displacements in global coordinate system

$ {}_0\underline{R} $ = transformation matrix

and $ {}_0\underline{\bar{e}}^T = \left[{}_0\bar{e}_{11}\ {}_2{}_0\bar{e}_{12}\ {}_2{}_0\bar{e}_{13}\right] $; $ {}_0\underline{\bar{u}}^T = \left[{}_0\bar{u}^1\ {}_0\bar{u}^2\ {}_0\bar{u}^3\ \cdots\ {}_0\bar{u}^{12}\right] $

(continued)

TABLE 4 (Continued)

$$\underset{\sim}{t}^{B}_{0L} = \underset{\sim}{t}^{B}_{0L0} + \underset{\sim}{t}^{B}_{0L1} \quad \text{where}$$

$$\underset{\sim}{t}^{B}_{0L0} = \begin{bmatrix} {}^{0}h^{1}_{1,1} & {}^{0}h^{1}_{2,1} & {}^{0}h^{1}_{3,1} & \cdots & {}^{0}h^{1}_{12,1} \\ ({}^{0}h^{1}_{1,2} + {}^{0}h^{2}_{1,1}) & ({}^{0}h^{1}_{2,2} + {}^{0}h^{2}_{2,1}) & ({}^{0}h^{1}_{3,2} + {}^{0}h^{2}_{3,1}) & \cdots & ({}^{0}h^{1}_{12,2} + {}^{0}h^{2}_{12,1}) \\ ({}^{0}h^{1}_{1,3} + {}^{0}h^{3}_{1,1}) & ({}^{0}h^{1}_{2,3} + {}^{0}h^{3}_{2,1}) & ({}^{0}h^{1}_{3,3} + {}^{0}h^{3}_{3,1}) & \cdots & ({}^{0}h^{1}_{12,3} + {}^{0}h^{3}_{12,1}) \end{bmatrix}$$

and

$$\underset{\sim}{t}^{B}_{0L1} = \begin{bmatrix} (\ell_{11}\,{}^{0}h^{1}_{1,1} + \ell_{21}\,{}^{0}h^{2}_{1,1} + \ell_{31}\,{}^{0}h^{3}_{1,1}) & & & \\ (\ell_{11}\,{}^{0}h^{1}_{1,2} + \ell_{12}\,{}^{0}h^{1}_{1,1} + \ell_{21}\,{}^{0}h^{2}_{1,2} + \ell_{22}\,{}^{0}h^{2}_{1,1} + \ell_{31}\,{}^{0}h^{3}_{1,2} + \ell_{32}\,{}^{0}h^{3}_{1,1}) & & & \\ (\ell_{11}\,{}^{0}h^{1}_{1,3} + \ell_{13}\,{}^{0}h^{1}_{1,1} + \ell_{21}\,{}^{0}h^{2}_{1,3} + \ell_{23}\,{}^{0}h^{2}_{1,1} + \ell_{31}\,{}^{0}h^{3}_{1,3} + \ell_{33}\,{}^{0}h^{3}_{1,1}) & & & \end{bmatrix}$$

$$\begin{matrix} (\ell_{11}\,{}^{0}h^{1}_{2,1} + \ell_{21}\,{}^{0}h^{2}_{2,1} + \ell_{31}\,{}^{0}h^{3}_{2,1}) & \cdots \\ (\ell_{11}\,{}^{0}h^{1}_{2,2} + \ell_{12}\,{}^{0}h^{1}_{2,1} + \ell_{21}\,{}^{0}h^{2}_{2,2} + \ell_{22}\,{}^{0}h^{2}_{2,1} + \ell_{31}\,{}^{0}h^{3}_{2,2} + \ell_{32}\,{}^{0}h^{3}_{2,1}) & \cdots \\ (\ell_{11}\,{}^{0}h^{1}_{2,3} + \ell_{13}\,{}^{0}h^{1}_{2,1} + \ell_{21}\,{}^{0}h^{2}_{2,3} + \ell_{23}\,{}^{0}h^{2}_{2,1} + \ell_{31}\,{}^{0}h^{3}_{2,3} + \ell_{33}\,{}^{0}h^{3}_{2,1}) & \cdots \end{matrix}$$

$$\begin{matrix} \cdots\ (\ell_{11}\,{}^{0}h^{1}_{12,1} + \ell_{21}\,{}^{0}h^{2}_{12,1} + \ell_{31}\,{}^{0}h^{3}_{12,1}) \\ \cdots\ (\ell_{11}\,{}^{0}h^{1}_{12,2} + \ell_{12}\,{}^{0}h^{1}_{12,1} + \ell_{21}\,{}^{0}h^{2}_{12,2} + \ell_{22}\,{}^{0}h^{2}_{12,1} + \ell_{31}\,{}^{0}h^{3}_{12,2} + \ell_{32}\,{}^{0}h^{3}_{12,1}) \\ \cdots\ (\ell_{11}\,{}^{0}h^{1}_{12,3} + \ell_{13}\,{}^{0}h^{1}_{12,1} + \ell_{21}\,{}^{0}h^{2}_{12,3} + \ell_{23}\,{}^{0}h^{2}_{12,1} + \ell_{31}\,{}^{0}h^{3}_{12,3} + \ell_{33}\,{}^{0}h^{3}_{12,1}) \end{matrix} \Bigg]$$

TABLE 4 (Continued)

where

$$\ell_{ij} = \frac{\partial {}^{t}_{0}\bar{u}_i}{\partial {}^{0}\bar{x}_j}$$

3. **Nonlinear Strain-Displacement Transformation Matrix**

$$ {}^{t}_{0}\bar{B}_{NL} = \begin{bmatrix} {}^{0}h^1_{1,1} & {}^{0}h^1_{2,1} & {}^{0}h^1_{3,1} & \cdots & {}^{0}h^1_{12,1} \\ {}^{0}h^2_{1,1} & {}^{0}h^2_{2,1} & {}^{0}h^2_{3,1} & \cdots & {}^{0}h^2_{12,1} \\ {}^{0}h^3_{1,1} & {}^{0}h^3_{2,1} & {}^{0}h^3_{3,1} & \cdots & {}^{0}h^3_{12,1} \\ {}^{0}h^1_{1,2} & {}^{0}h^1_{2,2} & {}^{0}h^1_{3,2} & \cdots & {}^{0}h^1_{12,2} \\ {}^{0}h^2_{1,2} & {}^{0}h^2_{2,2} & {}^{0}h^2_{3,2} & \cdots & {}^{0}h^2_{12,2} \\ {}^{0}h^3_{1,2} & {}^{0}h^3_{2,2} & {}^{0}h^3_{3,2} & \cdots & {}^{0}h^3_{12,2} \\ {}^{0}h^1_{1,3} & {}^{0}h^1_{2,3} & {}^{0}h^1_{3,3} & \cdots & {}^{0}h^1_{12,3} \\ {}^{0}h^2_{1,3} & {}^{0}h^2_{2,3} & {}^{0}h^2_{3,3} & \cdots & {}^{0}h^2_{12,3} \\ {}^{0}h^3_{1,3} & {}^{0}h^3_{2,3} & {}^{0}h^3_{3,3} & \cdots & {}^{0}h^3_{12,3} \end{bmatrix} $$

(continued)

TABLE 4 (Continued)

4. 2nd Piola-Kirchhoff Stress Matrix and Vector

$$ {}_0^{t}\underline{\underline{S}} = \begin{bmatrix} {}_0^{t}\underline{S}_{11}\underline{I}_3 & & \text{symmetric} \\ {}_0^{t}\underline{S}_{12}\underline{I}_3 & \underline{0} & \\ {}_0^{t}\underline{S}_{13}\underline{I}_3 & \underline{0} & \underline{0} \end{bmatrix} \qquad {}_0^{t}\underline{\underline{S}} = \begin{bmatrix} {}_0^{t}\underline{S}_{11} \\ {}_0^{t}\underline{S}_{12} \\ {}_0^{t}\underline{S}_{13} \end{bmatrix} $$

where $\underline{I}_3$ is a 3×3 identity matrix.

TABLE 5 MATRICES USED IN UPDATED LAGRANGIAN FORMULATION OF SHELL ELEMENT

1. Linear Strain-Displacement Transformation Matrix

$$ {}^t\underline{e} = {}^t_t\underline{B}_L \, \underline{u} $$

$$ {}^t\underline{e}^T = [{}^te_{11} \; {}^te_{22} \; {}^te_{33} \; {}^t2e_{12} \; {}^t2e_{13} \; {}^t2e_{23}] $$

$$ \underline{u}^T = [u_1^1 \; u_2^1 \; u_3^1 \; \alpha^1 \; \beta^1 \; ; \; u_1^2 \; u_2^2 \; \ldots \; ; \; u_1^N \; u_2^N \; u_3^N \; \alpha^N \; \beta^N] $$

Note: α^k and β^k (k = 1,2, .. N) are included in $\underline{u}^T$ only if node k is a mid-surface node

$$ {}^t_t\underline{B}_L = \left[\begin{array}{c|ccc|cc|cc|c} \cdots & {}^th_{k,1} & 0 & 0 & {}^tg^k_{11} & {}^tG^k_1 & {}^tg^k_{21} & {}^tG^k_1 & \\ & 0 & {}^th_{k,2} & 0 & {}^tg^k_{12} & {}^tG^k_2 & {}^tg^k_{22} & {}^tG^k_2 & \\ & 0 & 0 & {}^th_{k,3} & {}^tg^k_{13} & {}^tG^k_3 & {}^tg^k_{23} & {}^tG^k_3 & \\ & {}^th_{k,2} & {}^th_{k,1} & 0 & ({}^tg^k_{11}\ {}^tG^k_2 + {}^tg^k_{12}\ {}^tG^k_1) & & ({}^tg^k_{21}\ {}^tG^k_2 + {}^tg^k_{22}\ {}^tG^k_1) & & \cdots \\ & {}^th_{k,3} & 0 & {}^th_{k,1} & ({}^tg^k_{11}\ {}^tG^k_3 + {}^tg^k_{13}\ {}^tG^k_1) & & ({}^tg^k_{21}\ {}^tG^k_3 + {}^tg^k_{23}\ {}^tG^k_1) & & \\ & 0 & {}^th_{k,3} & {}^th_{k,2} & ({}^tg^k_{12}\ {}^tG^k_3 + {}^tg^k_{13}\ {}^tG^k_2) & & ({}^tg^k_{22}\ {}^tG^k_3 + {}^tg^k_{23}\ {}^tG^k_2) & & \end{array}\right] $$

include if node k is a mid-surface node

for nodal point k

TABLE 5 (Continued)

2. Nonlinear Strain-Displacement Transformation Matrix

$$
{}^{t}_{t}\underline{B}_{NL} = \left[\begin{array}{c:ccc:cccc:c}
\cdots & {}^{t}h_{k,1} & 0 & 0 & {}^{t}g^{k}_{11} & {}^{t}G^{k}_{1} & {}^{t}g^{k}_{21} & {}^{t}G^{k}_{1} & \\
 & 0 & {}^{t}h_{k,1} & 0 & {}^{t}g^{k}_{12} & {}^{t}G^{k}_{1} & {}^{t}g^{k}_{22} & {}^{t}G^{k}_{1} & \\
 & 0 & 0 & {}^{t}h_{k,1} & {}^{t}g^{k}_{13} & {}^{t}G^{k}_{1} & {}^{t}g^{k}_{23} & {}^{t}G^{k}_{1} & \\
 & {}^{t}h_{k,2} & 0 & 0 & {}^{t}g^{k}_{11} & {}^{t}G^{k}_{2} & {}^{t}g^{k}_{21} & {}^{t}G^{k}_{2} & \cdots \\
 & 0 & {}^{t}h_{k,2} & 0 & {}^{t}g^{k}_{12} & {}^{t}G^{k}_{2} & {}^{t}g^{k}_{22} & {}^{t}G^{k}_{2} & \\
 & 0 & 0 & {}^{t}h_{k,2} & {}^{t}g^{k}_{13} & {}^{t}G^{k}_{2} & {}^{t}g^{k}_{23} & {}^{t}G^{k}_{2} & \\
 & {}^{t}h_{k,3} & 0 & 0 & {}^{t}g^{k}_{11} & {}^{t}G^{k}_{3} & {}^{t}g^{k}_{21} & {}^{t}G^{k}_{3} & \\
 & 0 & {}^{t}h_{k,3} & 0 & {}^{t}g^{k}_{12} & {}^{t}G^{k}_{3} & {}^{t}g^{k}_{22} & {}^{t}G^{k}_{3} & \\
 & 0 & 0 & {}^{t}h_{k,3} & {}^{t}g^{k}_{13} & {}^{t}G^{k}_{3} & {}^{t}g^{k}_{23} & {}^{t}G^{k}_{3} &
\end{array}\right]
$$

include if node k is a mid-surface node

for nodal point k

TABLE 5 (Continued)

3. Stress Matrix

$$\underline{t}_{\tau} = \begin{bmatrix} t_{\tau_{11}} \underline{I}_3 & & \text{Sym.} \\ t_{\tau_{12}} \underline{I}_3 & t_{\tau_{22}} \underline{I}_3 & \\ t_{\tau_{13}} \underline{I}_3 & t_{\tau_{23}} \underline{I}_3 & t_{\tau_{33}} \underline{I}_3 \end{bmatrix}$$

where

$$\underline{I}_3 = \begin{bmatrix} 1 & 0 & 0 \\ 0 & 1 & 0 \\ 0 & 0 & 1 \end{bmatrix}$$

4. Stress Vector

$$\hat{\underline{t}}_{\tau}^{T} = [t_{\tau_{11}} \quad t_{\tau_{22}} \quad t_{\tau_{33}} \quad t_{\tau_{12}} \quad t_{\tau_{13}} \quad t_{\tau_{23}}]$$

TABLE 6 MATRICES USED IN TOTAL LAGRANGIAN FORMULATION OF SHELL ELEMENT

1. Linear Strain-Displacement Transformation Matrix

$$ {}_0\underline{e} = {}_{0\underline{B}_L}^{t}\underline{u}; \qquad {}_{0\underline{B}_L}^{t} = {}_{0\underline{B}_{L0}}^{t} + {}_{0\underline{B}_{L1}}^{t} $$

$$ {}_0\underline{e}^T = [{}_0e_{11}\ {}_0e_{22}\ {}_0e_{33}\ \ {}_0e_{12}\ {}_0e_{13}\ \ {}_0e_{23}] $$

$$ \underline{u}^T = [u_1^1\ u_2^1\ u_3^1\ \alpha^1\ \beta^1;\ \ u_1^2\ u_2^2\ \ldots\ ;\ u_1^N\ \ u_2^N\ \ u_3^N\ \ \alpha^N\ \ \beta^N] $$

Note: α^k and β^k (k=1,2, .. N) are included in $\underline{u}^T$ only if node k is a mid-surface node

$$ {}_{0\underline{B}_{L0}}^{t} = \left[\begin{array}{ccc:cc:c} \cdots & & & & & \cdots \\ {}_0h_{k,1} & 0 & 0 & {}^tg_{11}^k\ {}_0G_1^k & {}^tg_{21}^k\ {}_0G_1^k & \\ 0 & {}_0h_{k,2} & 0 & {}^tg_{12}^k\ {}_0G_2^k & {}^tg_{22}^k\ {}_0G_2^k & \\ 0 & 0 & {}_0h_{k,2} & {}^tg_{13}^k\ {}_0G_3^k & {}^tg_{23}^k\ {}_0G_3^k & \\ {}_0h_{k,2} & {}_0h_{k,1} & 0 & \left({}^tg_{11}^k\ {}_0G_2^k + {}^tg_{12}^k\ {}_0G_1^k\right) & \left({}^tg_{21}^k\ {}_0G_2^k + {}^tg_{22}^k\ {}_0G_1^k\right) & \cdots \\ {}_0h_{k,3} & 0 & {}_0h_{k,1} & \left({}^tg_{11}^k\ {}_0G_3^k + {}^tg_{13}^k\ {}_0G_1^k\right) & \left({}^tg_{21}^k\ {}_0G_3^k + {}^tg_{23}^k\ {}_0G_1^k\right) & \\ 0 & {}_0h_{k,3} & {}_0h_{k,2} & \left({}^tg_{12}^k\ {}_0G_3^k + {}^tg_{13}^k\ {}_0G_2^k\right) & \left({}^tg_{22}^k\ {}_0G_3^k + {}^tg_{23}^k\ {}_0G_2^k\right) & \end{array}\right] $$

include if node k is a mid-surface node

for nodal point k

TABLE 6 (Continued)

$$
{}_{0}^{t}\underline{B}_{L1} = \left[\cdots \;\vdots\; \begin{array}{ccc|cc}
{}_{\ell}{}_{11}\,{}_{0}^{}h_{k,1} & {}_{\ell}{}_{21}\,{}_{0}^{}h_{k,1} & {}_{\ell}{}_{31}\,{}_{0}^{}h_{k,1} & \phi_{11}^{k}\,{}_{0}^{}G_{1}^{k} & \phi_{21}^{k}\,{}_{0}^{}G_{1}^{k} \\
{}_{\ell}{}_{12}\,{}_{0}^{}h_{k,2} & {}_{\ell}{}_{22}\,{}_{0}^{}h_{k,2} & {}_{\ell}{}_{32}\,{}_{0}^{}h_{k,2} & \phi_{12}^{k}\,{}_{0}^{}G_{2}^{k} & \phi_{22}^{k}\,{}_{0}^{}G_{2}^{k} \\
{}_{\ell}{}_{13}\,{}_{0}^{}h_{k,3} & {}_{\ell}{}_{23}\,{}_{0}^{}h_{k,3} & {}_{\ell}{}_{33}\,{}_{0}^{}h_{k,3} & \phi_{13}^{k}\,{}_{0}^{}G_{3}^{k} & \phi_{23}^{k}\,{}_{0}^{}G_{3}^{k} \\
({}_{\ell}{}_{11}\,{}_{0}^{}h_{k,2}+ & ({}_{\ell}{}_{21}\,{}_{0}^{}h_{k,2}+ & ({}_{\ell}{}_{31}\,{}_{0}^{}h_{k,2}+ & (\phi_{12}^{k}\,{}_{0}^{}G_{1}^{k}+ & (\phi_{22}^{k}\,{}_{0}^{}G_{1}^{k}+ \\
\quad {}_{\ell}{}_{12}\,{}_{0}^{}h_{k,1}) & \quad {}_{\ell}{}_{22}\,{}_{0}^{}h_{k,1}) & \quad {}_{\ell}{}_{32}\,{}_{0}^{}h_{k,1}) & \quad \phi_{11}^{k}\,{}_{0}^{}G_{2}^{k}) & \quad \phi_{21}^{k}\,{}_{0}^{}G_{2}^{k}) \\
({}_{\ell}{}_{11}\,{}_{0}^{}h_{k,3}+ & ({}_{\ell}{}_{21}\,{}_{0}^{}h_{k,3}+ & ({}_{\ell}{}_{31}\,{}_{0}^{}h_{k,3}+ & (\phi_{13}^{k}\,{}_{0}^{}G_{1}^{k}+ & (\phi_{23}^{k}\,{}_{0}^{}G_{1}^{k}+ \\
\quad {}_{\ell}{}_{13}\,{}_{0}^{}h_{k,1}) & \quad {}_{\ell}{}_{23}\,{}_{0}^{}h_{k,1}) & \quad {}_{\ell}{}_{33}\,{}_{0}^{}h_{k,1}) & \quad \phi_{11}^{k}\,{}_{0}^{}G_{3}^{k}) & \quad \phi_{21}\,{}_{0}^{}G_{3}^{k}) \\
({}_{\ell}{}_{12}\,{}_{0}^{}h_{k,3}+ & ({}_{\ell}{}_{22}\,{}_{0}^{}h_{k,3}+ & ({}_{\ell}{}_{32}\,{}_{0}^{}h_{k,3}+ & (\phi_{13}^{k}\,{}_{0}^{}G_{2}^{k}+ & (\phi_{23}^{k}\,{}_{0}^{}G_{2}^{k}+ \\
\quad {}_{\ell}{}_{13}\,{}_{0}^{}h_{k,2}) & \quad {}_{\ell}{}_{23}\,{}_{0}^{}h_{k,2}) & \quad {}_{\ell}{}_{33}\,{}_{0}^{}h_{k,2}) & \quad \phi_{12}^{k}\,{}_{0}^{}G_{3}^{k}) & \quad \phi_{22}\,{}_{0}^{}G_{3}^{k}) \\
 & & & \text{include if node k is} & \\
 & & & \text{a mid-surface node} &
\end{array} \;\vdots\; \cdots \right]
$$

for nodal point k

where

$$
{}_{\ell}{}_{ij} = \frac{\partial\, {}^{t}u_{i}}{\partial\, {}^{0}x_{j}} \quad ; \quad \phi_{ij}^{k} = \sum_{m=1}^{3} {}^{t}g_{im}^{k}\, {}_{\ell}{}_{mj}
$$

TABLE 6 (Continued)

2. Nonlinear Strain-Displacement Transformation Matrix

$$
{}^{t}_{0}\underline{B}_{NL} = \left[\cdots \;\vdots\; \begin{array}{ccc:cc}
{}^{0}h_{k,1} & 0 & 0 & {}^{t}g^{k}_{11}\,{}^{0}G^{k}_{1} & {}^{t}g^{k}_{21}\,{}^{0}G^{k}_{1} \\
0 & {}^{0}h_{k,1} & 0 & {}^{t}g^{k}_{12}\,{}^{0}G^{k}_{1} & {}^{t}g^{k}_{22}\,{}^{0}G^{k}_{1} \\
0 & 0 & {}^{0}h_{k,1} & {}^{t}g^{k}_{13}\,{}^{0}G^{k}_{1} & {}^{t}g^{k}_{23}\,{}^{0}G^{k}_{1} \\
{}^{0}h_{k,2} & 0 & 0 & {}^{t}g^{k}_{11}\,{}^{0}G^{k}_{2} & {}^{t}g^{k}_{21}\,{}^{0}G^{k}_{2} \\
0 & {}^{0}h_{k,2} & 0 & {}^{t}g^{k}_{12}\,{}^{0}G^{k}_{2} & {}^{t}g^{k}_{22}\,{}^{0}G^{k}_{2} \\
0 & 0 & {}^{0}h_{k,2} & {}^{t}g^{k}_{13}\,{}^{0}G^{k}_{2} & {}^{t}g^{k}_{23}\,{}^{0}G^{k}_{2} \\
{}^{0}h_{k,3} & 0 & 0 & {}^{t}g^{k}_{11}\,{}^{0}G^{k}_{3} & {}^{t}g^{k}_{21}\,{}^{0}G^{k}_{3} \\
0 & {}^{0}h_{k,3} & 0 & {}^{t}g^{k}_{12}\,{}^{0}G^{k}_{3} & {}^{t}g^{k}_{22}\,{}^{0}G^{k}_{3} \\
0 & 0 & {}^{0}h_{k,3} & {}^{t}g^{k}_{13}\,{}^{0}G^{k}_{3} & {}^{t}g^{k}_{23}\,{}^{0}G^{k}_{3}
\end{array} \;\vdots\; \cdots \right]
$$

include if node k is a mid-surface node

for nodal point k

TABLE 6 (Continued)

3. Stress Matrix

$$
{}^{t}_{0}\underline{S} = \begin{bmatrix} {}^{t}_{0}S_{11}\,\underline{I}_3 & & \text{Symm.} \\ {}^{t}_{0}S_{12}\,\underline{I}_3 & {}^{t}_{0}S_{22}\,\underline{I}_3 & \\ {}^{t}_{0}S_{13}\,\underline{I}_3 & {}^{t}_{0}S_{23}\,\underline{I}_3 & {}^{t}_{0}S_{33}\,\underline{I}_3 \end{bmatrix}
$$

where

$$
\underline{I}_3 = \begin{bmatrix} 1 & 0 & 0 \\ 0 & 1 & 0 \\ 0 & 0 & 1 \end{bmatrix}
$$

4. Stress Vector

$$
{}^{t}_{0}\hat{\underline{S}}^{T} = \begin{bmatrix} {}^{t}_{0}S_{11} & {}^{t}_{0}S_{22} & {}^{t}_{0}S_{33} & {}^{t}_{0}S_{12} & {}^{t}_{0}S_{13} & {}^{t}_{0}S_{23} \end{bmatrix}
$$

TABLE 7. 3-D ELASTIC - PLASTIC INCREMENTAL CONSTITUTIVE MATRIX, VON MISES YIELD CONDITION, AND ISOTROPIC HARDENING

$$\underline{\bar{C}}^{EP} = \frac{E}{1+\nu}$$

$\frac{1-\nu}{1-2\nu} - \beta \bar{t}_{D_{11}}^2$	$\frac{\nu}{1-2\nu} - \beta \bar{t}_{D_{11}} \bar{t}_{D_{22}}$	$\frac{\nu}{1-2\nu} - \beta \bar{t}_{D_{11}} \bar{t}_{D_{33}}$	$-\beta \bar{t}_{D_{11}} \bar{t}_{D_{12}}$	$-\beta \bar{t}_{D_{11}} \bar{t}_{D_{23}}$	$-\beta \bar{t}_{D_{11}} \bar{t}_{D_{13}}$
	$\frac{1-\nu}{1-2\nu} - \beta \bar{t}_{D_{22}}^2$	$\frac{\nu}{1-2\nu} - \beta \bar{t}_{D_{22}} \bar{t}_{D_{33}}$	$-\beta \bar{t}_{D_{22}} \bar{t}_{D_{12}}$	$-\beta \bar{t}_{D_{22}} \bar{t}_{D_{23}}$	$-\beta \bar{t}_{D_{22}} \bar{t}_{D_{13}}$
		$\frac{1-\nu}{1-2\nu} - \beta \bar{t}_{D_{33}}^2$	$-\beta \bar{t}_{D_{33}} \bar{t}_{D_{12}}$	$-\beta \bar{t}_{D_{33}} \bar{t}_{D_{23}}$	$-\beta \bar{t}_{D_{33}} \bar{t}_{D_{13}}$
SYMMETRIC			$\frac{1}{2} - \beta \bar{t}_{D_{12}}^2$	$-\beta \bar{t}_{D_{12}} \bar{t}_{D_{23}}$	$-\beta \bar{t}_{D_{12}} \bar{t}_{D_{13}}$
				$\frac{1}{2} - \beta \bar{t}_{D_{23}}^2$	$-\beta \bar{t}_{D_{23}} \bar{t}_{D_{13}}$
					$\frac{1}{2} - \beta \bar{t}_{D_{13}}^2$

where

$$\beta = \frac{3}{2} \frac{1}{\bar{t}_{\sigma_y^2}} \frac{1}{1 + \frac{2}{3} \frac{EE_T}{E-E_T} \frac{1+\nu}{E}}$$

TABLE 8 SHELL ELEMENT INTERPOLATION MATRIX

$$\underline{u}^e = {}^0\underline{H}\,\underline{u}$$

where $\underline{u}^e = \begin{bmatrix} u_1 \\ u_2 \\ u_3 \end{bmatrix}$; interpolated displacement field in the element

$$\underline{u}^T = \left[u_1^1 \; u_2^1 \; u_3^1 \; \alpha^1 \; \beta^1 ; \; u_1^2 \; u_2^2 \; \ldots ; \; u_1^N \; u_2^N \; u_3^N \; \alpha^N \; \beta^N \right];$$

Note: α^k and β^k (k = 1,2 .. N) are included in $\underline{u}^T$ only if node k is a mid-surface node

and the interpolation matrix is:

$$ {}^0\underline{H} = \left[\begin{array}{c:ccc:cc:c} & h_k & 0 & 0 & {}^0g_{11}^k & {}^0g_{21}^k & \\ \ldots & 0 & h_k & 0 & {}^0g_{12}^k & {}^0g_{22}^k & \ldots \\ & 0 & 0 & h_k & {}^0g_{13}^k & {}^0g_{23}^k & \end{array} \right] $$

include if node k is a mid-surface node

for nodal point k

TABLE 9 INTERPOLATION FUNCTIONS FOR VARIABLE-NUMBER-NODES SHELL ELEMENT

9.A QUADRILATERAL ELEMENT

INTERPOLATION FUNCTIONS	POLYNOMIAL	NODES				INCLUDE IF NODE IS PRESENT								NODE #	INCLUDE IF ALL NODES ARE PRESENT			
		1	2	3	4	5	6	7	8	9	10	11	12	13	13	14	15	16
h_1	$P_1 = \frac{1}{4} R S$	P_1				$-\frac{1}{2}P_5$			$-\frac{1}{2}P_8$	$-\frac{1}{4}P_5 + \frac{1}{3}P_9$			$\frac{1}{8}P_8 - \frac{1}{3}P_{12}$	$\frac{1}{4}P_{13}$	$\frac{4}{9}P_{13}$	$\frac{2}{9}P_{14}$	$\frac{1}{9}P_{15}$	$\frac{2}{9}P_{16}$
h_2	$P_2 = \frac{1}{4} \bar{R} S$		P_2			$-\frac{1}{2}P_5$	$-\frac{1}{2}P_6$			$\frac{1}{8}P_5 - \frac{1}{3}P_9$	$-\frac{1}{4}P_6 + \frac{1}{3}P_{10}$			$\frac{1}{4}P_{13}$	$\frac{2}{9}P_{13}$	$\frac{4}{9}P_{14}$	$\frac{2}{9}P_{15}$	$\frac{1}{9}P_{16}$
h_3	$P_3 = \frac{1}{4} \bar{R} \bar{S}$			P_3			$-\frac{1}{2}P_6$	$-\frac{1}{2}P_7$			$\frac{1}{8}P_6 - \frac{1}{3}P_{10}$	$-\frac{1}{4}P_7 + \frac{1}{3}P_{11}$		$\frac{1}{4}P_{13}$	$\frac{1}{9}P_{13}$	$\frac{2}{9}P_{14}$	$\frac{4}{9}P_{15}$	$\frac{2}{9}P_{16}$
h_4	$P_4 = \frac{1}{4} R \bar{S}$				P_4			$-\frac{1}{2}P_7$	$-\frac{1}{2}P_8$			$\frac{1}{8}P_7 - \frac{1}{3}P_{11}$	$-\frac{1}{4}P_8 + \frac{1}{3}P_{12}$	$\frac{1}{4}P_{13}$	$\frac{2}{9}P_{13}$	$\frac{1}{9}P_{14}$	$\frac{2}{9}P_{15}$	$\frac{4}{9}P_{16}$
h_5	$P_5 = 2P_1 \bar{R}$					P_5				$\frac{1}{8}P_5 - P_9$				$-\frac{1}{2}P_{13}$	$-\frac{2}{3}P_{13}$			$-\frac{1}{3}P_{16}$
h_6	$P_6 = 2P_2 \bar{S}$						P_6				$\frac{1}{8}P_6 - P_{10}$			$-\frac{1}{2}P_{13}$	$-\frac{1}{3}P_{13}$	$-\frac{2}{3}P_{14}$		
h_7	$P_7 = 2P_3 R$							P_7				$\frac{1}{8}P_7 - P_{11}$		$-\frac{1}{2}P_{13}$		$-\frac{1}{3}P_{14}$	$-\frac{2}{3}P_{15}$	
h_8	$P_8 = 2P_4 S$								P_8				$\frac{1}{8}P_6 - P_{12}$	$-\frac{1}{2}P_{13}$			$-\frac{1}{3}P_{15}$	$-\frac{2}{3}P_{16}$
h_9	$P_9 = \frac{9}{16} P_5 \underset{\sim}{\bar{R}}$									P_9						$-\frac{2}{3}P_{14}$	$-\frac{1}{3}P_{15}$	
h_{10}	$P_{10} = \frac{9}{16} P_6 \underset{\sim}{\bar{S}}$										P_{10}						$-\frac{2}{3}P_{15}$	$-\frac{1}{3}P_{16}$
h_{11}	$P_{11} = \frac{9}{16} P_7 \underset{\sim}{R}$											P_{11}			$-\frac{1}{3}P_{13}$			$-\frac{2}{3}P_{16}$
h_{12}	$P_{12} = \frac{9}{16} P_8 \underset{\sim}{S}$												P_{12}		$-\frac{2}{3}P_{13}$	$-\frac{1}{3}P_{14}$		
h_{13}^*	$P_{13} = R \bar{R} S \bar{S}$													P_{13}				
h_{13}	$P_{13} = \langle RS \rangle \underset{\sim}{R}\underset{\sim}{S}$														P_{13}			
h_{14}	$P_{14} = \langle RS \rangle \underset{\sim}{\bar{R}}\underset{\sim}{S}$															P_{14}		
h_{15}	$P_{15} = \langle RS \rangle \underset{\sim}{\bar{R}}\underset{\sim}{\bar{S}}$																P_{15}	
h_{16}	$P_{16} = \langle RS \rangle \underset{\sim}{R}\underset{\sim}{\bar{S}}$																	P_{16}

* { ONE INTERNAL NODE CAN ONLY BE PRESENT
IF AND ONLY IF NO CUBIC NODES ARE PRESENT
AND ALL QUADRATIC NODES (NODES 1 TO 8) ARE PRESENT

NOTATIONS:

$$\begin{cases} R = (1+r) \\ S = (1+s) \end{cases} ; \quad \begin{cases} \bar{R} = (1-r) \\ \bar{S} = (1-s) \end{cases} ; \quad \begin{cases} \underset{\sim}{R} = (1+3r) \\ \underset{\sim}{S} = (1+3s) \end{cases} ; \quad \begin{cases} \underset{\sim}{\bar{R}} = (1-3r) \\ \underset{\sim}{\bar{S}} = (1-3s) \end{cases} ; \quad \left\{ \langle RS \rangle = \frac{81}{256} (1-r^2)(1-s^2) \right.$$

TABLE 9 (CONTINUED)

9.8 TRIANGULAR ELEMENT

INTERPOLATION FUNCTIONS	POLYNOMIAL	NODES			INCLUDE IF NODE IS PRESENT					
		1	2	3	5	6	7	9	10	11
h_1	$P_1 = L_1$	P_1			$-\frac{1}{2}P_5$		$-\frac{1}{2}P_7$	$-\frac{1}{4}P_5 + \frac{1}{3}P_9$		$\frac{1}{8}P_7 - \frac{1}{3}P_{11}$
h_2	$P_2 = L_2$		P_2		$-\frac{1}{2}P_5$	$-\frac{1}{2}P_6$		$\frac{1}{8}P_5 - \frac{1}{3}P_9$	$-\frac{1}{4}P_6 + \frac{1}{3}P_{10}$	
h_3	$P_3 = L_3$			P_3		$-\frac{1}{2}P_6$	$-\frac{1}{2}P_7$		$\frac{1}{8}P_6 - \frac{1}{3}P_{10}$	$-\frac{1}{8}P_7 + \frac{1}{3}P_{11}$
h_5	$P_5 = 4L_1L_2$				P_5			$\frac{1}{8}P_5 - P_9$		
h_6	$P_6 = 4L_2L_3$					P_6			$\frac{1}{8}P_6 - P_{10}$	
h_7	$P_7 = 4L_1L_3$						P_7			$\frac{1}{8}P_7 - P_{11}$
h_9	$P_9 = \frac{9}{2}L_1L_2(2-3L_1)$							P_9		
h_{10}	$P_{10} = \frac{9}{2}L_2L_3(2-3L_2)$								P_{10}	
h_{11}	$P_{11} = \frac{9}{2}L_1L_3(2-3L_3)$									P_{11}

REFERENCES

[1] Fung, Y.C., and Sechler, E.E., Editors, Thin Shell Structures, Prentice-Hall Inc., Englewood Cliffs, New Jersey, 1974.

[2] Timoshenko, S. and Woinowsky-Krieger, S. Theory of Plates and Shells, McGraw-Hill, New York, 1959.

[3] Gallagher, R.H., "Geometrically Nonlinear Shell Analysis", Proc. Int. Conf. in Nonlinear Solid and Structural Mech., Geilo, Norway, Col-1/Col-26, Sept. 1977.

[4] Zienkiewicz, O.C., The Finite Element Method, McGraw-Hill, New York, 1975.

[5] Gallagher, R.H., "Shell Elements," Proc. World Congress on F.E.M., in Struct. Mech. Vol. 1, Bournemouth, England, 1975.

[6] Morino, L., Leech, J.W., Witmer, E.A., "An Improved Numerical Calculation Technique for Large Elastic-Plastic Transient Deformation of Thin Shells", Transactions of the ASME, J. of Applied Mechanics, pp. 423-436, June (1975).

[7] Bushnell, D., Almorth, B.O. and Brogan, F., "Finite-Difference Energy Methods for Nonlinear Shell Analysis", J. of Computers and Structures, Vol. 1, pp. 261-387 (1971).

[8] Pian, T.H.H., Tong, P., "Basis of Finite Element Methods for Solid Continua, Int. J. Numer. Method in Eng. 1. pp.3-28 (1969).

[9] Atluri, S., Pian, T.H.H., "Theoretical Formulation of Finite Element Methods in Linear-Elastic Analysis of General Shells", J. of Structural Mechanics, No. 1, Vol. 1, pp. 1-41 (1972).

[10] Botoz, J.L., Bathe, K.J., Ho, L.W., "A Search for the Optimum Three-Noded Triangular Plate Bending Element", Acoustic and Virbration Lab. Report 82448-8, Dept. of Mechanical Engrg., M.I.T.

[11] Dhatt, G.S., "An Efficient Triangular Shell Element", AIAA J., Vol. 8, No. 11, pp. 2100-2102, November (1970).

[12] Yoshida, Y., "A Hybrid Stress Element for Thin Shell Analysis", Proc. Finite Element Methods in Engineering, University of South Wales, 1974.

[13] Olson, M.D., Bearden, T.W., "The Simple Flat Triangular Shell Element Revisited", to appear in Int. J. of Numer. Method in Eng.

[14] Argyris, H.H. and Dunne, P.C., "Nonlinear and Post-Building Analysis of Structures", U.S.-Germany Symp. on Formulations and Computational Algorithms in F.E.A., Bathe, K.J., et al (Eds.) M.I.T. Press, 1976.

[15] Horrigmoe, G., "Finite Element Instability Analysis of Free-Form Shells", Report #77-2, The Norwegian Institute of Technology, The University of Trondheim, Norway, May 1977.

[16] Horrigmoe, G., "Hybrid Stress Finite Element Model for Nonlinear Shell Problems", Proc. Sixth Canadian Conf. on Applied Mech., U.B.C. Vancouver, Canada, May 1977.

[17] Weeks, G.E., "Finite Element Model for Shells Based on the Discrete Kirchhoff Hypothesis", Int. J. for Numer. Meth. in Engng., Vol. 5, pp. 3-16 (1972).

[18] Atluri, S. and Pian, T.H.H., "Finite-Element Analysis of Shells of Revolution by Two Doubly Curved Quadrilateral Elements", J. Struct. Meth., Vol. 1, No. 3, pp. 393-416 (1973).

[19] Larsen, P.K., Popov, E.P., "Large Displacement Analysis of Viso-elastic Shells of Revolution", Computer Meths. in Applied Mechanics and Engng., Vol. 3, pp. 237-253 (1974).

[20] Wempner, G.A., Oden, T. and Kross, D.A., "Finite-Element Analysis of Thin Shells", Proc. ASCE, J. Engng. Mech. Div., pp. 1273-1294 (1968).

[21] Alaylioglu, H. and Ali, R., "A Hybrid Stress Doubly Curved Shell Finite Element", J. Computers and Structures, Vol. 7, pp. 477-480 (1977).

[22] Noor, A.K. and Hartley, S.J., "Nonlinear Shell Analysis via Mixed Isoparametric Elements", J. Computers of Structures, Vol. 7, pp. 615-626 (1977).

[23] Boland, P.L. and Pian, T.H.H., "Large Deflection Analysis of Thin Elastic Structures by the Assumed Stress Hybrid Finite Element Method", J. Computers and Structures, Vol.7 , pp. 1-24, (1977).

[24] Ahmad, S., Irons, B.M., Zienkiewicz, O.C., "Analysis of Thick and Thin Shell Structures by Curved Finite Elements", Int. J. Numer. Meth. in Engng., Vol. 2, pp. 419-451 (1970).

[25] Zienkiewicz, O.C., Taylor, R.L., Too, J.M., "Reduced Integration Technique in General Analysis of Plate and Shells", Int. J. Numer. Meth. in Engng., Vol. 3, pp. 275-290 (1971).

[26] Takemoto, H., Cook, R.D., "Some Modifications of an Isoparametric Shell Element", Int. J. Numer. Meth. in Engng., Vol. 7, pp. 401-405 (1973).

[27] Nicolas, V.T. and Citipitioglu, E., "A General Isoparametric Finite Element Program SDRC SUPERB", J. Computers of Structures, Vol. 7, pp. 303-313 (1977).

[28] Ramm, E., "A Plate/Shell Element for Large Deflections and Rotations", in Formulations and Computational Algorithsm in Finite Element Analysis, Bathe, K.J., Oden, J.T., and Wunderlick, W. (Eds.), M.I.T. Press, 1977.

[29] Kråkeland, B., "Large Displacement Analysis of Shells Considering Elasto-Plastic and Elasto-Viscoplastic Materials", Report No. 77-6, The Norwegian Institute of Technology, The University of Trondheim, Norway, Dec. 1977.

[30] Bathe, K.J., Bolourchi, S., "A Geometric and Material Nonlinear Plate and Shell Element", J. Computers and Structures, to appear.

[31] Hartung, R.F. and Ball, R.E., "A Comparison of Several Computer Solutions to Three Structural Shell Analysis Problems", Tech. Report AFFDLTR-73-15, Lockheed Palo Alto Research Laboratory, Palo Alto, California, 1973.

[32] Bathe, K.J., Bolourchi, S., Ramaswamy, S., Snyder, M.D., "Some Computational Capabilities for Nonlinear Finite Element Analysis", J. Nuclear Engng. and Design, Vol. 46, pp. 429-455 (1978).

[33] Bathe, K.J. and Wilson, E.L., Numerical Methods in Finite Element Analysis, Prentice-Hall, Inc., 1976.

[34] Bathe, K.J., Ramm, E. and Wilson, E.L., "Finite Element Formulations for Large Deformation Dynamics Analysis", Int. J. Numer. Meth. in Engng., Vol. 9, pp. 353-386 (1975).

[35] Bathe, K.J., "Static Dynamic Geometric and Material Nonlinear Analysis Using ADINA", Acoustics and Vibration Lab. Report 82448-2, Dept. of Mechanical Engng., M.I.T., May 1976.

[36] Malvern, L.E., Introduction to the Mechanics of a Continuous Medium, Prentice-Hall Inc., Englewood Cliffs, New Jersey, 1969.

[37] Fung, Y.C., Foundations of Solid Mechanics, Prentice-Hall Inc., Englewood Cliffs, New Jersey, 1965.

[38] Bathe, K.J., Ramm, E. and Wilson, E.L., "Finite Element Formulations for Large Displacement and Large Strain Analysis", University of California at Berkeley, Report UC-SESM 73-14, 1973.

[39] Bathe, K.J., "ADINA - A Finite Element Program for Automatic Dynamic Incremental Nonlinear Analysis", Acoustics and Vibration Lab, Report 82448-1, Dept. of Mechanical Engng., M.I.T., Sept. 1975.

[40] Bathe, K.J., Bolourchi, S., "Large Deflection Analysis of Three-Dimensional Beam Structures", Int. J. Numer. Meth. in Engng. (1979).

[41] Bolourchi, S., Bathe, K.J., "A Geometric and Material Nonlinear Three-dimensional Beam Element", Acoustics and Vibration Lab. Report 82448-4, Dept. of Mechanical Engng., M.I.T., 1977.

[42] Kråkeland, B. and Mo.O.,"Non-Linear Analysis of Stiffened Shells", UUAIE 7th Structural Analysis S.I.G. Meeting, Nice, France, Oct. 1978.

[43] Hammer, P.C., Marlowe, O.J. and Stroud, A.H., "Numerical Integration Over Simplexes and Cones", Math. Tables Aids Comp., Vol. 10, pp. 130-137 (1956).

[44] Hammer, P.C. and Stroud, A.H., "Numerical Evaluation of Multiple Integrals II", Math. Tables Aids Comp., Vol. 12, pp. 272-280 (1958).

[45] Stroud, A.H., "Numerical Integration Formulas of Degree Two", Mathematics of Computation, Vol, 14, pp. 21-26, (1960).

[46] Lannoy, F.G., "Triangular Finite Elements and Numerical Integration", J. Computers and Structures, Vol. 7, pp. 613, (1977).

[47] Cowper, G.R., "Gaussian Quadrature Formulas for Triangles", Int. J. of Numer. Methods in Engng., Vol. 7 , pp. 405-408 (1973).

[48] Lindberg, G.M., Olson, M.D., and Cowper, G.R., "New Developments in the Finite Element Analysis of Shells", National Research Council of Canada, Quarterly Bulletin of the Division of Mechanical Engng. and the National Aeronautical Establishment, Vol. 4, pp. 1-38, 1969.

[49] Liu, S.C. and Lin, T.H., "Elastic-Plastic Dynamic Analysis of Structures Using Known Elastic Solutions", to be published in Int. J. of Earthquake Engng. and Structure Dynamics.

[50] Jenkins, J.A., Seitz, T.B., and Przemieniecki, J.S., "Large Deflections of Diamond-Shaped Frames", Int. J. Solid Structures, Vol. 2, pp. 591-603, (1966).

[51] Levy, S., "Bending of Rectangular Plates with Large Deflections", Technical Note, National Advisory Committee for Aeronautics, No. 846, 1942.

[52] Snyder, M.D., and Bathe, K.J., "Formulation and Numerical Solution of Thermoelastic-Plastic-Creep Problems", Acoustics and Vibration Lab., Report 82448-3, Dept. of Mechanical Engng., M.I.T., June 1977.

[53] Hughes, T.J.R., Taylor, R.L. and Kanoknukulchai, W., "A Simple and Efficient Finite Element for Plate Bending", Int. J. Num. Meth. in Engng., Vol. 11, pp. 1529-1543 (1977).

[54] Sabir, A.B. and Lock, A.C., "The Application of Finite Elements to the Large Deflection Geometrically Nonlinear Behavior of Cylindrical Shells", in Variation Methods in Engineering, Brebbia, C.A. and Tottenham, H. (Editors), Southampton University Press, pp. 7/66-7/75, 1973.

[55] Dhatt, G.S., "Instability of Thin Shells by the Finite Element Method", IASS Symposium for Folded Plates and Prismatic Structures, Vienna, Vol. 1, 1970.

[56] Leicester, R.H., "Finite Deformations of Shallow Shells", ASCE, Vol. 94, EM6, pp. 1409-1423. (1968).

[57] Gallagher, R.H., "Finite Element Representations for Thin Shell Instability Analysis", in Buckling of Structures, by Budiansky, B. (Editor), Springer-Verlag, pp. 40-51, 1976.

[58] Wegner, R., "Finite Element Models for Reinforced Concrete", in Formulations and Computational Algorithms in Finite Element Analysis Bathe, K.J., Oden, J.T., and Wunderlich, W. (Eds.), M.I.T. Press, 1977.

BIOGRAPHICAL NOTE

The author was born on January 14, 1951, and was raised in Tehran, Iran. He attended Queen Mary College, London University at U.K. In July 1973, he received a Bachelor of Science Degree in Mechanical Engineering from Queen Mary College, where he was chosen as best student. He then attended M.I.T. and received a Master of Science Degree in Mechanical Engineering in February 1975. His Master's Thesis, under the direction of Professor Richard H. Lyon, was "Noise Reduction by Ballast in Rail Vehicle Track Structures". He has published a number of articles which are:

Bathe, K.J., and Bolourchi, S., "A Geometric and Material Nonlinear Plate and Shell Element", Journal of Computers and Structures, to appear.

Bathe, K.J., and Bolourchi, S., "Nonlinear Analysis of Three-Dimensional Beam Structures", International Journal Numerical Methods in Engineering, to appear.

Bathe, K.J., Bolourchi, S., Ramaswamy, S., Snyder, M.D., "Some Computational Capabilities for Nonlinear Finite Element Analysis", Journal Nuclear Engineering and Design, Vol. 46, pp. 429-455, 1978.

Bolourchi, S., and Bathe, K.J., "A Geometric and Material Nonlinear Three-Dimensional Beam Element", Report 82448-4 Acoustics and Vibration Lab., Mechanical Engineering Department, M.I.T., August 1977.

Bolourchi, S., 730 Problems in Logarithm and Algebra, Barani Publishing Company, Tehran, Iran (1968) (in Persian).